Electron- and photon-impact atomic ionization

I. Bray, D. V. Fursa, A. S. Kadyrov, A. T. Stelbovics

ARC Centre for Antimatter-Matter Studies, Curtin University, GPO Box U1987, Perth, WA 6845, Australia

A. S. Kheifets

Research School of Physical Sciences, The Australian National University, Canberra ACT 0200, Australia

Abstract

The last decade has seen extraordinary theoretical progress in the field of fully kinematically resolved atomic electron-impact ionization, and its closely related field of double photoionization. These processes were challenging to calculate due to formal and computational difficulties associated with breakup problems involving the long ranged Coulomb potential. Presently, however, these processes can be routinely calculated accurately for suitable targets, irrespective of the kinematics considered or the geometry of detectors. We report on the computational progress, and how it has resulted in a deeper understanding of the formalism of Coulomb few-body problems.

Keywords: electron-impact ionization, double photoionization

Contents

1. Introduction

Collisions in the realm of atomic physics not only have many practical applications, but also form the testing ground for the underlying quantum collision theory, made possible by the wealth of experimental data. Due to the long-range nature of the Coulomb potential charged particles continue to interact with each other even at infinite separation. For this reason the much studied problem of electron-impact ionization, and its very close relative of non-sequential double photoionization, have lacked a proper formal foundation despite many successful computational implementations. In fact it was

the success of the computational approaches to the problems that drove us to revisit the underlying formal theory.

The purpose of this article is to review the recent progress in formal ionization theory, and show how it relates to the successful computational techniques which aim to fully solve the ionization problems without resorting to approximations which limit the applicability of the methods. Such issues are best addressed using relative simple targets of atomic hydrogen and helium, where we can be very confident in the accuracy of the calculated target structure. Additionally, we shall restrict detailed discussion to the lower energies, where high-energy approximations are inaccurate.

We begin with the discussion of formal issues in Sec. 2 and the computational methods in Sec. 3. This is followed by applications to electron-impact ionization in Sec. 4 and double photoionization in Sec. 5.

2. Formal scattering theory for Coulomb few-body problems

Scattering in a three-body system at energies above the three-body breakup threshold is one of the central subjects of quantum mechanics. Enormous progress has been achieved in recent years in describing (e,2e) processes via the exterior complex scaling (ECS) [1–3], convergent close coupling (CCC) [4–6] , R-matrix with pseudostates (RMPS) [7–10] and time-dependent close-coupling (TDCC) [11] methods. As described in the forthcoming sections of the present review, kinematically complete picture of electron impact ionisation (of simple atoms) is well understood, with calculations fully supporting experimental observations. The electron-hydrogen breakup problem is considered as practically solved. In particular, the success of the ECS and CCC approaches to the fundamental Coulomb breakup problem caused re-examination of the underlying formal theory [12–14] which culminated in a surface-integral approach [15] to formulating scattering theory. We start from a brief review of this approach in a form applicable to arbitrary three-body systems with both short-range and Coulombic long-range potentials. The formalism is based on a surface-integral approach. New prior and post forms of the breakup amplitude for a three-body system will be given that are valid for both short-range and Coulombic potentials. This resolves a problem of the missing conventional post form of the Coulomb breakup amplitude. An essential feature of the surface-integral formulation is that it avoids any reference to the Green's functions and formal solutions of the Schrödinger equation in integral forms. Therefore, for the purpose of defining the scat-

tering amplitudes the knowledge of a complicated analytic structure of the Green's function in the complex-energy plane is not required. This constitutes a simpler yet more general alternative to formulations adopted in textbooks on scattering theory.

Microscopic many-particle systems with the long-range Coulomb interactions and cosmological many-body systems with the gravitational interactions are of fundamental importance for our understanding of the universe. Atomic and nuclear systems are governed by the pairwise Coulomb potential (in addition to other possible short-range interactions) which is proportional to the charges of interacting particles and inversely proportional to the interparticle distance (r). In case of cosmic objects the masses of the objects play the role of gravitational charges. This $1/r$ potential is arguably the most important interaction in the structure of the universe. The long-range character of this potential implies that there is interaction even at very large (in fact, infinitely large) distances. This leads to various divergency problems in many branches of physics from quantum mechanics to quantum electrodynamics, from field theories to statistical physics, from celestial mechanics to cosmology. Despite being identified from the very beginning of modern physics, these problems have resisted proper solution. As a result different renormalization theories have been developed aimed at their *ad hoc* resolution. However, such approaching have been possible only in some limited class of problems. One can think that a simple cut off beyond some finite range could be a remedy for these problems. Unfortunately, this is not the case for most systems of practical interest. This could be because limiting the range of the potential leads to the loss of information about the very nature of the field creating the potential that cannot be recovered by simply taking the screening range to infinity.

It is well known that conventional quantum-mechanical collision theory is valid only when particles interact via short-range potentials. For charged particles the theory requires modification due to the fact that the long range of the Coulomb potential distorts the incident and scattered waves right out to infinity. Formal scattering theory is generalized to include Coulomb long-range potentials using renormalization methods [16]. The renormalization theories lead to the correct cross sections for the two-body problem, however, the results from these procedures cannot be regarded as completely consistent. For instance, in screening-based renormalization methods different ways of screening lead to different asymptotic forms for the scattering wave function. These asymptotic forms differ from the exact one obtained

from the solution of the Schrödinger equation. Moreover the renormalization methods give rise to a scattering amplitude that does not exist on the energy shell. In other words, the resulting amplitude cannot be directly used for calculating cross sections. This is because the amplitude obtained in these methods has complex factors which are divergent on the energy shell. Therefore, these factors must be removed (renormalized) before approaching the on-shell point. Furthermore, the renormalization factors depend on the way the limits are taken when the on-shell point is approached. In other words, depending on the way you take the limits different factors need to be removed. Thus, the *ad-hoc* renormalization procedure is not logically consistent. In quantum collision theory it is customary to define the scattering amplitude in terms of the scattering wavefunction and the potential of interaction. Despite the fact that the Coulomb wavefunction and the Coulomb potential are both known analytically, the conventional theory has not been able to provide such a standard definition for the amplitude of scattering of two charged particles, which yields the Rutherford cross section.

The situation with the Coulomb few-body scattering problem is significantly more complicated. Rigorous scattering theory for a system of three particles valid for short-range potentials was given by Faddeev [17, 18]. For the charged particles with the long-range Coulomb interaction the theory has faced difficulties associated with the compactness of the underlying equations. A renormalization method was implemented successfully for the three-body problem when only two particles are charged [19]. There are no compact integral equations yet known for collisions of more than two charged particles that are satisfactory above the breakup threshold [16]. Furthermore, there is no theoretical proof or practical evidence that a renormalization approach can be applied to the Faddeev equations for the three-body Coulomb problem. This has serious consequences especially for three-body problems in atomic physics where all three particles are charged.

As far as breakup of a bound state of two particles in a system of three charged particles is concerned, the key problem is how to extract the scattering information from the wavefunction when the latter is available. The conventional theory fails to provide a formal post-form definition of the breakup amplitude for three charged particles in terms of the total wavefunction with outgoing scattered waves describing the process. Therefore, the Coulomb interaction is screened and the formula for the short-range case is used. However, it is well known that the short-range definition of the breakup amplitude diverges when the screening radius is taken to infinity.

Thus we have a situation where we cannot use the theory unless we screen the Coulomb interaction, and when we do, we end up with quantities which diverge as screening is removed. This leaves no choice but to use renormalization to fix unphysical results. As mentioned above this is not possible in all cases of interest. Therefore, a new approach to the Coulomb three-body problem that does not need renormalization is required.

Despite the aforementioned problems remarkable progress has been achieved in atomic physics in describing (e,2e) processes via the exterior complex-scaling (ECS) [1, 2] and the convergent close-coupling (CCC) [4] methods. As we mentioned earlier, the success of the ECS and CCC approaches to the Coulomb breakup problem caused us to reexamine the underlying formal theory [12–15]. In the ECS method the amplitude is calculated from Peterkop's trial integral [20] which is likely to be some kind of approximation to the exact breakup amplitude in the post form (unavailable in conventional scattering theory). In the CCC method one of the electrons is treated using a square-integrable (L^2) representation, and the breakup amplitude can be related to a particular form of Peterkop's integral. Despite the success of the computational methods in describing the measured cross sections, the traditional formal theory of scattering was unable to provide a definition for the breakup amplitude in terms of the scattered wave. This has been a long-standing problem [14].

In this Section we briefly review a surface-integral approach [15] to formulating scattering theory. This approach represents an extension of the general formalism of scattering theory to systems of two and three charged particles with long-range Coulombic interactions. The essential feature of the surface-integral formulation of scattering theory is that it avoids the reference to the Green's function and formal solution for the scattered wavefunction in the integral form. Wave functions we deal with in scattering theory go beyond the Hilbert space. Since these functions are not square-integrable (L^2) their scalar products can be unbounded. While this fact is not a problem on its own, nevertheless, non-L^2 functions do make certain integrals emerging in the theory divergent. In case of integrals containing the interaction potential a standard procedure, which ensures their existence, is limiting the range of the potential. However, this irreversibly distorts the nature of the problem. The surface-integral approach usees a different way to deal with the aforementioned problem. Here, first the scattering problem is formulated in a finite region of coordinate space, and then extended to the full space. This leads to new more general definitions for scattering amplitude valid for

arbitrary interactions including Coulombic long-range ones. Details of the surface-integral formalism can be found in Ref. [15].

2.1. Formal problems of the conventional theory of ionisation

We start from giving some more details of two problems of formal scattering theory mentioned above. Consider scattering of electron e_1 with incident momentum $\boldsymbol{k}_i$ off a hydrogen atom (p, e_2) in initial state $\phi_i(\boldsymbol{r}_2)$ of energy E_i. Assume that the energy of the projectile $k_i^2/2$ is enough to break up the target. The ionization amplitude in the *prior* form is well defined and given according to [21]

$$T(\boldsymbol{k}_1, \boldsymbol{k}_2) \;=\; \int d\boldsymbol{r}_1 d\boldsymbol{r}_2 \Psi_0^{-*}(\boldsymbol{r}_1, \boldsymbol{r}_2) \overline{V}_i \Phi_i(\boldsymbol{r}_1, \boldsymbol{r}_2), \tag{1}$$

where Ψ_0^- is the total scattering wave function developing into an initial state of three particles in the continuum with incoming scattered-wave boundary condition and describes

$$\left.\begin{array}{l} e_1 + e_2 + p \\ e_1 + (p, e_2) \\ e_2 + (p, e_1) \end{array}\right\} \;\rightarrow\; e_1 + e_2 + p \tag{2}$$

processes. The wave function Ψ_0^- satisfies the Schrödinger equation

$$(E - H)\Psi_0^-(\boldsymbol{r}_1, \boldsymbol{r}_2) = 0, \tag{3}$$

where $H = H_0 + V$ is the total three-body Hamiltonian, $H_0 = -\Delta_{\boldsymbol{r}_1}/2 - \Delta_{\boldsymbol{r}_2}/2$ is the free three-body Hamiltonian, V is the full interaction and $E = k_i^2/2 + E_i = k_1^2/2 + k_2^2/2$ is the total energy of the system, $\overline{V}_i = V - V_i$ in Eq. (1) is the interaction of the incident electron with the target particles, $\boldsymbol{r}_1$ and $\boldsymbol{r}_2$ are the coordinates of the electrons relative to the proton and $\boldsymbol{k}_1$ and $\boldsymbol{k}_2$ are their momenta. The wave function representing the initial two-fragment channel is given by a product of the incident plane wave and the initial bound-state wave function

$$\Phi_i(\boldsymbol{r}_1, \boldsymbol{r}_2) = e^{i\boldsymbol{k}_i \cdot \boldsymbol{r}_1} \phi_i(\boldsymbol{r}_2). \tag{4}$$

V_i is the potential responsible for the bound state in the initial channel. According to our particular choice of the initial channel, V_i is the Coulomb interaction of electron e_2 and the proton.

The ionization amplitude given in the form (1) is difficult to calculate because it requires the total scattering wave function Ψ_0^-, which evolves into a free three-particle state (in a time-reversal picture). Asymptotic boundary condition that helps to choose the right solution from the infinite set of solutions to the differential equation has a complicated form. For this reason, it is very difficult to solve Eq. (3) using direct integration methods. In addition, for the ionization amplitude to be calculated from this definition, a knowledge of Ψ_0^- in the entire space is necessary. Therefore, this form of the ionization amplitude has mostly been used in distorted-wave Born-type calculations (see, e.g. [22–25] and references therein). In terms of numerical calculations, it is always more convenient to work with the wave function Ψ_i^+ that describes

$$e_1 + (p, e_2) \;\; \rightarrow \;\; \left\{ \begin{array}{l} e_1 + e_2 + p \\ e_1 + (p, e_2) \\ e_2 + (p, e_1) \end{array} \right. \tag{5}$$

processes. The total scattering wave function Ψ_i^+ is a solution of the Schrödinger equation

$$(E - H)\Psi_i^+(\boldsymbol{r}_1, \boldsymbol{r}_2) = 0, \tag{6}$$

with outgoing scattered-wave boundary condition. The advantage of Ψ_i^+ over its time-reversal counterpart Ψ_0^- is that the wave function Ψ_i^+ develops from the exact initial state Φ_i given by a product of a plane wave and hydrogen bound state wave function. In order to calculate the ionization amplitude from Ψ_i^+ we need a post-form definition of the amplitude. According to the conventional scattering theory this forms is written as

$$T(\boldsymbol{k}_1, \boldsymbol{k}_2) \;\; = \;\; \int d\boldsymbol{r}_1 d\boldsymbol{r}_2 \Phi_0^*(\boldsymbol{r}_1, \boldsymbol{r}_2) V \Psi_i^+(\boldsymbol{r}_1, \boldsymbol{r}_2), \tag{7}$$

where

$$\Phi_0(\boldsymbol{r}_1, \boldsymbol{r}_2) \;\; = \;\; e^{i\boldsymbol{k}_1 \cdot \boldsymbol{r}_1 + i\boldsymbol{k}_2 \cdot \boldsymbol{r}_2}. \tag{8}$$

I.e., the final state of the two unbound electrons is described by the plane waves. The problem with the definition (7) is that it is valid only for particles interacting via short-range potentials. It cannot be applied for charged particles with the long-range Coulomb interaction. An attempt to apply it to

breakup processes with charged particles leads to divergent results. As mentioned in the Introduction, the prescription from the conventional scattering theory is to screen the Coulomb interactions, use Eq. (7) and then in the obtained result take the screening radius to infinity. However, this procedure has not been shown to be valid neither theoretically, nor by practical calculations. Then the question is how do we calculate the ionisation amplitude if we somehow managed to solve Eq. (6) and obtained Ψ_i^+?

Trying to resolve this problem Peterkop [26] (see also [27]) developed 50 years ago the so-called effective-charge formalism for electron-impact ionisation. He considered the integral

$$I_{z_1,z_2}(\boldsymbol{k}_1,\boldsymbol{k}_2) \;=\; \int d\boldsymbol{r}_1 d\boldsymbol{r}_2 \Psi_i^+(\boldsymbol{r}_1,\boldsymbol{r}_2)(H-E)\Phi_{z_1,z_2}^{(2\mathrm{C})-*}(\boldsymbol{r}_1,\boldsymbol{r}_2), \qquad (9)$$

where the function $\Phi_{z_1,z_2}^{(2\mathrm{C})-}$ is a product of the two Coulomb (2C) wave functions with effective charges z_1 and z_2:

$$\Phi_{z_1,z_2}^{(2\mathrm{C})-}(\boldsymbol{r}_1,\boldsymbol{r}_2) \;=\; e^{i\boldsymbol{k}_1\cdot\boldsymbol{r}_1+i\boldsymbol{k}_2\cdot\boldsymbol{r}_2}\,\psi_{z_1}(\boldsymbol{k}_1,\boldsymbol{r}_1)\,\psi_{z_2}(\boldsymbol{k}_2,\boldsymbol{r}_2), \qquad (10)$$

with incoming wave boundary condition. The Coulomb part is given by

$$\psi_\nu(\boldsymbol{k},\boldsymbol{r}) \;=\; \Gamma(1+i\nu/k)\exp(\pi\nu/2k)\,{}_1F_1(-i\nu/k,1;-i(kr+\boldsymbol{k}\cdot\boldsymbol{r})), \qquad (11)$$

where ${}_1F_1$ is the confluent hypergeometric function.

Using Eq. (6) and Green's theorem [28] the volume integral in Eq. (9) can be written as a surface integral

$$\begin{aligned} I_{z_1,z_2}(\boldsymbol{k}_1,\boldsymbol{k}_2) \;=\; & \frac{1}{2}\lim_{R\to\infty} R^5 \int d\hat{\boldsymbol{r}}_1 d\hat{\boldsymbol{r}}_2 \int_0^{\pi/2} d\alpha \sin^2\alpha\cos^2\alpha \\ & \times\left[\Phi_{z_1,z_2}^{(2\mathrm{C})-*}\frac{\partial\Psi_i^+}{\partial R} - \Psi_i^+\frac{\partial\Phi_{z_1,z_2}^{(2\mathrm{C})-*}}{\partial R}\right], \end{aligned} \qquad (12)$$

where $R=(r_1^2+r_2^2)^{1/2}$ is a hyperradius, $(\hat{\boldsymbol{r}}_1,\hat{\boldsymbol{r}}_2,\alpha)$ is a 5-dimensional hyperangle, with $\alpha=\arctan(r_2/r_1)$.

The advantage of the integral form (12) is that it is readily expanded in partial-waves leading to a sum of one-dimensional integrals. On the other hand Eq. (1) reduces to a two-dimensional integral upon partial wave expansion. Most importantly, the integral I_{z_1,z_2} depends only on the asymptotic

behavior of the wave functions Ψ_i^+ and $\Phi_{z_1,z_2}^{(2C)-}$ on an infinitely large hypershpere and, therefore, knowledge of the wave function Ψ_i^+ over the entire space is not required. But how does integral I_{z_1,z_2} relate to the ionization amplitude?

Let us define the domain Ω_0 to correspond to the space where all interparticle distances are large, i.e. r_1, r_2, $r_3\,(\boldsymbol{r}_3 = \boldsymbol{r}_1 - \boldsymbol{r}_2) \to \infty$, in a manner that $r_1/r_2 \to \text{const} \neq 0$. In this domain the asymptotic behavior of Ψ_i^+ was found by Peterkop [29] and is written, in the leading order of R, as

$$\Psi_i^+(\boldsymbol{r}_1, \boldsymbol{r}_2) \quad \xrightarrow{\Omega_0} \quad A(\hat{\boldsymbol{r}}_1, \hat{\boldsymbol{r}}_2, \alpha)\; R^{-5/2} e^{i\kappa R + i\gamma \ln(\kappa R)}, \tag{13}$$

where $\kappa = (2E)^{1/2}$,

$$\gamma = \frac{1}{\kappa}\left[\frac{1}{\cos\alpha} + \frac{1}{\sin\alpha} - \frac{1}{\sqrt{1 - \hat{\boldsymbol{r}}_1 \cdot \hat{\boldsymbol{r}}_2\, \sin 2\alpha}}\right], \tag{14}$$

and A is Peterkop's ionization amplitude. Peterkop showed that integral I_{z_1,z_2} exists and differs from amplitude A only by a factor:

$$A(\hat{\boldsymbol{k}}_1, \hat{\boldsymbol{k}}_2, \alpha') \;=\; \frac{\kappa^{3/2}}{(2\pi)^{5/2}} e^{i\beta(R) + i\pi/4} I_{z_1,z_2}(\boldsymbol{k}_1, \boldsymbol{k}_2), \tag{15}$$

where $\alpha' = \arctan(k_2/k_1)$. However, the phase factor $\beta(R)$ diverges as $R \to \infty$ unless the so-called Peterkop condition

$$\frac{z_1}{k_1} + \frac{z_2}{k_2} \;=\; \frac{1}{k_1} + \frac{1}{k_2} - \frac{1}{|\boldsymbol{k}_1 - \boldsymbol{k}_2|}, \tag{16}$$

is satisfied. In this case $\beta(R)$ vanishes for large R. The relation (15) is known as the Peterkop integral representation for the ionization amplitude.

Thus, in Peterkop's effective charge approach z_1 and z_2 depend on vectors $\boldsymbol{k}_1$ and $\boldsymbol{k}_2$. For this reason this method was not very useful in practice for it was not clear how to implement condition (16) in realistic calculations. Numerical problems associated with the effective charge approach were discussed by McCurdy et al. [30]. Their calculations showed that use of effective charges z_1 and z_2 leads to severe numerical problems due to nonorthogonality of the Coulomb wave of a non-unit effective charge to the bound states of hydrogen. From a formal point of view, even if the Peterkop condition is satisfied, one could not establish the ionization amplitude in full. This is because, as mentioned by Peterkop [27], an arbitrary part of the complex

amplitude A in asymptotic form (13) can be moved to the phase factor and the resulting wave function would still be a solution to the original Eq. (6) transformed into the six-dimensional hyperspace. Thus, the remaining part of A can equally well be called an ionization amplitude and there is no way of choosing between the different phase possibilities which is clearly unsatisfactory.

In order to explain the origin of the problems with the Peterkop formulation, summarized by Eqs. (12) and (15), we need to distinguish all possible geometries where the condition $R \to \infty$ is satisfied. In addition to the Ω_0 domain defined earlier, we identify the domain where $r_1 \to \infty$, $r_2 \to \infty$ with limited r_3 as Ω_3 and when r_2 (or r_1) goes to infinity but r_1 (r_2) remains limited as Ω_2 (Ω_1). Domains Ω_1, Ω_2 and Ω_3 correspond to $\alpha \to \pi/2$, $\alpha \to 0$ and $\alpha \to \pi/4$ in the surface integral (12), respectively. The problems with Peterkop's integral representation for the ionization amplitude originate from the fact that the Peterkop asymptotic form used to calculate the integral (12) is valid only in Ω_0. It is clearly seen from Eq. (14) that the Peterkop form cannot be used when $\alpha \to 0$ and $\alpha \to \pi/2$. This wave function is singular also when $\alpha \to \pi/4$ if $\hat{\boldsymbol{r}}_1 \cdot \hat{\boldsymbol{r}}_2 = 1$. At the same time integration over α runs through all these points. Thus, in the integral representation suggested by Peterkop the contributions from Ω_1, Ω_2 and Ω_3 domains are either missing, or taken into account incorrectly.

Since the Peterkop condition turned out to be impossible to satisfy in practice, for almost four decades the formalism had looked like an elaborate theory without practical implications. A breakthrough came in the form of ECS method [30]. These authors practically demonstrated that for calculations of the cross sections using the integral representation of Eq. (15) for the breakup amplitude there was no need to satisfy the associated Peterkop condition. Moreover, they showed that in calculations it was more convenient to choose the trial function $\Phi^{2C}_{z_1,z_2}$ in Eq. (9) as a combination of two two-particle scattering states. In the hydrogen ionization problem this corresponds to taking $z_1 = z_2 = 1$ in Eq. (10). Since these two-particle scattering states are orthogonal to bound-state wavefunctions of the relevant pair of particles, this lead to faster convergence of the resulting integral [30]. Despite this breakthrough in practical calculations the origin of the Peterkop integral remained unclear. Also remained ununderstood the reason why one could ignore the Peterkop condition and still get the correct cross sections. The latter was addressed in Ref. [13] where the Peterkop formalism was generalised to all domains Ω_i, $i = 0 - 3$, of coordinate space and

demonstrated to be valid for arbitrary choice of $z_1 = z_2 = 1$, thereby relaxing the Peterkop condition altogether. This analysis lead to a surface-integral formulation of the scattering theory which showed that the Peterkop integral was an approximation to a missing post form of the ionisation amplitude.

2.2. Surface-integral approach

Here we give an overview of the surface-integral approach [15] to scattering theory in a general form applicable for an arbitrary system of three charged particles. We use the Jacobi coordinates where $\boldsymbol{r}_\alpha$ is the relative coordinate, and $\boldsymbol{k}_\alpha$ is the relative momentum, between particles β and γ, $\boldsymbol{\rho}_\alpha$ is the relative coordinate of the center of mass of the pair (β, γ) and particle α, with $\boldsymbol{q}_\alpha$ being the canonically conjugate relative momentum. Accordingly, μ_α is the reduced mass of particles β and γ and M_α is the reduced mass of the pair (β, γ) and particle α. Here $\alpha, \beta, \gamma = 1, 2, 3$, and $\alpha \neq \beta \neq \gamma$.

We are interested in scattering of particle α with incident momentum $\boldsymbol{q}_{\alpha n}$ off a bound pair (β, γ) in initial state $\phi_{\alpha n}(\boldsymbol{r}_\alpha)$ of energy $E_{\alpha n}$. Here n denotes a full set of quantum numbers of the bound state (β, γ) in channel α. Assume that the energy of the projectile $q_{\alpha n}^2/2M_\alpha$ is enough to break up the target. Therefore, in addition to direct scattering and rearrangement $(\beta + (\gamma, \alpha))$ channels, there is a breakup one. We call this $2 \to 3$ process. In order to find the amplitudes of direct scattering, rearrangement and breakup in this collision we need the total scattering wavefunction developed from the initial channel αn and three different asymptotic wavefunctions corresponding to three final-state channels. The same amplitudes can be found in the so-called prior forms as well, which requires the knowledge of the other three types of the total scattering wavefunctions being developed to three different final-state wavefunctions. Thus, in any case, we require a set of four total scattering wavefunctions together with their corresponding asymptotic forms in all relevant asymptotic domains.

There are two distinct types of asymptotic domains. Let us call Ω_0 the asymptotic domain, where all interparticle distances are large, i.e, $r_\alpha \to \infty$, $\rho_\alpha \to \infty$, so that r_α/ρ_α is non-zero. In addition, we call Ω_α the asymptotic regime, where $\rho_\alpha \to \infty$, however r_α satisfies the constraint $r_\alpha/\rho_\alpha \to 0$.

The total three-body wavefunction describing the $2 \to 3$ processes satisfies the Schrödinger equation

$$(E - H)\Psi^+_{\alpha n}(\boldsymbol{r}_\alpha, \boldsymbol{\rho}_\alpha) \;=\; 0, \tag{17}$$

with outgoing-wave boundary conditions, where $H = H_0 + V$, $H_0 = -\Delta_{\boldsymbol{r}_\alpha}/2\mu_\alpha - \Delta_{\boldsymbol{\rho}_\alpha}/2M_\alpha$ is the free Hamiltonian, $V = V_\alpha(\boldsymbol{r}_\alpha) + V_\beta(\boldsymbol{r}_\beta) + V_\gamma(\boldsymbol{r}_\gamma)$ is the full interaction and $E = E_{\alpha n} + q^2_{\alpha n}/2M_\alpha = k^2_\alpha/2\mu_\alpha + q^2_\alpha/2M_\alpha$ is the total energy of the system. We split the wavefunction $\Psi^+_{\alpha n}$ into the initial-channel wave $\Phi^+_{\alpha n}$ and scattered wave $\Psi^{\mathrm{sc}+}_{\alpha n}$:

$$\Psi^+_{\alpha n}(\boldsymbol{r}_\alpha, \boldsymbol{\rho}_\alpha) = \Phi^+_{\alpha n}(\boldsymbol{r}_\alpha, \boldsymbol{\rho}_\alpha) + \Psi^{\mathrm{sc}+}_{\alpha n}(\boldsymbol{r}_\alpha, \boldsymbol{\rho}_\alpha). \tag{18}$$

A slightly different scattering process may also take place within the same three-body system at the same total energy E, the one where in the initial channel (in the time-reversed picture this will be the final state) all three particles are in the continuum which we call $3 \to 3$ scattering. The wavefunction Ψ^-_0 describing this process is also an eigenstate of the same Hamiltonian H,

$$(E - H)\Psi^-_0(\boldsymbol{r}_\alpha, \boldsymbol{\rho}_\alpha) = 0, \tag{19}$$

but with incoming scattered-wave boundary conditions. In the total wavefunction $\Psi^-_0(\boldsymbol{r}_\alpha, \boldsymbol{\rho}_\alpha)$ we separate the part describing the unscattered state of three free particles, denoted $\Phi^-_0(\boldsymbol{r}_\alpha, \boldsymbol{\rho}_\alpha)$ and which Ψ^-_0 is being developed to (in the absence of the Coulomb interaction this would simply be the three-body plane wave),

$$\Psi^-_0(\boldsymbol{r}_\alpha, \boldsymbol{\rho}_\alpha) = \Phi^-_0(\boldsymbol{r}_\alpha, \boldsymbol{\rho}_\alpha) + \Psi^{\mathrm{sc}-}_0(\boldsymbol{r}_\alpha, \boldsymbol{\rho}_\alpha). \tag{20}$$

Asymptotic boundary conditions that the wavefunctions $\Psi^+_{\alpha n}$ and Ψ^-_0 satisfy are compiled in Ref. [15].

Now we use $\Psi^+_{\alpha n}$ and Ψ^-_0 to derive amplitudes for different scattering processes. This time we need an incomplete inner product in the six-dimensional configuration space. Such a product of two arbitrary functions Ψ_i and Ψ_f is written as a volume integral

$$\left\langle \Psi_f | \Psi_i \right\rangle_{R_0} = \int_{R \le R_0} d\boldsymbol{r}_\alpha d\boldsymbol{\rho}_\alpha \Psi^*_f(\boldsymbol{r}_\beta, \boldsymbol{\rho}_\beta)\Psi_i(\boldsymbol{r}_\alpha, \boldsymbol{\rho}_\alpha), \tag{21}$$

where the integration is limited to the volume of a six-dimensional hypersphere of radius R_0. A hyperradius in the six-dimensional configurations space is defined according to $R = \left(\mu_\alpha r^2_\alpha + M_\alpha \rho^2_\alpha\right)^{1/2}$.

Taking into account Eq. (18) we can write Eq. (17) as

$$(E - H)\Psi^{\mathrm{sc}+}_{\alpha n}(\boldsymbol{r}_\alpha, \boldsymbol{\rho}_\alpha) \;=\; (H - E)\Phi^+_{\alpha n}(\boldsymbol{r}_\alpha, \boldsymbol{\rho}_\alpha). \tag{22}$$

Let us multiply Eq. (22) by $\Psi_0^{-*}(\boldsymbol{r}_\alpha, \boldsymbol{\rho}_\alpha)$ from the left and integrate the result over the volume of a hypersphere of radius R_0:

$$\left\langle \Psi_0^- | (E-H) \Psi_{\alpha n}^{\mathrm{sc}+} \right\rangle_{R_0} = \left\langle \Psi_0^- | (H-E) \Phi_{\alpha n}^+ \right\rangle_{R_0}. \quad (23)$$

We also have

$$\left\langle (E-H) \Psi_0^- | \Psi_{\alpha n}^{\mathrm{sc}+} \right\rangle_{R_0} = 0, \quad (24)$$

which is true for any R_0 simply due to Eq. (19). Now we subtract Eq. (24) from (23) to get

$$\left\langle \Psi_0^- | (E-H) \Psi_{\alpha n}^{\mathrm{sc}+} \right\rangle_{R_0} - \left\langle (E-H) \Psi_0^- | \Psi_{\alpha n}^{\mathrm{sc}+} \right\rangle_{R_0} = \left\langle \Psi_0^- | (H-E) \Phi_{\alpha n}^+ \right\rangle_{R_0}. \quad (25)$$

Despite of the fact that both Ψ_0^- and $\Psi_{\alpha n}^{\mathrm{sc}+}$ are non-L^2 functions, terms of the form $\left\langle \Psi_0^- | (E-V) | \Psi_{\alpha n}^{\mathrm{sc}+} \right\rangle_{R_0}$ are finite due to the limited space (regardless of the long-range nature of the potential). Therefore, canceling them we look at the limit of this equation as $R_0 \to \infty$

$$\lim_{R_0 \to \infty} \left[-\left\langle \Psi_0^- | H_0 \Psi_{\alpha n}^{\mathrm{sc}+} \right\rangle + \left\langle H_0 \Psi_0^- | \Psi_{\alpha n}^{\mathrm{sc}+} \right\rangle \right]_{R_0} = \lim_{R_0 \to \infty} \left\langle \Psi_0^- | (H-E) \Phi_{\alpha n}^+ \right\rangle_{R_0}. \quad (26)$$

As in the two-body case, the meaning of this quantity will become clear when we evaluate the limits.

Parameter R_0 can go to infinity with the system being in Ω_0 or Ω_α, $\alpha = 1, 2, 3$. An essential feature of the term on the LHS of Eq. (26) is that it is easily transformed into an integral over the hypersurface of radius R_0 so that the result depends only on the behavior of the wavefunctions on this surface. For this integral the knowledge of the wavefunctions anywhere inside the surface is not required. Then it can be evaluated using the asymptotic forms of the wavefunctions in the corresponding asymptotic domain.

Let us start with the Ω_0 domain. If $R_0 \to \infty$ in Ω_0 then for the LHS of Eq. (26) we have

$$\begin{aligned} \mathrm{LHS} = & \frac{1}{2(\mu_\alpha M_\alpha)^{3/2}} \lim_{R_0 \to \infty} R_0^5 \int d\hat{\boldsymbol{r}}_\alpha d\hat{\boldsymbol{\rho}}_\alpha \int_0^{\pi/2} d\varphi_\alpha \sin^2 \varphi_\alpha \cos^2 \varphi_\alpha \\ & \times \left[\Psi_0^{-*}(\boldsymbol{r}_\alpha, \boldsymbol{\rho}_\alpha) \frac{\partial}{\partial R} \Psi_{\alpha n}^{\mathrm{sc}+}(\boldsymbol{r}_\alpha, \boldsymbol{\rho}_\alpha) - \Psi_{\alpha n}^{\mathrm{sc}+}(\boldsymbol{r}_\alpha, \boldsymbol{\rho}_\alpha) \frac{\partial}{\partial R} \Psi_0^{-*}(\boldsymbol{r}_\alpha, \boldsymbol{\rho}_\alpha) \right]_{R=R_0}, \end{aligned} \quad (27)$$

where $\varphi_\alpha = \arctan\left[(\mu_\alpha/M_\alpha)^{1/2}\, r_\alpha/\rho_\alpha\right]$ is a hyperangle, $0 \le \varphi_\alpha \le \pi/2$. Here we first transformed H_0 from $(\boldsymbol{r}_\alpha, \boldsymbol{\rho}_\alpha)$ into $(R, \widehat{\boldsymbol{r}}_\alpha, \widehat{\boldsymbol{\rho}}_\alpha, \varphi_\alpha)$-variables and then made use of Green's theorem to transform the volume integral into the surface integral. Now we can use the asymptotic forms for the wave functions [15] and perform differentiation to find out that this is an extremely oscillatory integral as $R_0 \to \infty$. Therefore, only points of stationary phase in φ_α, if there are any, should contribute to the integral. Calculating the integral by means of the stationary-phase method we arrive at

$$\text{LHS} \;=\; T\left(\boldsymbol{k}_\alpha, \boldsymbol{q}_\alpha\right), \tag{28}$$

where $T(\boldsymbol{k}_\alpha, \boldsymbol{q}_\alpha)$ is the amplitude of the of the scattered wave in Ω_0. Therefore, in Ω_0 Eq. (26) is written as

$$T(\boldsymbol{k}_\alpha, \boldsymbol{q}_\alpha) \;=\; \lim_{R_0\to\infty} \left\langle \Psi_0^- | (H-E)\Phi_{\alpha n}^+ \right\rangle_{R_0}. \tag{29}$$

In other words, if scattering takes place into the Ω_0 domain then the expression $\lim_{R_0\to\infty} \left\langle \Psi_0^- | (H-E)\Phi_{\alpha n}^+ \right\rangle_{R_0}$ represents the breakup amplitude. If after the collision the products of scattering turn out to be in Ω_α or in Ω_β domains then we have to distinguish whether all three particles are in the continuum or only one. If all three are in the continuum then similarlarly to the Ω_0 case we can show that $\lim_{R_0\to\infty} \left\langle \Psi_0^- | (H-E)\Phi_{\alpha n}^+ \right\rangle_{R_0}$ again represents the breakup amplitude. Thus, Eq. (29) defines the breakup amplitude in all asymptotic domains.

If after the collision the products of scattering form a two-fragment channel then instead of Ψ_0^- we will need the total scattering wavefunction which develops into the wavefunction of this two-fragment channel. We start from Ω_α domain which corresponds to direct scattering. In this case the total scattering wavefunction we need is $\Psi_{\alpha m}^-$. Let us multiply Eq. (22) by $\Psi_{\alpha m}^{-*}(\boldsymbol{r}_\alpha, \boldsymbol{\rho}_\alpha)$ from the left and integrate the result over the volume of a hypersphere of radius R_0:

$$\left\langle \Psi_{\alpha m}^- | (E-H)\Psi_{\alpha n}^{\mathrm{sc}+} \right\rangle_{R_0} \;=\; \left\langle \Psi_{\alpha m}^- | (H-E)\Phi_{\alpha n}^+ \right\rangle_{R_0}. \tag{30}$$

Now we subtract $\left\langle (E-H)\Psi_{\alpha m}^- | \Psi_{\alpha n}^{\mathrm{sc}+} \right\rangle_{R_0} = 0$ from Eq. (30) to get

$$-\left\langle \Psi_{\alpha m}^- | H_0 \Psi_{\alpha n}^{\mathrm{sc}+} \right\rangle_{R_0} + \left\langle H_0 \Psi_{\alpha m}^- | \Psi_{\alpha n}^{\mathrm{sc}+} \right\rangle_{R_0} = \left\langle \Psi_{\alpha m}^- | (H-E)\Phi_{\alpha n}^+ \right\rangle_{R_0}. \tag{31}$$

We again consider the limit of this equation as $R_0 \to \infty$. Since this time $R_0 \to \infty$ in Ω_α then on the LHS of Eq. (31) we have

$$\begin{aligned} \text{LHS} &= \frac{1}{2M_\alpha} \lim_{R_0\to\infty} R_0^2 \int d\boldsymbol{r}_\alpha d\hat{\boldsymbol{\rho}}_\alpha \left[\Psi^{-*}_{\alpha m}(\boldsymbol{r}_\alpha, \boldsymbol{\rho}_\alpha) \frac{\partial}{\partial \rho_\alpha} \Psi^{\mathrm{sc}+}_{\alpha n}(\boldsymbol{r}_\alpha, \boldsymbol{\rho}_\alpha) \right. \\ &\left. - \Psi^{\mathrm{sc}+}_{\alpha n}(\boldsymbol{r}_\alpha, \boldsymbol{\rho}_\alpha) \frac{\partial}{\partial \rho_\alpha} \Psi^{-*}_{\alpha m}(\boldsymbol{r}_\alpha, \boldsymbol{\rho}_\alpha) \right]_{\rho_\alpha = R_0}. \end{aligned} \tag{32}$$

Here we transformed only one of the volume integrals into the surface integral (the wave functions fall off exponentially in the other two-body subspace). Using the asymptotic forms of the wavefunctions [15] and the orthogonality of the the two-particle bound state wavefunctions and calculating the integral we arrive at

$$\text{LHS} = F(\boldsymbol{q}_{\alpha m}, \boldsymbol{q}_{\alpha n}), \tag{33}$$

where $F(\boldsymbol{q}_{\alpha m}, \boldsymbol{q}_{\alpha n})$ is the amplitude of the wave scattered into channel α. Thus as $R_0 \to \infty$ Eq. (31) is in fact written as

$$F(\boldsymbol{q}_{\alpha m}, \boldsymbol{q}_{\alpha n}) = \lim_{R_0\to\infty} \left\langle \Psi^-_{\alpha m} | (H - E) \Phi^+_{\alpha n} \right\rangle_{R_0}. \tag{34}$$

In other words we have got a definition for the direct scattering (elastic and excitation) amplitude. Finally, taking $R_0 \to \infty$ in Ω_β (i.e., the final state belongs to channel β) and calculating the limit of Eq. (31) we get a definition for the amplitude of the rearrangement scattering

$$G(\boldsymbol{q}_{\beta m}, \boldsymbol{q}_{\alpha n}) = \lim_{R_0\to\infty} \left\langle \Psi^-_{\beta m} | (H - E) \Phi^+_{\alpha n} \right\rangle_{R_0}. \tag{35}$$

Now we derive the scattering and breakup amplitudes in post form. Taking into account Eq. (20) we can write Eq. (19) as

$$(E - H)\Psi^{\mathrm{sc}-}_0(\boldsymbol{r}_\alpha, \boldsymbol{\rho}_\alpha) = (H - E)\Phi^-_0(\boldsymbol{r}_\alpha, \boldsymbol{\rho}_\alpha). \tag{36}$$

Let us take the complex conjugate of Eq. (36) and multiply it by $\Psi^+_{\alpha n}(\boldsymbol{r}_\alpha, \boldsymbol{\rho}_\alpha)$ from right. Then integrating the result over the volume of a hypersphere of radius R_0 we get

$$\left\langle (E - H)\Psi^{\mathrm{sc}-}_0 | \Psi^+_{\alpha n} \right\rangle_{R_0} = \left\langle (H - E)\Phi^-_0 | \Psi^+_{\alpha n} \right\rangle_{R_0}. \tag{37}$$

We also consider

$$\left\langle \Psi_0^{\rm sc-}|(E-H)\Psi_{\alpha n}^{+}\right\rangle_{R_0} \;=\; 0, \tag{38}$$

which is again valid for any R_0 due to Eq. (17). Now we subtract Eq. (38) from (37)

$$\left\langle (E-H)\Psi_0^{\rm sc-}|\Psi_{\alpha n}^{+}\right\rangle_{R_0} - \left\langle \Psi_0^{\rm sc-}|(E-H)\Psi_{\alpha n}^{+}\right\rangle_{R_0} = \left\langle (H-E)\Phi_0^{-}|\Psi_{\alpha n}^{+}\right\rangle_{R_0}, \tag{39}$$

which reduces to

$$-\left\langle H_0\Psi_0^{\rm sc-}|\Psi_{\alpha n}^{+}\right\rangle_{R_0} + \left\langle \Psi_0^{\rm sc-}|H_0\Psi_{\alpha n}^{+}\right\rangle_{R_0} = \left\langle (H-E)\Phi_0^{-}|\Psi_{\alpha n}^{+}\right\rangle_{R_0}. \tag{40}$$

Calculations of the limit of the LHS of Eq. (40) are similar to those of Eq. (26) leading to Eqs. (29), (34) and (35). Depending on whether the $R_0 \to \infty$ limit is taken in domains Ω_0, Ω_α or Ω_β we have

$$T(\boldsymbol{k}_\alpha, \boldsymbol{q}_\alpha) \;=\; \lim_{R_0\to\infty} \left\langle (H-E)\Phi_0^{-}|\Psi_{\alpha n}^{+}\right\rangle_{R_0}, \tag{41}$$

$$F(\boldsymbol{q}_{\alpha m}, \boldsymbol{q}_{\alpha n}) \;=\; \lim_{R_0\to\infty} \left\langle (H-E)\Phi_{\alpha m}^{-}|\Psi_{\alpha n}^{+}\right\rangle_{R_0}, \tag{42}$$

$$G(\boldsymbol{q}_{\beta m}, \boldsymbol{q}_{\alpha n}) \;=\; \lim_{R_0\to\infty} \left\langle (H-E)\Phi_{\beta m}^{-}|\Psi_{\alpha n}^{+}\right\rangle_{R_0}, \tag{43}$$

respectively. These are the post forms of the amplitudes.

As it will be shown in the following subsection the prior and post forms of the breakup amplitude can take surface-integral forms (see Eqs. (61) and (63)). These surface integrals are similar in form to those calculated earlier. They can be calculated using the same analysis and shown to yield the same result, i.e. the breakup amplitude. Therefore Eq. (26) and the limit of (40) as $R_0 \to \infty$ represent the breakup amplitude. The same is true for the surface-integral representations of the direct scattering and rearrangement amplitudes. Therefore, Eqs. (29), (34) and (35) can in fact be written as

$$T^{\rm pr}(\boldsymbol{k}_\alpha, \boldsymbol{q}_\alpha) = \left\langle \Psi_0^{-}|\overrightarrow{H}-E|\Phi_{\alpha n}^{+}\right\rangle, \tag{44}$$

$$F^{\rm pr}(\boldsymbol{q}_{\alpha m}, \boldsymbol{q}_{\alpha n}) = \left\langle \Psi_{\alpha m}^{-}|\overrightarrow{H}-E|\Phi_{\alpha n}^{+}\right\rangle, \tag{45}$$

$$G^{\rm pr}(\boldsymbol{q}_{\beta m}, \boldsymbol{q}_{\alpha n}) = \left\langle \Psi_{\beta m}^{-}|\overrightarrow{H}-E|\Phi_{\alpha n}^{+}\right\rangle \tag{46}$$

and Eqs. (41)-(43) as

$$T^{\rm pt}(\boldsymbol{k}_\alpha, \boldsymbol{q}_\alpha) = \left\langle \Phi_0^{-}|\overleftarrow{H}-E|\Psi_{\alpha n}^{+}\right\rangle, \tag{47}$$

$$F^{\rm pt}(\boldsymbol{q}_{\alpha m}, \boldsymbol{q}_{\alpha n}) = \left\langle \Phi_{\alpha m}^{-}|\overleftarrow{H}-E|\Psi_{\alpha n}^{+}\right\rangle, \tag{48}$$

$$G^{\rm pt}(\boldsymbol{q}_{\beta m}, \boldsymbol{q}_{\alpha n}) = \left\langle \Phi_{\beta m}^{-}|\overleftarrow{H}-E|\Psi_{\alpha n}^{+}\right\rangle. \tag{49}$$

Thus we get alternative representations for the breakup, scattering and rearrangement amplitudes. In particular, the definition given in Eq. (47) resolves the problem of the post form of the Coulomb breakup amplitude mentioned earlier.

We note that when the interactions between all three pairs are short ranged then

$$\Phi^{\pm}_{\alpha n}(\boldsymbol{r}_\alpha, \boldsymbol{\rho}_\alpha) \;\; \rightarrow \;\; e^{i\boldsymbol{q}_{\alpha n}\cdot\boldsymbol{\rho}_\alpha}\phi_{\alpha n}(\boldsymbol{r}_\alpha). \tag{50}$$

This state satisfies the equation

$$(H-E)e^{i\boldsymbol{q}_{\alpha n}\cdot\boldsymbol{\rho}_\alpha}\phi_{\alpha n}(\boldsymbol{r}_\alpha) \;\; = \;\; \overline{V}_\alpha e^{i\boldsymbol{q}_{\alpha n}\cdot\boldsymbol{\rho}_\alpha}\phi_{\alpha n}(\boldsymbol{r}_\alpha), \tag{51}$$

where $\overline{V}_\alpha = V - V_\alpha$. At the same time if we have 3 particles in the final channel then

$$\Phi^{-}_{0}(\boldsymbol{r}_\alpha, \boldsymbol{\rho}_\alpha) \;\; \rightarrow \;\; e^{i\boldsymbol{k}_\alpha\cdot\boldsymbol{r}_\alpha + i\boldsymbol{q}_\alpha\cdot\boldsymbol{\rho}_\alpha}, \tag{52}$$

for which we have

$$(H-E)e^{i\boldsymbol{k}_\alpha\cdot\boldsymbol{r}_\alpha + i\boldsymbol{q}_\alpha\cdot\boldsymbol{\rho}_\alpha} \;\; = \;\; Ve^{i\boldsymbol{k}_\alpha\cdot\boldsymbol{r}_\alpha + i\boldsymbol{q}_\alpha\cdot\boldsymbol{\rho}_\alpha}. \tag{53}$$

Therefore, the new generalized forms of the amplitudes (44)-(49) reduce to the standard definitions

$$T^{\rm pr}(\boldsymbol{k}_\alpha, \boldsymbol{q}_\alpha) = \left\langle \Psi^{-}_{0}|\overline{V}_\alpha|\phi_{\alpha n}, \boldsymbol{q}_{\alpha n}\right\rangle, \tag{54}$$

$$F^{\rm pr}(\boldsymbol{q}_{\alpha m}, \boldsymbol{q}_{\alpha n}) = \left\langle \Psi^{-}_{\alpha m}|\overline{V}_\alpha|\phi_{\alpha n}, \boldsymbol{q}_{\alpha n}\right\rangle, \tag{55}$$

$$G^{\rm pr}(\boldsymbol{q}_{\beta m}, \boldsymbol{q}_{\alpha n}) = \left\langle \Psi^{-}_{\beta m}|\overline{V}_\alpha|\phi_{\alpha n}, \boldsymbol{q}_{\alpha n}\right\rangle \tag{56}$$

and

$$T^{\rm pt}(\boldsymbol{k}_\alpha, \boldsymbol{q}_\alpha) = \left\langle \boldsymbol{q}_\alpha, \boldsymbol{k}_\alpha|V|\Psi^{+}_{\alpha n}\right\rangle, \tag{57}$$

$$F^{\rm pt}(\boldsymbol{q}_{\alpha m}, \boldsymbol{q}_{\alpha n}) = \left\langle \boldsymbol{q}_{\alpha m}, \phi_{\alpha m}|\overline{V}_\alpha|\Psi^{+}_{\alpha n}\right\rangle, \tag{58}$$

$$G^{\rm pt}(\boldsymbol{q}_{\beta m}, \boldsymbol{q}_{\alpha n}) = \left\langle \boldsymbol{q}_{\beta m}, \phi_{\beta m}|\overline{V}_\beta|\Psi^{+}_{\alpha n}\right\rangle. \tag{59}$$

When the interactions have the Coulomb tail Eqs. (51) and (53) are not satisfied. For this reason the standard definitions (54)-(59) become invalid.

As mentioned earlier both prior and post forms of the scattering and breakup amplitudes take surface integral forms. The post form of the breakup

amplitude $T^{\rm pt}(\boldsymbol{k}_\alpha, \boldsymbol{q}_\alpha)$ is given by Eq. (41). Using Eq. (17) which is valid for any R_0 we can write this as

$$T^{\rm pt}(\boldsymbol{k}_\alpha, \boldsymbol{q}_\alpha) \;=\; \lim_{R_0\to\infty} \left[\left\langle H_0\Phi_0^-|\Psi_{\alpha n}^+\right\rangle - \left\langle \Phi_0^-|H_0\Psi_{\alpha n}^+\right\rangle\right]_{R_0}. \qquad (60)$$

Transforming the volume integral into a surface integral we get

$$T^{\rm pt}(\boldsymbol{k}_\alpha, \boldsymbol{q}_\alpha) = -\frac{1}{2(\mu_\alpha M_\alpha)^{3/2}} \lim_{R_0\to\infty} R_0^5 \int d\hat{\boldsymbol{r}}_\alpha d\hat{\boldsymbol{\rho}}_\alpha \int_0^{\pi/2} d\varphi_\alpha \sin^2\varphi_\alpha \cos^2\varphi_\alpha \times \left[\Psi_{\alpha n}^+(\boldsymbol{r}_\alpha, \boldsymbol{\rho}_\alpha)\frac{\partial}{\partial R}\Phi_0^{-*}(\boldsymbol{r}_\alpha, \boldsymbol{\rho}_\alpha) - \Phi_0^{-*}(\boldsymbol{r}_\alpha, \boldsymbol{\rho}_\alpha)\frac{\partial}{\partial R}\Psi_{\alpha n}^+(\boldsymbol{r}_\alpha, \boldsymbol{\rho}_\alpha)\right]_{R=R_0}. \qquad (61)$$

Thus the breakup amplitude in the post form is written as a five-dimensional surface integral. In the prior form of this amplitude and also both in the post and prior forms of scattering and rearrangement amplitudes only one of the three-dimensional volume integrals can be transformed into a surface integral. Consider, for instance, the prior form of the breakup amplitude. Using Eq. (19) we get from Eq. (29)

$$T^{\rm pr}(\boldsymbol{k}_\alpha, \boldsymbol{q}_\alpha) \;=\; \lim_{R_0\to\infty} \left[\left\langle \Psi_0^-|H_0\Phi_{\alpha n}^+\right\rangle - \left\langle H_0\Psi_0^-|\Phi_{\alpha n}^+\right\rangle\right]_{R_0}. \qquad (62)$$

This can be written as

$$T^{\rm pr}(\boldsymbol{k}_\alpha, \boldsymbol{q}_\alpha) = -\frac{1}{2M_\alpha} \lim_{R_0\to\infty} R_0^2 \int d\boldsymbol{r}_\alpha d\hat{\boldsymbol{\rho}}_\alpha \times \left[\Psi_0^{-*}(\boldsymbol{r}_\alpha, \boldsymbol{\rho}_\alpha)\frac{\partial}{\partial \rho_\alpha}\Phi_{\alpha n}^+(\boldsymbol{r}_\alpha, \boldsymbol{\rho}_\alpha) - \Phi_{\alpha n}^+(\boldsymbol{r}_\alpha, \boldsymbol{\rho}_\alpha)\frac{\partial}{\partial \rho_\alpha}\Psi_0^{-*}(\boldsymbol{r}_\alpha, \boldsymbol{\rho}_\alpha)\right]_{\rho_\alpha=R_0}. \qquad (63)$$

Note that above we took into account the fact that the surface integral in the other two-body space is zero as $r_\alpha \to \infty$ (the function $\Phi_{\alpha n}^+$ falls off

exponentially in this variable). Similarly we get

$$
\begin{aligned}
F^{\rm pr}(\boldsymbol{q}_{\alpha m},\boldsymbol{q}_{\alpha n}) &= -\frac{1}{2M_\alpha}\lim_{R_0\to\infty} R_0^2\int d\boldsymbol{r}_\alpha d\hat{\boldsymbol{\rho}}_\alpha \\
&\times\left[\Psi^{-*}_{\alpha m}(\boldsymbol{r}_\alpha,\boldsymbol{\rho}_\alpha)\frac{\partial}{\partial\rho_\alpha}\Phi^{+}_{\alpha n}(\boldsymbol{r}_\alpha,\boldsymbol{\rho}_\alpha)\right. \\
&\left.-\Phi^{+}_{\alpha n}(\boldsymbol{r}_\alpha,\boldsymbol{\rho}_\alpha)\frac{\partial}{\partial\rho_\alpha}\Psi^{-*}_{\alpha m}(\boldsymbol{r}_\alpha,\boldsymbol{\rho}_\alpha)\right]_{\rho_\alpha=R_0}, \qquad (64)\\
G^{\rm pr}(\boldsymbol{q}_{\beta m},\boldsymbol{q}_{\alpha n}) &= -\frac{1}{2M_\alpha}\lim_{R_0\to\infty} R_0^2\int d\boldsymbol{r}_\alpha d\hat{\boldsymbol{\rho}}_\alpha \\
&\times\left[\Psi^{-*}_{\beta m}(\boldsymbol{r}_\alpha,\boldsymbol{\rho}_\alpha)\frac{\partial}{\partial\rho_\alpha}\Phi^{+}_{\alpha n}(\boldsymbol{r}_\alpha,\boldsymbol{\rho}_\alpha)\right. \\
&\left.-\Phi^{+}_{\alpha n}(\boldsymbol{r}_\alpha,\boldsymbol{\rho}_\alpha)\frac{\partial}{\partial\rho_\alpha}\Psi^{-*}_{\beta m}(\boldsymbol{r}_\alpha,\boldsymbol{\rho}_\alpha)\right]_{\rho_\alpha=R_0}, \qquad (65)
\end{aligned}
$$

and in post forms

$$
\begin{aligned}
F^{\rm pt}(\boldsymbol{q}_{\alpha m},\boldsymbol{q}_{\alpha n}) &= -\frac{1}{2M_\alpha}\lim_{R_0\to\infty} R_0^2\int d\boldsymbol{r}_\alpha d\hat{\boldsymbol{\rho}}_\alpha \\
&\times\left[\Psi^{+}_{\alpha n}(\boldsymbol{r}_\alpha,\boldsymbol{\rho}_\alpha)\frac{\partial}{\partial\rho_\alpha}\Phi^{-*}_{\alpha m}(\boldsymbol{r}_\alpha,\boldsymbol{\rho}_\alpha)\right. \\
&\left.-\Phi^{-*}_{\alpha m}(\boldsymbol{r}_\alpha,\boldsymbol{\rho}_\alpha)\frac{\partial}{\partial\rho_\alpha}\Psi^{+}_{\alpha n}(\boldsymbol{r}_\alpha,\boldsymbol{\rho}_\alpha)\right]_{\rho_\alpha=R_0}, \qquad (66)\\
G^{\rm pt}(\boldsymbol{q}_{\beta m},\boldsymbol{q}_{\alpha n}) &= -\frac{1}{2M_\beta}\lim_{R_0\to\infty} R_0^2\int d\boldsymbol{r}_\beta d\hat{\boldsymbol{\rho}}_\beta \\
&\times\left[\Psi^{+}_{\alpha n}(\boldsymbol{r}_\beta,\boldsymbol{\rho}_\beta)\frac{\partial}{\partial\rho_\beta}\Phi^{-*}_{\beta m}(\boldsymbol{r}_\beta,\boldsymbol{\rho}_\beta)\right. \\
&\left.-\Phi^{-*}_{\beta m}(\boldsymbol{r}_\beta,\boldsymbol{\rho}_\beta)\frac{\partial}{\partial\rho_\beta}\Psi^{+}_{\alpha n}(\boldsymbol{r}_\beta,\boldsymbol{\rho}_\beta)\right]_{\rho_\alpha=R_0}. \qquad (67)
\end{aligned}
$$

What is the advantage of the surface-integral representations over the volume-integral forms? As we can see from the surface-integral forms for the amplitudes, they are ideal for practical calculations in partial waves as integrals over solid angles are taken [13]. Moreover, the corresponding results depend only on the behavior of the wavefunctions on the hypersurface of radius R_0, meaning that for these integrals the knowledge of the wavefunctions

anywhere inside the surface is not required. Therefore, they can be evaluated using the asymptotic forms of the wavefunctions in the corresponding asymptotic domain. The main advantage of the surface forms is that the asymptotic channel wavefunctions Φ_0^-, $\Phi_{\alpha m}^{\pm}$ and $\Phi_{\beta m}^-$ necessary for extracting the breakup, scattering and rearrangement amplitudes do not have to be exact. They can be replaced by other suitable functions making sure that magnitudes of the amplitudes are still calculated exactly. The question is what properties trial functions, capable of replacing aforementioned three functions, should posses?

Let us assume that as a result of solving the Schrödinger equation scattering wave $\Psi_{\alpha n}^+$ (or $\Psi_{\alpha n}^{\mathrm{sc}+}$) became available. First consider the way of extracting the direct scattering amplitude. According to Eq. (66), in order to extract this amplitude we need $\Phi_{\alpha m}^-$, or its partial waves. Consider the following trial surface integral instead

$$F_{R_0}(\boldsymbol{q}_{\alpha m}, \boldsymbol{q}_{\alpha n}) \;=\; \left\langle \Phi_{\alpha m} | \overleftarrow{H} - E | \Psi_{\alpha n}^+ \right\rangle_{R_0}, \tag{68}$$

where

$$\Phi_{\alpha m} \;=\; e^{i\boldsymbol{q}_{\alpha m}\boldsymbol{\rho}_\alpha} \phi_{\alpha m}(\boldsymbol{r}_\alpha). \tag{69}$$

After some algebra similar to what we have used in the previous section we arrive at

$$\lim_{R_0\to\infty} F_{R_0}(\boldsymbol{q}_{\alpha m}, \boldsymbol{q}_{\alpha n}) \;=\; F(\boldsymbol{q}_{\alpha m}, \boldsymbol{q}_{\alpha n}) \lim_{R_0\to\infty} \exp\left[-i\eta_{\alpha m}/q_{\alpha m} \ln(2q_{\alpha m}R_0)\right], \tag{70}$$

with a divergent phase. From this result we conclude that

$$|\lim_{R_0\to\infty} F_{R_0}(\boldsymbol{q}_{\alpha m}, \boldsymbol{q}_{\alpha n})| \;=\; |F(\boldsymbol{q}_{\alpha m}, \boldsymbol{q}_{\alpha n})|. \tag{71}$$

Similarly, for the magnitude of the rearrangement amplitude we get

$$|G(\boldsymbol{q}_{\alpha m}, \boldsymbol{q}_{\alpha n})| \;=\; |\lim_{R_0\to\infty} G_{R_0}(\boldsymbol{q}_{\alpha m}, \boldsymbol{q}_{\alpha n})|, \tag{72}$$

where

$$G_{R_0}(\boldsymbol{q}_{\beta m}, \boldsymbol{q}_{\alpha n}) \;=\; \left\langle \Phi_{\alpha m} | \overleftarrow{H} - E | \Psi_{\alpha n}^+ \right\rangle_{R_0}, \tag{73}$$

and

$$\Phi_{\beta m} \;=\; e^{i\boldsymbol{q}_{\beta m}\cdot\boldsymbol{\rho}_\beta}\phi_{\beta m}(\boldsymbol{r}_\beta). \tag{74}$$

Finally we consider breakup. The breakup amplitude in terms of $\Psi^+_{\alpha n}$ is given by Eq. (47) as a volume integral and Eq. (61) as a surface integral. These forms require Φ_0^-. Though the latter is known, its partial waves have complicated analytical form [13]. Therefore we consider the following surface integral

$$I_{R_0}(\boldsymbol{k}_\alpha,\boldsymbol{q}_\alpha) \;=\; \big\langle\tilde{\Phi}_0|\overleftarrow{H}-E|\Psi^+_{\alpha n}\big\rangle_{R_0}, \tag{75}$$

where $\tilde{\Phi}_0$ is a trial function. The trial function can be the three-body plane wave or any other function containing the three-body plane wave as a leading term at large distances. Another requirement is that it must be easily expandable in partial waves. Consider the case when

$$\tilde{\Phi}_0(\boldsymbol{r}_\alpha,\boldsymbol{\rho}_\alpha) \;=\; e^{i\boldsymbol{k}_\alpha\cdot\boldsymbol{r}_\alpha+i\boldsymbol{q}_\alpha\cdot\boldsymbol{\rho}_\alpha}. \tag{76}$$

Then we get, after some algebra [12, 13],

$$\lim_{R_0\to\infty} I_{R_0}(\boldsymbol{q}_\alpha,\boldsymbol{q}_\alpha) \;=\; T(\boldsymbol{q}_\alpha,\boldsymbol{q}_\alpha)\lim_{R_0\to\infty}\exp\left[-i\lambda_0\ln(2\kappa R_0)-i\sigma_0\right]. \tag{77}$$

The phase factor on the RHS diverges logarithmically as $R_0\to\infty$. However, we can again write that

$$|\lim_{R_0\to\infty} I_{R_0}(\boldsymbol{q}_\alpha,\boldsymbol{q}_\alpha)| \;=\; |T(\boldsymbol{q}_\alpha,\boldsymbol{q}_\alpha)|. \tag{78}$$

Thus in order to extract the *magnitude* of the scattering amplitudes it is not necessary to use the exact asymptotic state. The same can be done using much simpler trial functions. And that is the main advantage of the surface-integral representations.

A similar approach to atomic ionization problem is known as the Peterkop effective-charge formalism [26, 31]. The Peterkop integral discussed earlier can be written as

$$I_{z_1,z_2}(\boldsymbol{q}_\alpha,\boldsymbol{q}_\alpha) \;=\; \big\langle\Phi^{(2C)-}_{z_1,z_2}|\overleftarrow{H}-E|\Psi^+_{\alpha n}\big\rangle, \tag{79}$$

where $\Phi^{(2C)-}_{z_1,z_2}$ is a trial function taken as a product of two Coulomb waves of effective charges z_1 and z_2. Though Eq. (79) has no mathematical meaning

as it is written since the RHS is divergent, however, if we assume that it is written in the sense of Eq. (75) for a finite R_0, then as $R_0 \to \infty$ Eq. (78) would hold.

The CCC [5] and RMPS [7–10] methods are the other two successful approaches to atomic breakup problem. After inserting the projection operator into the exact post form of the ionization amplitude these approaches end up with a representation for the ionisation amplitude similar to the Peterkop trial integral (see Eqs. (106)-(107) and (118)). The choice of effective potentials in this case corresponds to $z_1 = 0$ for more energetic of the electrons and $z_2 = 1$ for the other (before the antisymmetrization). Though they do not use the surface-integral technique for calculating the amplitude, the obtained representation is further built into resulting scattering equations.

Thus the new post form of the breakup amplitude given in Eq. (47) in particular explains the origin of the Peterkop integral, a cornerstone of the highly successful ECS, CCC and R-matrix approaches to Coulomb breakup problems in atomic physics. Comparison of Eq. (79) with Eq. (47) shows that the Peterkop integral is simply an approximation to the exact breakup amplitude in its post form, where the exact three-body state Φ_0^- is replaced by the trial function Φ_{z_1,z_2}. It is remarkable that with any choice of the effective charges the difference between the breakup amplitude and Peterkop's integral reduces to a phase factor which does not affect the calculated cross sections [12, 13] provided $\Psi_{\alpha n}^+$ is accurate and R_0 is asymptotically large.

In order to solve a scattering problem, first, one has to find the total wavefunction describing the scattering process. The second part consists in the extraction of the necessary scattering amplitudes from this wave function for the purpose of calculating the cross sections. So far the surface-integral approach has resolved problems of the theory related to extracting the information about the scattering event. When the total scattering wavefunction is available the scattering amplitudes can be reliably extracted from it using the new definitions regardless the long-range nature of the interactions. Once the amplitudes are available calculations of corresponding cross sections are straightforward (see, e.g., [32]). As mentioned earlier, there are sophisticated numerical methods which can provide reliable numerical solution to the Schrödinger equation in some special cases. However, in case of three distinguishable particles where rearrangement is possible the Schrödinger equation cannot provide a unique answer. This is because of the fact that it is impossible to specify all asymptotic boundary conditions using one set of the Jacobi variables. To overcome this difficulty Faddeev [17] suggested a set

of equations which incorporates all the required asymptotic boundary conditions. However, as mentioned earlier in case of charged particles the Faddeev equations become noncompact. In other words they cannot be solved using standard numerical techniques though noncompactness generally does not exclude existence of analytic solutions. At the same time our results show that problems with the Faddeev equations are more serious than noncompactness. Equivalent sets of the Faddeev equations can be written for the wavefunction, resolvent of the Green's function or T-matrix. Let us consider the equations for the components of the three-body T-matrix. The starting point for these equations are old (conventional) definitions in terms of the interaction potentials which are simply not correct for charged particles. This implies that any results derived from old definitions are valid strictly for short-range potentials. For the Coulombic potentials they might be simply incorrect. Thus, the Faddeev equations in the presence of long-range Coulomb interactions require careful inspection. It may be possible to formulate the Faddeev equations in a form that would not require screening and renormalization along the lines of the present surface-integral formalism.

The main ingredient of the Faddeev equations is the off-the-energy-shell two-body T-matrix. For charged particles it is the off-shell Coulomb two-body T-matrix. The theory of the Coulomb T-matrix, which started from pioneering work of Schwinger in the 1940's (first published in Ref. [33]), is believed to be well developed and complete [16]. However, as we mentioned earlier the off-shell Coulomb T-matrix has no on-shell limit. It diverges as the on-shell point is approached where physical observables are extracted. Therefore, it cannot be directly used to calculate the physical Coulomb scattering amplitude. In particular, it appears obvious that if used it can only exacerbate the problems of the Faddeev equations. The theory is based on the conception that the Coulomb T-matrix cannot be defined directly on the energy shell. However, in the present work we have shown this to be a misconception and introduced the on-shell Coulomb T-matrix which directly gives the physical scattering amplitude. In other words, the on-shell Coulomb T-matrix presented here has no singularities and therefore does not require renormalisation. This means that the conventional theory of the Coulomb T-matrix must be abandoned altogether and a new theory be developed. We believe a new off-shell Coulomb T-matrix should be introduced as an analytic extension into the complex-energy plane of the on-shell T-matrix presented in this work.

We started with a general comment about divergence problems in different

branches of physics, associated with fields creating $1/r$ potentials. These annoying difficulties are consequences of imperfections in the existing theories. Renormalization is used to deal with such problems in quantum electrodynamics (QED). QED has experienced extraordinary success since Feynman, Schwinger and Tomonaga suggested the renormalization method. However, certain dissatisfaction with this theory remains [34–36]. Berestetskii, Lifshitz and Pitaevskii [37] start their well-known textbook emphasizing that "there is as yet no logically consistent and complete relativistic quantum theory. ... The lack of complete logical consistency in this theory is shown by the occurrence of divergent expressions when the mathematical formalism is directly applied, although there are quite well-defined ways of eliminating these divergences. Nevertheless, such methods remain, to a considerable extent, semiempirical rules, and our confidence in the correctness of the results is ultimately based only on their excellent agreement with experiment, not on the internal consistency or logical ordering of the fundamental principles of the theory." While another popular author Ryder [38] concludes that "despite the comparative success of renormalisation theory the feeling remains that there ought to be a more satisfactory way of doing things." Unfortunately, these concerns are largely ignored by the scientific community. We believe there must be a logically consistent solution to these problems where the mathematical formalism is directly applicable without the need for renormalization. In our case, utilising a surface-integral approach and focusing on integrated properties removes screening and renormalisation requirements in scattering theory. We suggest that a similar integrated approach may help eliminate renormalisation requirements in QED and other fields. This looks feasible at least in the case of the infrared divergencies.

3. Computational methods for Coulomb breakup problems

3.1. Exterior complex scaling

As we have already seen, specifying the asymptotic form of the scattering wave function for electron–impact ionization is a major challenge due to the long–range Coulomb force. In order to carry out numerical calculations for ionization one needs the partial–wave forms as well and they are not in easily accessible analytic forms amenable to practical calculations. Indeed very few numerical studies have been carried out, mostly in the Temkin–Poet model [39–41] that has simpler boundary conditions for the scattered wave. Therefore alternative methods applying the direct ionization boundary condition

have been sought. The CCC approach that has been successfully applied to ionization [42, 43] has the virtue of replacing continuum waves in the ionization channel by positive energy pseudo–states that at large distances approach zero magnitude. In this sense the continuum boundary condition of three free particles is replaced by one with a single continuum particle and an excited bound–state with positive energy. Exterior Complex Scaling (ECS) is another method that also seeks to eliminate the complexity of dealing with the true ionization boundary condition. In this method whose application to atomic collisions was championed by Rescigno, McCurdy and co-workers in the late 1990's [1, 44, 45] the three-body Schrödinger equation in coordinate space is solved by rotating the configuration space coordinates into the complex plane at sufficiently large distances $r \geq R_0$, where the asymptotic form of the boundary condition can be employed. For all intents and purposes R_0 may be considered to play the same role as that defined in the previous section on the formal scattering theory.

The method can be illustrated simply by means of the example of a one–dimensional scattering problem with a short-range potential $U(r)$. Consider the radial (s-wave) Schrödinger equation

$$\left(\frac{d^2}{dr^2} + k^2\right) \psi_k^+(r) = U(r)\psi_k^+(r). \tag{80}$$

The scattering solution needs two boundary conditions; as usual $\psi_k^+(0) = 0$ and secondly the asymptotic behaviour for large r,

$$\psi_k^+(r) \underset{r\to\infty}{\sim} \sin kr + e^{\mathrm{i}kr} e^{\mathrm{i}\delta} \sin\delta, \tag{81}$$

where the scattering information is contained in the the phase-shift $\delta(k)$. Let us now split, as in the previous section, $\psi_k^+(r)$ as the sum of the initial state $\phi_k(r) = \sin(kr)$, and $\psi_k^{\mathrm{sc}+}(r)$ which asymptotically contains the outgoing scattered wave and has the form

$$\psi_k^{\mathrm{sc}+} \underset{r\to\infty}{\sim} e^{\mathrm{i}kr} e^{\mathrm{i}\delta} \sin\delta. \tag{82}$$

Now it is possible to express Eq. (80) using this decomposition as

$$\left(\frac{d^2}{dr^2} + k^2 - U(r)\right) \psi_k^{\mathrm{sc}+}(r) = U(r)\phi_k(r), \tag{83}$$

In practice this equation for unknown $\psi^{\rm sc+}$ is easily solved numerically for short-range potentials using difference equation techniques and propagating out from $r = 0$ to large r where the asymptotic form (82) is valid given the known initial state.

In situations where the asymptotic forms are very difficult to formulate or to adapt to practical numerical calculations the propagation method flounders. One way to overcome this problem is to use exterior complex scaling. At a large finite distance from the origin (R_0) that is in the asymptotic region we choose to rotate the r–space into the complex plane:

$$z(r) = \begin{cases} r, & r < R_0 \\ R_0 + (r - R_0)e^{{\rm i}\theta}, & r \geq R_0. \end{cases} \tag{84}$$

The angle of rotation is within the range $0 < \theta < \pi/2$ so that when this transformation is applied to the outgoing wave for $r > R_0$ one has

$$\begin{aligned} e^{{\rm i}kr} \rightarrow e^{{\rm i}kz(r)} &= e^{-k(r-R_0)\sin\theta} e^{{\rm i}k(R_0+(r-R_0)\cos\theta)} & (85) \\ &\rightarrow 0 \text{ as } r \rightarrow \infty. & (86) \end{aligned}$$

Thus by using this rotation one can replace the asymptotic scattering boundary condition by the much simpler one that at some distance not far beyond R_0, $\psi_k^{\rm sc+} \approx 0$. However there remains a subtlety to consider when applying this transformation to Eq.(83), namely that the initial state $\phi_k = \sin kr$ has both incoming and outgoing waves. Unfortunately the incoming wave *diverges* exponentially under the transformation. In numerical implementation it has been found that the empirical procedure of applying a smooth cut–off to the incoming portion beyond R_0 is completely satisfactory if one wishes to extract scattering information in the asymptotic region below R_0. Mathematical justifications of this empirical procedure has been provided quite recently [46, 47].

In this example the scattering information, is contained in the coefficient $e^{{\rm i}\delta}\sin\delta$ of the scattered wave. It can be extracted directly using $e^{{\rm i}\delta}\sin\delta = \lim_{r\rightarrow\infty} \psi^{\rm sc+}e^{-{\rm i}kr}$ but one can use the more general (and elegant) surface integral approach to scattering theory employed in section 2.

Consider the integral

$$t_R(k) = \frac{1}{k}\int_0^R \psi_k^+(r)\left(\frac{d^2}{dr^2} + k^2 - U(r)\right)\phi_k(r). \tag{87}$$

We begin by noting that apart from a kinematic factor it is the partial wave form of the on–shell post version of the scattering amplitude defined by Eq. (41) in a one-dimensional case. Making use of Eq.(80) it is straightforward to derive

$$t_R(k) = \frac{1}{k}[\psi_k^+(R)\phi_k'(R) - \phi_k(R)\psi_k^{+\prime}(R)]. \tag{88}$$

This is essentially the analogue of the surface integral form (61) for a volume integral of dimensionality one. It is then straightforward to use the asymptotic forms to deduce that

$$t(k) = \lim_{R\to\infty} t_R(k) = e^{\mathrm{i}\delta}\sin\delta. \tag{89}$$

There has been considerable testing of the method for ionization in the Temkin–Poet model [39–41] where there are several approaches that have provided converged results [48–53]. The ECS approach has demonstrated it can compute with high accuracy across the full range of electron impact energies. The method has been successfully applied to the full problem for ionization [1] as well as discrete scattering [54]. A useful variant of the approach called the propagating ECS method (PECS) [3, 55] has been applied to the near threshold ionization region for the full problem and essential elements of the interesting threshold effects predicted by Wannier [56] have been confirmed [3, 54, 57].

Because the method is so computationally intensive there has been relatively little work carried out beyond the three–body problem. The method has been applied to four–body problems only in the context of an extended Temkin–Poet model [58–61].

3.2. Time-dependent close-coupling

Similarly to ECS method the time-dependent close-coupling (TDCS) is a direct approach to the solution of the three-body Schrödinger equation which allows to circumvent the difficulties associated with formulating the correct asymptotic boundary conditions. This, however, is conducted in the time domain [11, 62–64],

$$i\frac{\partial\Psi(x_1,x_2,t)}{\partial t} = H(\boldsymbol{r}_1,\boldsymbol{r}_2)\Psi(x_1,x_2,t), \tag{90}$$

where the symbol $x = (\boldsymbol{r}, s)$ stands for the combined space $\boldsymbol{r}$ and spin s coordinates. The total Hamiltonian for electron scattering from hydrogen is

given by

$$H = K_1 + K_2 - \frac{1}{r_1} - \frac{1}{r_2} + -\frac{1}{|\boldsymbol{r}_1 - \boldsymbol{r}_2|}. \tag{91}$$

The total wave function is expand in coupled spherical harmonics

$$\Psi(x_1, x_2, t) = \sum_{Sl_1,l_2} \frac{1}{r_1 r_2} P^{LS}_{l_1 l_2}(r_1, r_2, t) Y^L_{l_1 l_2}(\hat{\boldsymbol{r}}_1, \hat{\boldsymbol{r}}_2) \chi^S_{\frac{1}{2}\frac{1}{2}} \tag{92}$$

where L and S are the total orbital and spin angular momentum. The coupled spherical harmonic is given by

$$Y^L_{l_1 l_2}(\hat{\boldsymbol{r}}_1, \hat{\boldsymbol{r}}_2) = \sum_{m_1 m_2} C^{l_1 l_2 L}_{m_1 m_2 0} Y_{l_1 m_1}(\hat{\boldsymbol{r}}_1) Y_{l_2 m_2}(\hat{\boldsymbol{r}}_2), \tag{93}$$

where $C^{l_1 l_2 L}_{m_1 m_2 0}$ is a Clebsh-Gordan coefficient, and $Y_{lm}(\hat{\boldsymbol{r}})$ is a spherical harmonic. The coupled two-electron spin wave function $\chi^S_{\frac{1}{2}\frac{1}{2}}$ is defined similarly to (93). Substitution of the expansion (92) into time-dependent Schrödinger equation (90) and projection onto coupled spherical harmonics and spin wave functions leads to a set of coupled partial differential equations for each target symmetry

$$i\frac{\partial P^{LS}_{l_1 l_2}(r_1, r_2, t)}{\partial t} = T_{l_1 l_2}(r_1, r_2) P^{LS}_{l_1 l_2}(r_1, r_2, t) + \sum_{l'_1 l'_2} U^L_{l_1 l_2, l'_1 l'_2} P^{LS}_{l'_1 l'_2}(r_1, r_2, t), \tag{94}$$

where $T_{l_1 l_2}(r_1, r_2)$ contains all one-electron operators and $U^L_{l_1 l_2, l'_1 l'_2}(r_1, r_2)$ contains the electron-electron interaction.

The set of coupled equations (94) can be written as

$$i\frac{\partial \boldsymbol{P}^{LS}}{\partial t} = \boldsymbol{H}^L \boldsymbol{P}^{LS}, \tag{95}$$

where the dimension of vector $\boldsymbol{P}^{LS}$ is equal to the number of $l_1 l_2$ pairs. Each vector component P^{LS}_i is represented on a two-dimensional lattice as an array of dimension $\bar{N}$. Similarly, the matrix $\boldsymbol{H}^L$ has dimensions of $N \times N$, and each of its components is an array of dimension $\bar{N} \times \bar{N}$. As matrix $\boldsymbol{H}^L$ is time independent the time evolution of the radial wave functions is given simply by

$$\boldsymbol{P}^{LS}(t + \Delta t) = \exp(-i\boldsymbol{H}^L \Delta t) \boldsymbol{P}^{LS}(t). \tag{96}$$

Choosing the time step Δt sufficient;y small the radial wave function can be propagated in time [62, 63]. This allows to obtain a lattice representation of the radial wave function.

At time $t = 0$ the wave function is constructed as

$$P^{LS}_{l_1 l_2}(r_1, r_2, t = 0) = \frac{1}{\sqrt{2}} \left(G_{k_1 l_1}(r_1) P_{1s}(r_2) + (-1)^S \delta_{0,l_1} G_{k_2 l_2}(r_2) P_{1s}(r_1), \right) \tag{97}$$

where $G_{kl}(r)$ is a radial wave-packet for linear momentum k [63]. At an appropriate time $t = T$ after the collision, when only an outgoing wave is present for each reaction channel, the ionization scattering amplitude is simply defined as the overlap between two Coulomb waves and the calculated two-electron wave function,

$$f^{(S)}(\boldsymbol{q}_1, \boldsymbol{q}_2) = \langle \boldsymbol{q}_1^{(-)} \boldsymbol{q}_2^{(-)} \chi^S_{\frac{1}{2}\frac{1}{2}} | \Psi(t = T) \rangle. \tag{98}$$

We cannot offer a formal proof as to why Eq. (98) should yield the correct ionization amplitude. It is clear that the projection by the two non-interacting Coulomb waves eliminates any orthogonal components in the total wavefunction. We suppose that Eq. (98) is a good approximation to the standard interpretation in terms of a probability amplitude of finding the system in a state with the electrons having the desired momenta. The TDCS method was successfully applied to the calculation of fully-differential cross sections for electron impact ionization of hydrogen [11, 64] and helium [65, 66] atoms.

3.3. Convergent close-coupling

The convergent close-coupling (CCC) method is a technique for treating a projectile-target collision problem. The aim is to solve such systems at any collision energy for the major scattering and ionization processes. Initially, the method was implemented for the simplest well-studied Coulomb three-body problem of electron scattering on atomic hydrogen for excitation [42] and total ionization [43]. A few years later it was shown to work for fully differential ionization as well [5]. The technique has been generalised to other projectiles, including photons [67], positrons [68, 69], and more recently to heavy projectiles such as antiprotons [70].

The fundamental strength of the method is the rigorous treatment of the atomic target countably infinite discrete spectrum and its uncountably

infinite continuum in the evaluation of collision data. Specifically, the target spectrum is expanded using a complete Laguerre basis

$$\xi_{kl}(r) = \left(\frac{\lambda_l (k-1)!}{(2l+1+k)!}\right)^{1/2} (\lambda_l r)^{l+1} \exp(-\lambda_l r/2) L_{k-1}^{2l+2}(\lambda_l r), \qquad (99)$$

where the $L_{k-1}^{2l+2}(\lambda_l r)$ are the associated Laguerre polynomials, and k ranges from 1 to the basis size N_l. This ensures that with increasing basis size the negative-energy states converge to the true eigenstates $|\phi_n\rangle$, while the positive-energy states provide for an increasingly dense discretisation of the continuum. Most importantly, the summation over all of the square-integrable Laguerre-based target states provides a quadrature rule for the summation and integration over the true target discrete and continuous eigenstates [71]. Specifically, we write

$$I = \sum\!\!\!\!\!\!\int_n |\phi_n\rangle\langle\phi_n| = \lim_{N\to\infty} \sum_{n=1}^{N} |\phi_n^{(N)}\rangle\langle\phi_n^{(N)}| \equiv \lim_{N\to\infty} I^{(N)}. \qquad (100)$$

The target states are typically obtained by diagonalising the target Hamiltonian $H_{\rm T}$ to yeild

$$\langle\phi_f^{(N)}|H_{\rm T}|\phi_i^{(N)}\rangle = \epsilon_f^{(N)}\delta_{fi}. \qquad (101)$$

Another alternative is to generate Box-based eigenstates by generating a discrete set of states $\phi_n^{(R_0)}(r)$ which are zero at a specified value of $r = R_0$, and then set to be zero for $r > R_0$. Being eigenstates they also satisfy Eq. (101), and so may readily be used in the CCC formalism instead of the Laguerre-based states [72]. Increasing R_0 allows for more discrete eigenstates to fit in the box and increases the density of positive-energy states. Whereas in the Laguerre basis the maximum number of states for each l is N_l, in the box-basis case there is no relation between N_l and R_0. For any specified R_0 we can take as many N_l as we like.

The target states are used to expand the total wavefunction $|\Psi_i^{(+)}\rangle$ of the projectile-atom scattering system, i.e.

$$\begin{aligned} 0 = (E-H)|\Psi_i^{(+)}\rangle &\approx (E-H) I^{(N)} |\Psi_i^{(+)}\rangle \\ &= (E-H) \sum_{n=1}^{N} |\phi_n^{(N)} f_{ni}^{(N+)}\rangle \\ &\equiv (E-H)|\Psi_i^{(N+)}\rangle, \end{aligned} \qquad (102)$$

where E and H are the total energy and Hamiltonian, respectively. The unknown one-electron functions $f_{ni}^{(N+)}(r)$ are to be determined from solution of the resulting close-coupling equations. The key idea here is that with increasing N the expansion approaches the identity operator I.

The close-coupling equations can be written in several forms, as discussed above, all of which should yield identical results if the same states $|\phi_n^{(N)}\rangle$ are used in the expansion. In the CCC method the equations take the form of coupled Lippmann-Schwinger equations for the transition amplitude

$$\begin{aligned}\langle \boldsymbol{k}_f \phi_f^{(N)} | T | \phi_i^{(N)} \boldsymbol{k}_i \rangle &= \langle \boldsymbol{k}_f \phi_f^{(N)} | V | \phi_i^{(N)} \boldsymbol{k}_i \rangle \\ &\quad + \sum_{n=1}^{N} \int d^3k \frac{\langle \boldsymbol{k}_f \phi_f^{(N)} | V | \phi_n^{(N)} \boldsymbol{k} \rangle \langle \boldsymbol{k} \phi_n^{(N)} | T | \phi_i^{(N)} \boldsymbol{k}_i \rangle}{E + i0 - \epsilon_n^{(N)} - k^2/2} \end{aligned} \tag{103}$$

where $E = \epsilon_i + k_i^2$ for projectile of incident momentum $\boldsymbol{k}_i$ on the initial target state of energy ϵ_i. The operator V contains all particle interactions, as well as ensuring the required symmetry properties for the total wavefunction [42].

Without loss of generality in the following we proceed by ignoring symmetrisation parts of V and write

$$\begin{aligned} H &= H_{\rm asym} + V \\ &= H_{\rm T} + K_0 + V, \end{aligned} \tag{104}$$

where the asymptotic Hamitonian is a combination of the target Hamiltonian and the projectile kinetic energy operator K_0. The transition amplitudes are then

$$\begin{aligned}\langle \boldsymbol{k}_f \phi_f^{(N)} | T | \phi_i^{(N)} \boldsymbol{k}_i \rangle &= \langle \boldsymbol{k}_f \phi_f^{(N)} | \overleftarrow{H} - E | \Psi_i^{(N+)} \rangle \\ &= \langle \boldsymbol{k}_f \phi_f^{(N)} | V | \Psi_i^{(N+)} \rangle \end{aligned} \tag{105}$$

for $\epsilon_f^{(N)} < E$, i.e. all open states. For negative-energy final eigenstates these are the required scattering amplitudes. In the case of ionization we start with Eq.(47)

$$\begin{aligned}\langle \Phi_0^- | \overleftarrow{H} - E | \Psi_i^{(+)} \rangle &\approx \langle \Phi_f | I^{(N)} (\overleftarrow{H} - E) I^{(N)} | \Psi_i^{(+)} \rangle \\ &= \langle \boldsymbol{k}_f \boldsymbol{q}_f^{(-)} | I^{(N)} (\overleftarrow{H} - E) | \Psi_i^{(N+)} \rangle \\ &= \sum_{n=1}^{N} \langle \boldsymbol{q}_f^{(-)} | \phi_n^{(N)} \rangle \langle \boldsymbol{k}_f \phi_n^{(N)} | (\overleftarrow{H} - E) | \Psi_i^{(N+)} \rangle \\ &= \langle \boldsymbol{q}_f^{(-)} | \phi_f^{(N)} \rangle \langle \boldsymbol{k}_f \phi_f^{(N)} | V | \Psi_i^{(N+)} \rangle, \quad \text{for } q_f^2/2 = \epsilon_n^{(N)}, \end{aligned} \tag{106}$$

$$
\begin{aligned}
&= \langle \boldsymbol{q}_f^{(-)} | \phi_f^{(N)} \rangle \langle \boldsymbol{k}_f \phi_f^{(N)} | T | \phi_i \boldsymbol{k}_i \rangle \\
&\equiv f_i^{(N)}(\boldsymbol{q}_f, \boldsymbol{k}_f),
\end{aligned} \tag{107}
$$

where we set $\langle \Phi_f | = \langle \boldsymbol{k}_f \boldsymbol{q}_f^{(-)} |$ because in the close-coupling approximation asymptotically the projectile electron $\langle \boldsymbol{k}_f |$ is always a plane wave due to being shielded by the square-integrable target states, ensuring the other electron being a pure Coulomb wave $\langle \boldsymbol{q}_f^{(-)} |$. The summation in (106) only disappears whenever $q_f^2/2 = \epsilon_n^{(N)}$ for some n, as then $\langle \boldsymbol{q}_f^{(-)} | \phi_n^{(N)} \rangle = \delta_{fn} \langle \boldsymbol{q}_f^{(-)} | \phi_f^{(N)} \rangle$. In practice, we evaluate (107) at all values of f and interpolate onto the experimental values. Note that Bray and Fursa [73] derived (107) without knowing the origin of (47), and that there is a pure Coulomb phase associated only with the electron of momentum $\boldsymbol{q}_f$.

Thus we have a very simple way of generating the ionization amplitudes from the close-coupling formalism. We just take the amplitudes for excitation of the positive-energy states, and multiply them by the given overlap, which may be seen as restoring the continuum normalisation. The first attempt at applying the close-coupling formalism to ionization, by Curran and Walters [74], which was followed by Bray et al. [75], had the perspective of using the close-coupling expansion to reconstruct the total wavefunction. This runs into problems when the channel functions are not consistent with the close-coupling expansion leading to non-existent matrix elements. For this reason we abandoned such an approach and developed the one above, which turned out to be much simpler and internally consistent.

3.4. R-matrix with pseudo-states

Application of the R-matrix method to electron scattering from atoms was originally aimed to study low energy processes [76, 77]. The approach starts with the multichannel expansion of the total wave function

$$
\Psi(x_1, ..., x_{M+1}) = \mathcal{A} \sum_i^N \phi_i(x_1, ..., x_M) F_i + \sum_j c_j \xi_j(x_1, ..., x_{M+1}). \tag{108}
$$

Here M is the number of electrons in the target atom, $\phi_i(x_1, ..., x_M)$ are the target wave functions, F_i are corresponding channel functions, and N is number of the target states included in the close-coupling expansion. The $\xi(x_1, ..., x_{M+1})$ are short-ranged functions describing the important correlations that may be missing in the first term of (108).

Substitution of the expansion (108) into the Schrödinger equation, and projecting on target states ϕ_i and correlation functions ξ_j, leads to formulation of a set of close-coupling integro-differential equations for the channel functions

$$\left(\frac{d^2}{dr^2} - \frac{l_i(li+1)}{r_2} + \frac{2Z}{r} + k_i^2\right) F_i(r) = \sum_j (V_{ij} + W_{ij}) F_j(r), \tag{109}$$

where V_{ij} represents a local direct potential and W_{ij} represents a non-local exchange and correlation potential.

The R-matrix method offers an efficient way of solution of the set of close-coupling equations (109). It makes use of a separate treatment of two regions; in the inner region ($0 < r < a$) interaction between target and projectile electrons is accounted for without approximations while in the outer region ($r > a$) only the direct interaction is retained. Solution of Eq. (109) in the outer region can be obtained relatively easily [78]. Matching solution in the inner and outer region at the boundary $r = a$ allows to obtain the scattering information. For n_a open channels, functions F_{ij} have the following asymptotic form

$$F_{ij}(r) \underset{r\to\infty}{\sim} k_i^{-1/2}(\mathcal{F}_i + \mathcal{G}_i K_{ij}),\ i,j = 1,...,n_a. \tag{110}$$

Here $\mathcal{F}_i$ and $\mathcal{G}_i$ are regular and irregular Riccarti-Bessel functions, respectively, and K_{ij} is the reaction K-matrix.

In the inner region the solution of the Schrödinger equation for the total wave function at energy E is sought as an expansion in an energy-independent basis set

$$\Psi_E = \sum_k A_{Ek} \Psi_k. \tag{111}$$

The basis set Ψ_k is constructed as

$$\Psi_k(x_1,...,x_{M+1}) = \mathcal{A} \sum_{ij} \phi_i(x_1,...,x_M) u_j(x_{M+1}) a_{ijk} + \sum_j \xi_j(x_1,...,x_{M+1}) b_{jk}, \tag{112}$$

where u_j are continuum functions describing the projectile electron. A discrete set of such functions at energies e_j is obtained as solutions of single-particle Schrödinger equation that satisfy the logarithmic derivative boundary condition at the R-matrix boundary

$$\left.\frac{a}{u_j}\frac{du_j}{dr}\right|_{r=a} = b, \tag{113}$$

where b is an arbitrary constant. Coefficients a_{ijk}, b_{jk} as well as associated energies E_k are determined by diagonalizing the total projectile and target electron Hamiltonian

$$\langle \Psi_k | H | \Psi_n \rangle = E_k \delta_{kn}. \tag{114}$$

Following the standard R-matrix formulation, we define

$$F_{ik}(r) = \sum_j u_j(r) a_{ijk} \tag{115}$$

Then the radial function describing the projectile electron in channel i at energy E is

$$F_i = \sum_k A_{Ek} F_{ik}. \tag{116}$$

One can show that coefficients A_{Ek} can be expressed as [76]

$$A_{Ek} = \frac{1}{2a(E_k - E)} \sum_i F_{ik} \left(a \frac{dF_i}{dr} - bF_i \right)_{|r=a}. \tag{117}$$

In order to obtain the reaction K-matrix the matching at the R-matrix boundary $r = a$ is performed by substituting the asymptotic form (110) into left and right-hand sides of Eq. (116). If the R-matrix radius a is not in the asymptotic region for the potential V_{ij} the set of linear independent fundamental solutions of Eq. (109) have to be used instead of Riccarti-Bessel functions $\mathcal{F}_i$ and $\mathcal{G}_i$. This leads to a system of linear equations for reaction K-matrix, and when solved the K, S, and T-matrix for excitation of various target states become available.

Computationally, the most demanding step in the R-matrix method is the setting up of the Hamiltonian matrix (114) and its digonalization. The size of the Hamiltonian matrix grows rapidly with the increase of the R-matrix radius a, maximum collision energy of interest, and number of target states included in the close-coupling expansion. Traditionally the R-matrix method was applied at collision energies below the ionization threshold. However, with the substantial growth of computational resources over last two decades the target state expansion in Eq. (112) can be expanded to include a large number of target pseudo-states [7–9]. Such a modification of the R-matrix method allowed its application at energies above the ionization threshold, and it became known as the R-matrix with pseudo-states method. As in the CCC method, it makes use of a square-integrable representation of the

target atom continuum, and yields the scattering T-matrix for excitation of the positive-energy pseudo-states.

As soon as the transition amplitudes $\langle \boldsymbol{k}_f \phi_f^{(N)} | T | \phi_i^{(N)} \boldsymbol{k}_i \rangle$ for a set of positive-energy pseudo-states are known the calculation of the ionization amplitudes can proceed in the same way as for the CCC method, see Eq. (107). However, Zatsarinny and Bartschat [10] suggested the following modification to the Eq. (106),

$$\begin{aligned} \langle \Phi_0^- | \overleftarrow{H} - E | \Psi_i^{(+)} \rangle &\equiv \sum_{n=1}^{N} \langle \boldsymbol{q}_f^{(-)} | \phi_n^{(N)} \rangle \langle \boldsymbol{k}_f \phi_n^{(N)} | T | \phi_i \boldsymbol{k}_i \rangle \\ &\approx \sum_{n=1}^{N} \langle \boldsymbol{q}_f^{(-)} | \phi_n^{(N)} \rangle \langle \boldsymbol{k}_n \phi_n^{(N)} | T | \phi_i \boldsymbol{k}_i \rangle. \end{aligned} \tag{118}$$

Here $\boldsymbol{q}_f^{(-)}$ is a true continuum wave function of the target atom at energy $q_f^2/2 = E - k_f^2/2$ obtained as a result of a solution of electron scattering on the corresponding positively charged ion. Note that the replacement of $\boldsymbol{k}_f$ to $\boldsymbol{k}_n$ in the T-matrix on the right-hand side of Eq. (118) produces an on-shell T-matrix that is available from the performed scattering calculation. At this moment we cannot provide any formal justification for this ansatz (118). We note, however, that for the first time very good agreement with experiment for e-He (e,2e) processes where the residual He^+ ion is left in excited states (2s+2p) was able to be obtained [10], see Sec. 4.2.4 for more detail.

3.5. Integro-differential close-coupling

The integro-differential close-coupling (IDCC) [74] represents a standard formulation of the close-coupling method, which pioneered the application to ionization calculations. The method starts with a multichannel expansion of the total wave function and formulates a set of close-coupling integro-differential equations (109) for the channel functions. These equations are solved in coordinate space. The definition of ionization amplitude for the e-H system that was adopted by Curran and Walters [74] can be thought of as starting again with Eq. (47)

$$\begin{aligned} \langle \Phi_0^- | \overleftarrow{H} - E | \Psi_i^{(+)} \rangle &\approx \langle \boldsymbol{q}_1^{(-)} \boldsymbol{q}_2^{(-)} | (\overleftarrow{H} - E) I^{(N)} | \Psi_i^{(+)} \rangle \\ &= \langle \boldsymbol{q}_1^{(-)} \boldsymbol{q}_2^{(-)} | (\overleftarrow{H} - E) | \Psi_i^{(N+)} \rangle. \end{aligned} \tag{119}$$

Note that the target state projection operator $I^{(N)}$ appears only once on the right-hand side of Eq. (119). This leads to an approximation of the total wave

function $\Psi_i^{(+)}$ by the close-coupling solution $\Psi_i^{(N+)}$. The asymptotic final state is chosen as a product of two Coulomb waves $\boldsymbol{q}_1^{(-)}$ and $\boldsymbol{q}_2^{(-)}$ calculated for charges z_1 and z_2 that satisfy the condition [79]

$$\frac{z_1}{q_1} + \frac{z_2}{q_2} = \frac{1}{q_1} + \frac{1}{q_2} - \frac{1}{|\boldsymbol{q}_1 - \boldsymbol{q}_2|} \tag{120}$$

The choice of the asymptotic final state is arbitrary in case of exact total wave function $\Psi_i^{(+)}$, but for the approximate solution $\Psi_i^{(N+)}$ it is more crucial. For the case of asymmetric energy sharing ($q_1 \gg q_2$) considered by Curran and Walters [74] the most important physics can be accounted for by choosing projectile electron to be described by a plane wave ($z_1 = 0$, $\boldsymbol{k}_1 \equiv \boldsymbol{q}_1$) and ejected electron as a Coulomb wave ($z_2 = 1$). Note that condition (120) is satisfied only approximately in this case. The expression for the ionization amplitude can now be written as

$$\langle \boldsymbol{k}_1 \boldsymbol{q}_2^{(-)}| \left(-\frac{1}{r} + \frac{1}{r_{12}} \right) (1 + (-1)^S P_{12}) \sum_n |f_n^{(N+)}(\boldsymbol{r}_1)\phi_n^{(N)}(\boldsymbol{r}_2)\rangle, \tag{121}$$

where we have substituted close-coupling expansion for the $\Psi_i^{(N+)}$ and P_{12} is a space exchange operator. The ionization amplitude (121) is commonly separated into the direct and exchange terms.

With channel functions known from the solution of close-coupling equations Curran and Walters [74] have evaluated integrals in (121) numerically. Note that for the exchange amplitude such direct evaluation of matrix element leads to the direct overlap of two continuum functions that generally does not converge, though Curran and Walters [74] suggested a work-around for this problem. It is these issues, also faced by Bray et al. [75] utilising the CCC method, that lead to the reassessment of how to apply the close-coupling method to ionization problems [73].

4. Electron-impact ionization

4.1. Hydrogen

4.1.1. S-wave model

Before engaging in comparison with experiment it is instructive to consider the consequences of using a square-integrable basis on calculating break-up processes. The S-wave model that restricts the collision problem to just

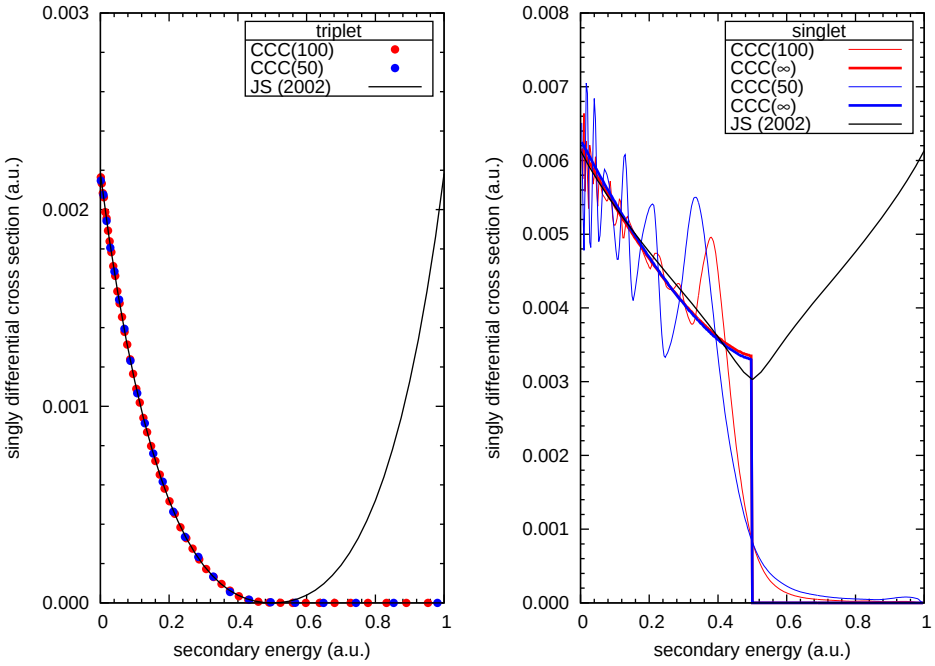

Figure 1: (Colour online) Singly differential cross sections calculated using the CCC method with 100 and 50 Laguerre-based functions, see text. Comparison is given with the benchmark results of Jones and Stelbovics [50]. In the singlet case, the estimates labeled CCC(∞) are derived from the corresponding calculations, see text.

states of zero orbital angular momentum is ideal for this. In the case of e-H scattering this is often referred to as the Temkin-Poet model due to their provision of benchmark results for the problem [39, 40]. It was originally used to validate the convergence of the CCC method to the correct results [4] for elastic and discrete excitation processes. It is also an ideal model for understanding how the close-coupling formalism may be applied to ionization processes due to the availability of highly accurate results for these processes too [50].

In figure 1 we present the singly differential cross sections (SDCS) for 40.8 eV (1.5 a.u.) electrons incident on the ground state of atomic hydrogen ($\epsilon_i = -0.5$ a.u., hence E=1 a.u.), calculated using the CCC(N) method within the S-wave model. The conversion of the cross sections for positive-energy states to the SDCS is given by Bray and Fursa [80]. Basically, for total spin S the total ionization cross section $\sigma_{\rm I}^{(S)}$ is the integral from 0 to total

energy E, which is also the sum of cross sections for all open positive-energy states. Beginning with the triplet case, the dots represent the individual cross sections of the positive-energy states for the two Laguerre bases. We see that there is excellent agreement with the benchmark calculations of Jones and Stelbovics [50], but only on the interval $[0, E/2]$. Due to the identical nature of the two electrons we would expect the SDCS to be symmetric about $E/2 = 0.5$ a.u.. However, in a unitary theory like CCC yielding symmetric SDCS would effectively double-count the ionization processes, and so the formalism yields near-zero cross sections for those states whose energy is greater than $E/2$. In other words, the formalism attempts to enforce the integration to end at $E/2$, as would be expected for identical electrons. This has a reasonable physical interpretation. The usage of the Laguerre basis ensures that the target-space electron is always bound and shields the scattered electron. For target electron energies $\epsilon_n^{(N)} < E/2$ this makes physical sense, i.e. we have the slow electron shielding the fast one. However for $\epsilon_n^{(N)} > E/2$ we have the unphysical case of the fast electron shielding the slow one, and it is somewhat satisfying that such cases yield near-zero cross sections.

Turning now to the singlet case, we see an even more interesting situation. Rather than presenting the CCC results with dots at the secondary energies $0 \leq \epsilon_n^{(N)} \leq E$, we connect the results with lines to ensure the nature of the oscillations is clearly visible. We see that the cross sections are non-zero predominantly for $0 \leq \epsilon_n^{(N)} \leq E/2$, and near zero elsewhere. The larger calculation has smaller oscillations which are around the benchmark provided by Jones and Stelbovics [50]. When such oscillations were first identified the suggestion was made that convergence should be to a step-function [81]. Further analysis by Stelbovics [82] suggested that solving the close-coupling equations for the complex amplitudes was in effect like taking a Fourier expansion of a complex function that had a step at $E/2$. Owing to the size of the step being zero in the triplet case (Pauli Principle ensures zero cross section at $E/2$) the results remain smooth. In the single case, the size of the step is non-zero and so the convergence of the amplitudes is to half the step height, or a quarter for the cross sections. The two curves, labeled CCC(∞) were derived from the two CCC calculations while preserving the integral and utilising the cross section at $E/2$. We see very good agreement with the results of [50]. It does not matter whether the method of solution of the close-coupling equations is with the use of the R-matrix technique [83] or the J-matrix method [53], the same analysis applies.

The vital conclusion that we draw from the study of the S-wave model is that the apparent conflict with formal scattering theory can be resolved. Specifically, the physical ionization amplitudes come only from the region of $0 \leq \epsilon_n^{(N)} \leq E/2$. Hence there is no double counting of the ionization processes in the unitary CCC theory, though a little care needs to be taken for the equal energy-sharing case.

All full applications of the close-coupling method to break-up processes are affected by the above analysis. In particular, Stelbovics [82] noted that the required ionisation amplitude $F_S^{(N)}(\boldsymbol{q}, \boldsymbol{k})$ is defined as

$$F_S^{(N)}(\boldsymbol{q}, \boldsymbol{k}) = f_S^{(N)}(\boldsymbol{q}, \boldsymbol{k}) + (-1)^S f_S^{(N)}(\boldsymbol{k}, \boldsymbol{q}), \tag{122}$$

but only if $f_S^{(N)}(\boldsymbol{q}, \boldsymbol{k})$ (see Eq. (107)) is zero for $q > k$, i.e. if the step function is satisfied to sufficient numerical precision. Subsequently, for $k = q$ it was found that $f_S^{(N)}(\boldsymbol{q}, \boldsymbol{k}) \approx (-1)^S f_S^{(N)}(\boldsymbol{k}, \boldsymbol{q})$ holds, so that

$$2\left(|f_S^{(N)}(\boldsymbol{q}, \boldsymbol{k})|^2 + |f_S^{(N)}(\boldsymbol{k}, \boldsymbol{q})|^2\right) \approx |f_S^{(N)}(\boldsymbol{q}, \boldsymbol{k}) + (-1)^S f_S^{(N)}(\boldsymbol{k}, \boldsymbol{q})|^2, \tag{123}$$

see Eq. (15) of Bray [84]. Thus in CCC calculations the equal energy-sharing amplitudes arise entirely ab initio. However, the asymmetric amplitudes will show minor oscillations that may be eliminated with the aid of a smooth $N = \infty$ estimate of the SDCS, as was obtained in Fig. 1.

Before we look at fully differential cross sections at various energies it is important to establish the accuracy of the method for the total ionization cross section at all energies of interest. This is presented in Fig. 2. It was the outstanding agreement between the CCC theory and experiment for total ionization, without any double-counting problems, that lead to our extension of the CCC method to fully differential ionization processes.

4.1.2. Low energies

We now turn to full calculations of e-H ionization, starting with the low energies, while restricting our discussion to primarily fully differential cross sections. Atomic hydrogen is the ideal testing ground for electron-impact excitation and ionization theories. Unfortunately, the experimental difficulties of creating a beam of atomic hydrogen suitable for collision studies are quite substantial, as is putting the measured data onto an absolute scale [86]. This typically leads to larger experimental uncertainties for e-H ionisation as compared to say to the e-He case, and is particularly a problem at low energies where the cross sections are small.

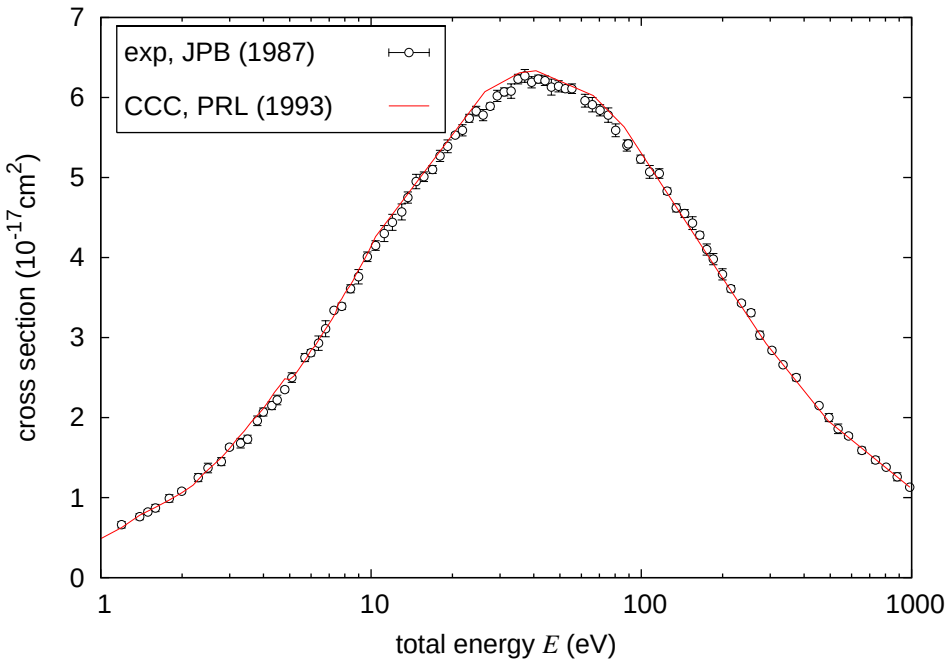

Figure 2: Total electron-impact ionization cross section of the ground state of atomic hydrogen. Experiment is due to Shah et al. [85] and the CCC results are from Bray and Stelbovics [43].

As far as we are aware detailed fully differential cross sections, whose geometries are summarized in figure 3, for e-H ionization are only available for incident energies of 15.6 eV [86, 87], 17.6 eV [87, 88], 20 eV, 25 eV, 30 eV [89, 90], 27.2 eV [91], 54.4 eV [92] and 150 eV [93]. The first five energies have data for equal energy-sharing, while the latter two, as well as at 27.2 eV, have asymmetric energy sharing data. Only the data at 15.6 eV, 17.6 eV, 54.4 eV and 150 eV have been put on the absolute scale. All data are for the coplanar geometry ($\psi = 0°$ in figure 3). Note that doubly differential ionization cross sections (the equivalent of excitation differential cross sections) are also available [94].

There have been many theories applied to fully differential ionization at the lowest energy case[1] of 15.6 eV. Though one would expect only non-perturbative approaches to work well here we have some first order theories

[1]There is the single geometry of $\theta_{AB} = 180°$ available at 14.6 eV [86]

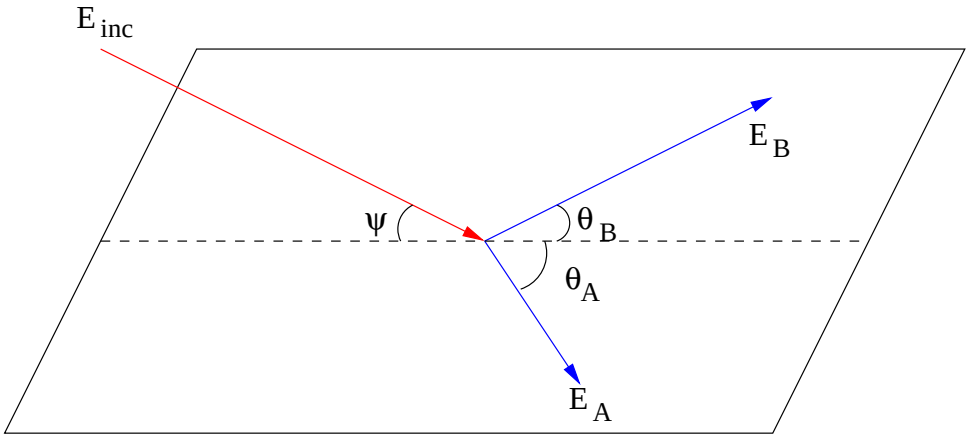

Figure 3: Parametrization of electron-impact single ionization fully differential cross sections. An electron of energy $E_{\rm inc}$ is incident at an angle ψ relative to the plane formed by the two outgoing electrons of energies E_A and E_B.

capturing much of the electron-electron correlations, see for example Jones et al. [95] and references therein. However, a fully quantitative agreement can only be obtained utilising non-perturbative approaches such as ECS, TDCC, and CCC. The excellent agreement between these three theories in both shape and magnitude is demonstrated in Fig. 4. Though we note that the demonstrated quantitative agreement is only possible when experimental mean values, which have an uncertainty of 35%, are divided by two. This requirement was identified quite early, even when the full understanding of the CCC method had not yet emerged [96].

It is quite remarkable to see such good agreement between the ECS, TDCC and CCC calculations for all of the geometries presented in figure 4. There are three distinct geometries presented which are slices in the three-dimensional surface that is a function of the scattering angles θ_A and θ_B. The symmetric geometry ($\theta_A = -\theta_B$) has the detectors on the opposite sides of the incident beam. It is particularly helpful in checking the accuracy of the CCC calculations by checking how close to zero the cross sections are when the two electrons go out together in the forward or backward angles. Such cross sections can only come out to be small through the destructive interference of the underlying partial-wave scattering amplitudes. This requires sufficiently large target-space orbital angular momentum l. Presently, we took $l \leq l_{\rm max} = 6$, with $N_l = 70 - l$ and $\lambda_l = 2$, while keeping all open and a few closed states. The fixed-θ_A geometries provide for a set of

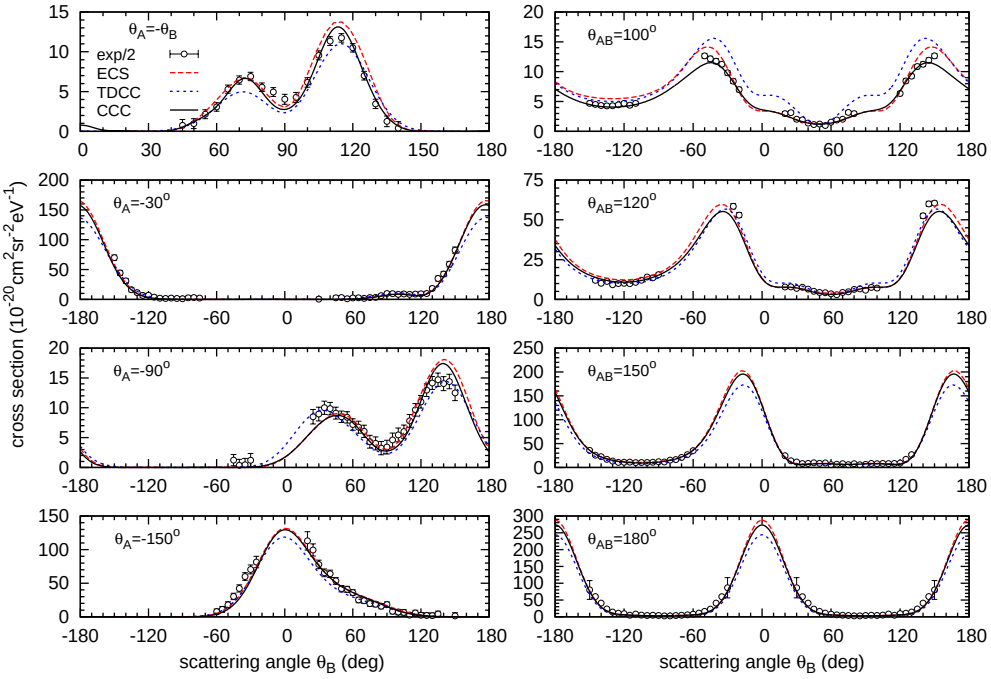

Figure 4: Coplanar fully differential cross sections for 15.6 eV electrons incident on the ground state of atomic hydrogen with 1 eV outgoing electrons. The exterior complex scaling (ECS) results are due to Baertschy et al. [2]. The time-dependent close-coupling (TDCC) results are due to Colgan and Pindzola [11]. The Laguerre-based CCC calculations are described in the text. The absolute experimental values, with an uncertainty of 35%, due to Röder et al. [86], have been divided by two for best visual fit to theory.

systematic slices through the cross section surface. As with the symmetric geometry, we expect near zero cross sections whenever $\theta_A \approx \theta_B$. Lastly, the fixed-$\theta_{AB} = \theta_B - \theta_A$ geometries are very useful for seeing quantitatively the effect of electron-electron correlation in the final state. For the smaller θ_{AB} we expect generally smaller cross sections. The maximal values of the cross sections arise in the Wannier geometry of $\theta_{AB} = 180°$. Note how the maxima only arise when one of the electrons is scattered into the forward direction.

It is our contention that the 15.6 eV case is sufficient to demonstrate that the ECS, TDCC, and CCC theories are able to solve the e-H ionization problem at any energy. However, having to divide the experimental values by two has to be of some concern, even when the stated absolute uncertainty is 35%. We therefore turn to the 17.6 eV case, the next energy at which absolute data are available. In this case there was some problem with internal consistency of the measured data, but this was resolved in the final presentation by Röder et al. [88]. Colgan and Pindzola [11] have already shown excellent agreement between the ECS, TDCC and CCC calculations at 17.6 eV. Following Röder et al. [88], they did not scale experiment by any factor, and found the theoretical results systematically a little lower than experiment. Keeping in mind that the absolute uncertainty is 40% [86], in figure 5 we divide the experiment by 1.4 for best overall visual fit to theory.

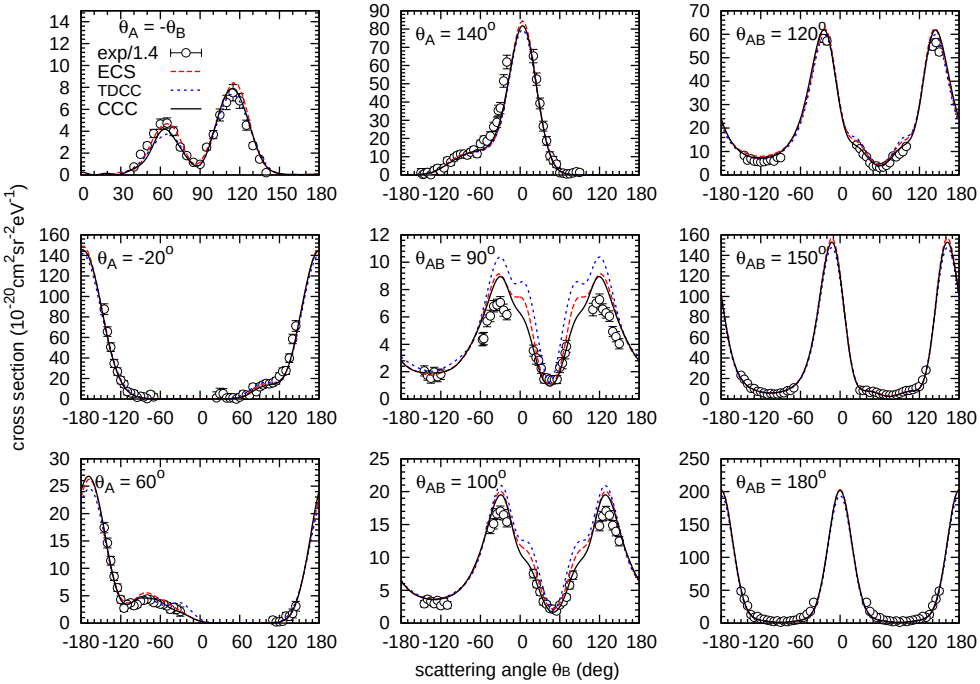

Figure 5: Coplanar fully differential cross sections for 17.6 eV electrons incident on the ground state of atomic hydrogen with 2 eV outgoing electrons. The ECS and TDCC results are as for Fig. 4. The CCC calculation is described in the text. The absolute experimental values, with an uncertainty of 40%, due to Röder et al. [88], have been divided by 1.4 for best visual fit to theory.

The present CCC calculations supersede those presented by Röder et al. [88]. We increased $l_{\max}$ from 5 to 7, while leaving $N_l = 50 - l$ and $\lambda_l = 2$. The effect of the increased $l_{\max}$ was to reduce the cross section at the forward scattering angles of the $\theta_A = -\theta_B$ geometry. The agreement demonstrated in figure 5 between theory and experiment is quite remarkable, and gives us further confidence that the ECS, TDCC and CCC theories are able to fully solve such ionization problems.

4.1.3. Intermediate energies

The 20, 25, and 30 eV electron-impact ionization data [89, 90] is for equal energy-sharing, and remains on a relative scale, but is internomalised across the various geometries, but not energy.

It is very instructive to compare the Laguerre-based (CCC-L) and Box-based (CCC-B) approaches to electron-atom ionization collision problems.

In the former, the extent of the radial functions depends on the combination of Laguerre basis N_l, the Laguerre exponential fall-off parameter λ_l, and the energy of the state. Roughly, the number of oscillations in all positive-energy states is the same, with the lower energy states therefore extending further in coordinate space. However, in CCC-B all positive energy states stop at $r = R_0$, with higher energy states having many more oscillations than the lower energy ones. The usage of $\lambda_l = \lambda$ allows for a systematic convergence study [97]. It was the varying of λ_l to avoid interpolation across the complex amplitudes that resulted in some of the discrepancies in the earlier applications of the CCC-L method [84].

One advantage of the CCC-B approach is that the positive target-state energies are linear in momentum, whereas they grow almost exponentially for CCC-L. This means that in the case of equal-energy sharing cases at the higher energies, CCC-B is a little more advantages by providing a more dense discretization around the required energy point. Accordingly, in Fig. 6 the CCC calculations are all performed in the CCC-B mode with all having $l_{\max} = 7$, $N_l = 25 - l$, but with R_0=90, 70, and 60 a.u. for the incident electron energies of 20, 25, and 30 eV, respectively. Comparison is given with experiment and the ECS calculations, with outstanding agreement found in all cases.

4.1.4. High energies

At the higher energies of 54.4 and 150 eV the experimental data is absolute, and is for asymmetric energy sharing. These two cases were the first to be considered when developing the CCC approach to ionization [75]. At that time we followed the approach of Curran and Walters [74], but ran into problems with non-existent integrals. The present implementation is much simpler, having no reconstruction of the total wavefunction, and derives the ionization amplitudes directly from the excitation amplitudes of the positive-energy pseudostates. At the time the 54.4 eV data was not available on the absolute scale, but it is now [98], and is presented in Fig. 7. Excellent agreement is found between experiment and the CCC calculations after the former have been uniformely divided by 0.8, which is well withing the experimental uncertainty of 35%. For interest, we ran the CCC calculations in the distorted-wave Born approximation (DWBA) mode (coupling excluded) which gives a qualitative account of the experimental observations. The same distorting potential (ground state) is used for the initial and final projectile space electrons, with the ejected electron treated via the positive-energy pseu-

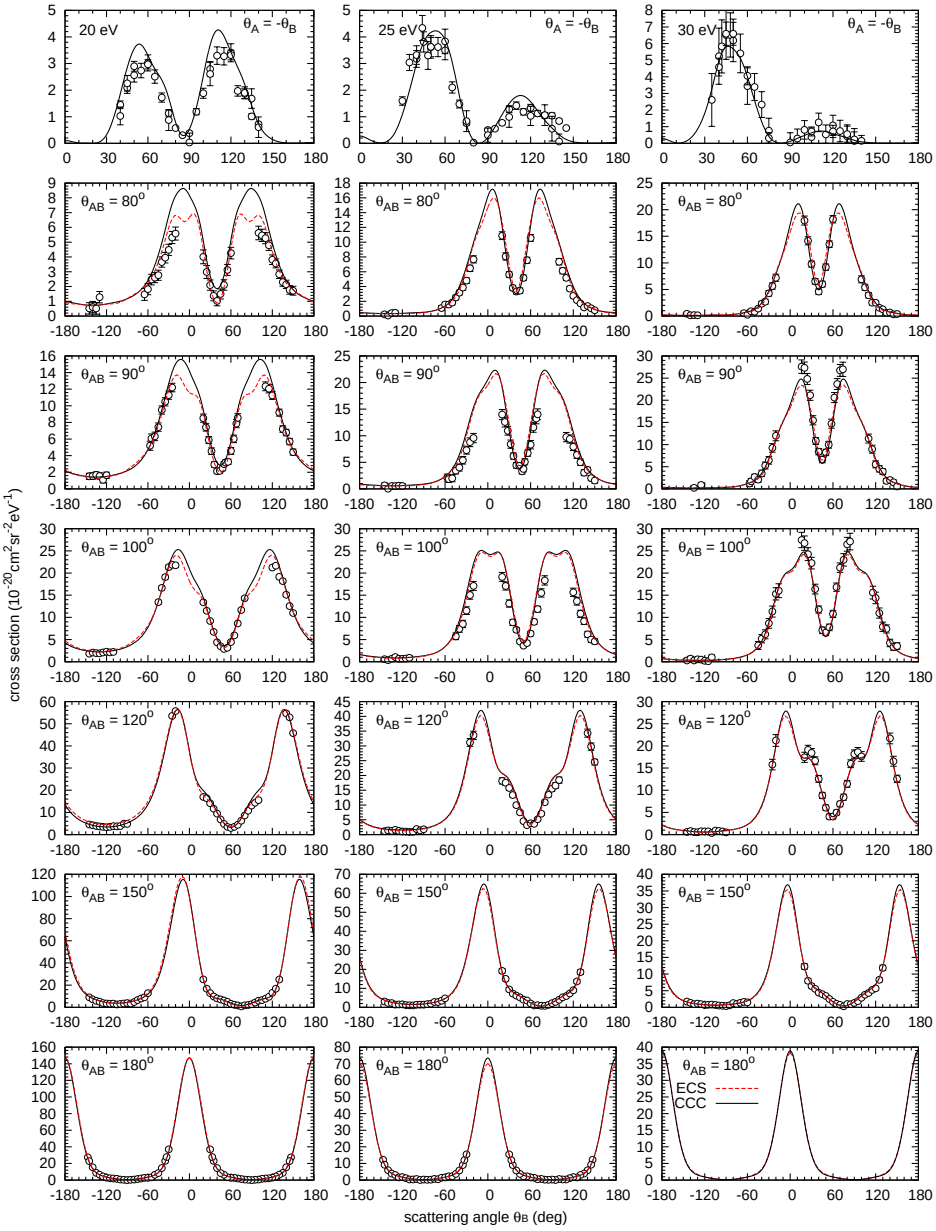

Figure 6: Coplanar fully differential cross sections for 20 eV (left), 25 eV (center) and 30 eV (right) electrons incident on the ground state of atomic hydrogen with equal energy outgoing electrons. The ECS theory is due to Baertschy et al. [2]. The CCC calculation is described in the text. The relative experimental values, due to Röder et al. [89] and Whelan et al. [90], are internormalised at each energy across the various geometries.

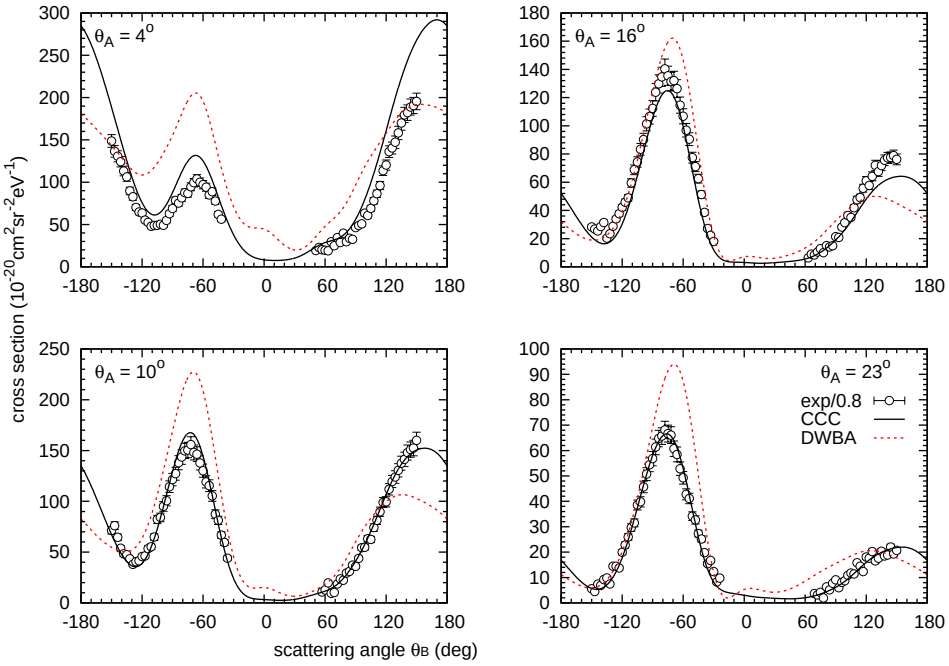

Figure 7: Coplanar fully differential cross sections for 54.4 eV electrons incident on the ground state of atomic hydrogen with an outgoing electron of energy E_B=5 eV. The fast electron of energy E_A=35.8 eV is detected at the specified θ_A angles. The relative experimental data presented by Brauner et al. [92], have been put on the absolute scale with an uncertainty of 35% by Jochen Röder [98], and divided by 0.8 for best visual fit to the CCC theory. The CCC and DWBA calculations are described in the text.

dostates. Note that the DWBA results typically vary with the choice of the distorting potential, whereas the CCC results must be independent of such a choice.

The 150 eV case is presented in Fig. 8 for completeness. This has been a solved problem for a very long time, and we see that the DWBA and CCC results are barely distinguishable. Here we took the opportunity to update the CCC results using the present CCC approach to ionization that superceded the one originally applied [75]. We set $l_{\max} = 6$ and $N_l = 25 - l$ with $\lambda_l = 2$. The DWBA mode turns off exchange and coupling.

We conclude this section by supporting the comments of Rescigno et al. [1] that the electron-impact ionization problem has been reduced to simply a computational one. Presently, we have the ECS, TDCC and CCC methods that are all able to solve such problems. Interestingly, computational progress

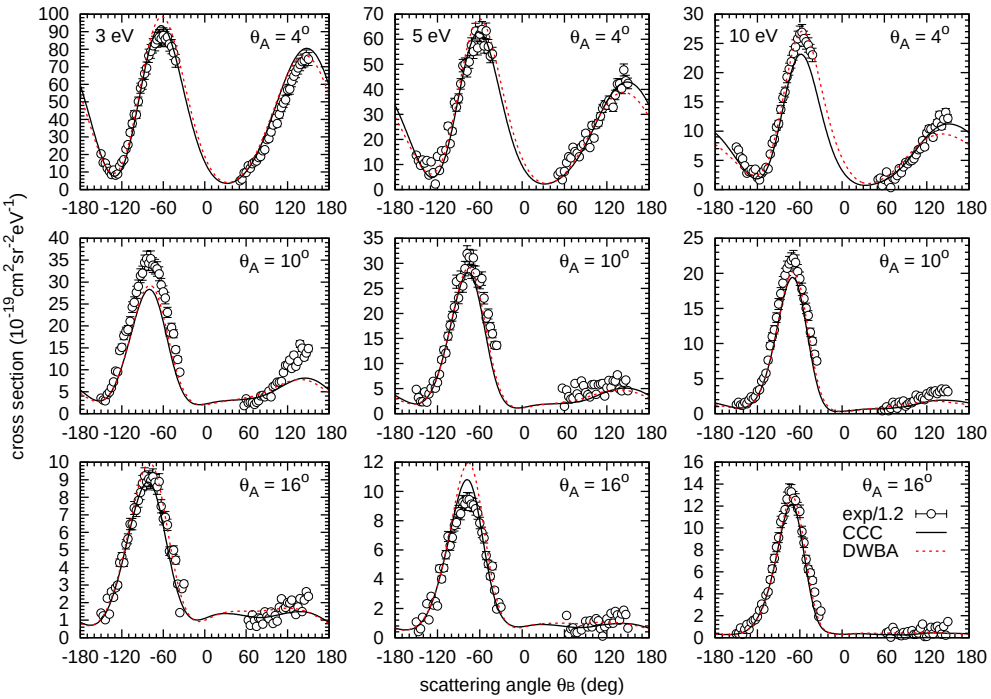

Figure 8: Coplanar fully differential cross sections for 150 eV electrons incident on the ground state of atomic hydrogen with outgoing electrons of energy E_B= 3 eV (left), 5 eV (center) and 10 eV (right). The fast electron is detected at the specified θ_A angles. text. The absolute experimental data, due to Ehrhardt et al. [93], has been divided by 1.2 for best visual fit to theory. The CCC and DWBA calculations are described in the text.

was possible without a full understanding of the origins of something as fundamental as the ionization amplitude [15].

4.2. Helium

Whereas atomic hydrogen is the ideal target for theorists, helium is the ideal target for experimentalists whilst maintaining the theoretical need for simplicity. It turns out that the helium atom is very well described by the frozen-core model, where one of the electrons occupies the $He^+(1s)$ orbital [99]. Thus, the appropriately symmetrised configurations are of the form $\{1s, nl\}$. The greatest error is in the ionization energy of the ground $\{1s, 1s'\}$ state, being 23.74 eV rather than the experimental value of 24.58 eV. The CCC method for helium within the frozen-core model has been thoroughly tested for electron-impact excitation of $n \leq 3$ singlet and triplet states [99, 100]. Nevertheless, due to the structural approximations, we can-

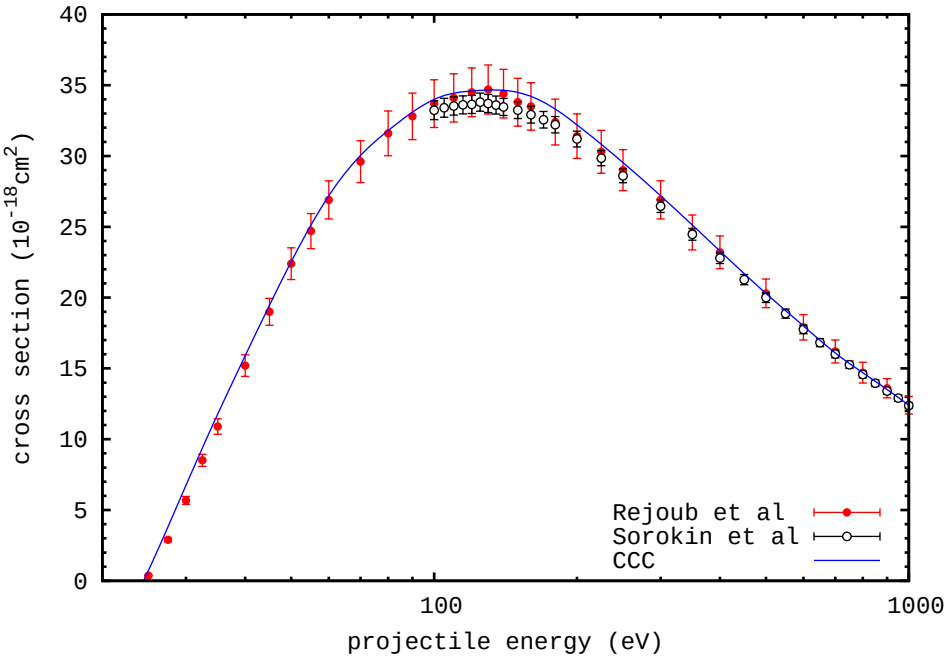

Figure 9: The total electron-impact single ionization cross section of the ground state of helium. The experiments are due to Rejoub et al. [105] and Sorokin et al. [106], and the CCC theory from Bray and Fursa [102].

not expect the same level of precision as for atomic hydrogen. The extension to electron-impact ionization processes for helium [73] follows in the same way as for atomic hydrogen, though the treatment of the equal-energy sharing case required more sophistication [101].

As for atomic hydrogen we begin by examining the total electron-impact (single) ionization cross section of helium, given in Fig. 9. Here we present the comparison between the multi-configurational structure model for helium and the more recent experiments. The difference between the frozen-core and multi-configuration results is relatively small and has already been discussed in some detail [102]. The key point is that as for atomic hydrogen the CCC theory yields excellent agreement with experiment across all energies of interest. As far as we are aware it remains the only theory to date that is able to do so. The ECS method has not yet been extended to full e-He problems, though some progress in this direction has been made [60]. The TDCC implementation for helium [103, 104] uses the configuration average approx-

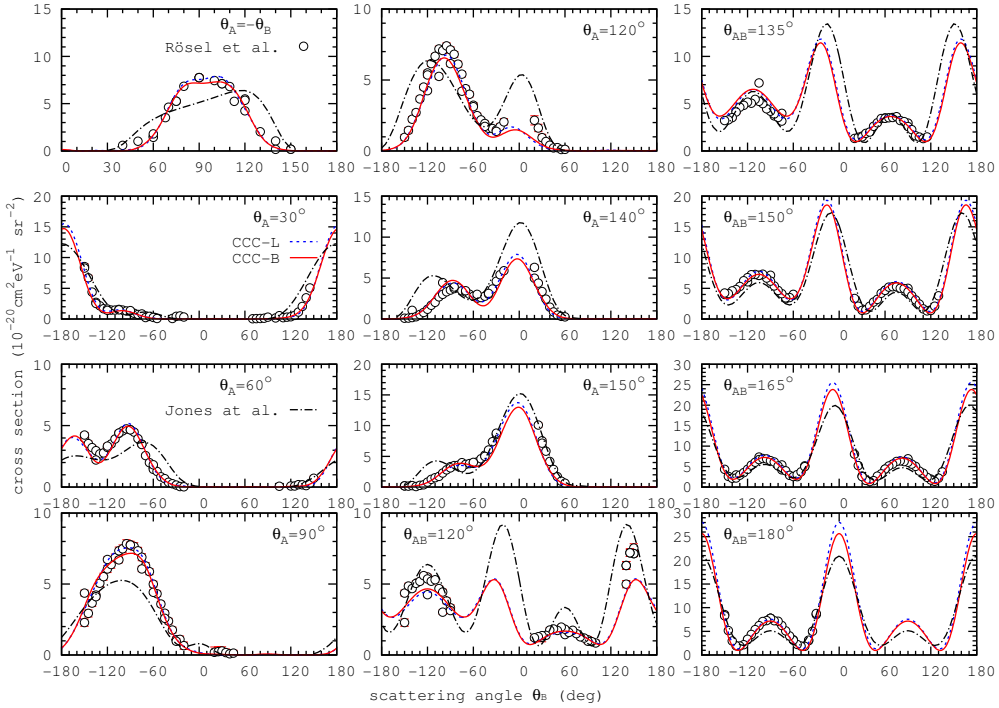

Figure 10: Fully differential cross sections for 26.6 eV electron-impact ionization of the ground state of helium with 1 eV outgoing electrons in the coplanar geometry. The experiment, with an absolute uncertainty of 22%, and the Jones et al. calculations are presented by Rösel et al. [107]. The CCC calculations are due to Stelbovics et al. [101]. Note, wherever possible points from overlapping geometries are also plotted, giving an indication of internal consistency.

imation, and so has difficulty at low energies when electron flux needs to be correctly subdivided between the singlet and triplet states. An all-electron TDCC implementation [65] should be able to do this, but it is particularly computationally expensive. RMPS approach should work well, but has concentrated on ionization-plus-excitation processes [10].

The electron-impact fully differential single ionization problem is arguably the most studied for the helium target than any other, both experimentally and theoretically. Accordingly, it is not practical to review all of the available studies, and we choose some specific highlights. It is our contention that this problem is as solved as it is for atomic hydrogen, though some few nagging discrepancies with experiment remain.

4.2.1. Low energies

The lowest energy for which e-He fully differential cross sections exist is 26.6 eV. In this case coplanar kinematics with 1 eV outgoing electrons were chosen. This is the most difficult case to calculate due to the very low energies involved with the competing elastic and excitation cross sections being considerably larger. The comparison between the Laguerre- and Box-based CCC theory and the experiment and calculations of Rösel et al. [107] are presented in Fig. 10. We see vey good agreement between the two CCC calculations and the experiment. Remarkably, the first order calculations of Jones et al are only in marginally worse agreement with experiment.

As in the case of atomic hydrogen it is tempting to conclude that the e-He single ionization problem is also solved for all practical purposes. Particularly so since similarly good agreement between the CCC theory and experiment is also found for 32.6 eV incident energy with 4 eV outgoing electrons [101]. However, thus far we have only looked at the coplanar case. Out-of-plane measurement are only available for the intermediate and high energy cases.

4.2.2. Intermediate energies

We'll define, somewhat aribitrarily, the intermediate energy range of interest to be above 32.6 eV and below 100 eV. Here data are available for both equal- and unequal-energy-sharing kinematics. Additionally, data for out-of-plane geometries are also available. While we will restrict ourselves to the geometries conveniently parametrised as in Fig. 3, there are others as well, see Röder et al. [108] for example of good agreement between theory and experiment at 40 eV, and 44.6 eV [109]. Note that in the latter case the factor of two difference was derived from first principles subsequently [101].

We'll begin by revisiting the 50 eV e-He case ($E = 25.4$ eV) first considered by Röder et al. [111]. Here, we have three energy-sharings measured for $E_B = 4$ eV, $E_B = 10$ eV, and $E_A = E_B = 12.7$ eV. Only the data for the asymmetric energy-sharing cases has been put on the absolute scale. This case is interesting because it relates to the step-function issues discussed earlier in Section 4.1.1. We begin by considering the singly differential cross section (SDCS), presented in Fig. 11. Here we have the results of a $l_{\max} = 6$, 50 a.u. box-based 283-state CCC calculation which shows oscillations for $E_B \leq E/2$, and falls off smoothly to zero for $E_B > E/2$. The curve labeled CCC(∞) is the corresponding step function estimate. It preseves the integral of the CCC(283) curve, that yields the kind of agreement with experiment presented in Fig. 9, with the height of the step being four times the presented

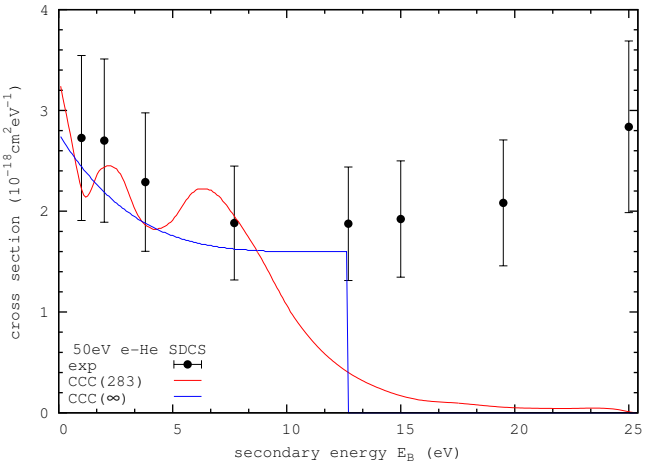

Figure 11: The 50 eV electron-impact on the ground state of helium singly differential cross section. The experiment is due to Röder et al. [110], and the present CCC calculations are described in the text.

CCC(283) result. The coherent combination of the ionization amplitudes at $E_B = E/2$ yields cross sections of the correct magnitude ab initio [101], but for the oscillations for $E_B \leq E/2$ invite some further attention, particularly for $E_B = 10$ eV. In this case we can be sure that the raw CCC(283) fully differential cross sections, will be substantially too low upon integration over the angular coordinates. Accordingly, we multiply them uniformly by the ratio of the CCC(∞) and CCC(283) results for each $E_B < E/2$ of interest. The resultant cross sections and comparison with experiment are presented in Fig. 12.

We see excellent agreement with experiment, which is of considerable improvement over what was presented earlier [111]. In part this is due to the much larger calculations now possible, but also due to the greater understanding of how the close-coupling method should be applied to ionizing processes.

Thus far we have concentrated on cases where there is clearly good agreement between theory and experiment. However, this is not always the case. In Fig. 13 we summarise an extraordinary situation that exists for 64.6 eV electron-impact ionisation of the ground state of helium with equal energy (20 eV) outgoing electrons. This case has been studied in great detail already [113] using the CCC theory and TDCC [114, 115] methods. Here we

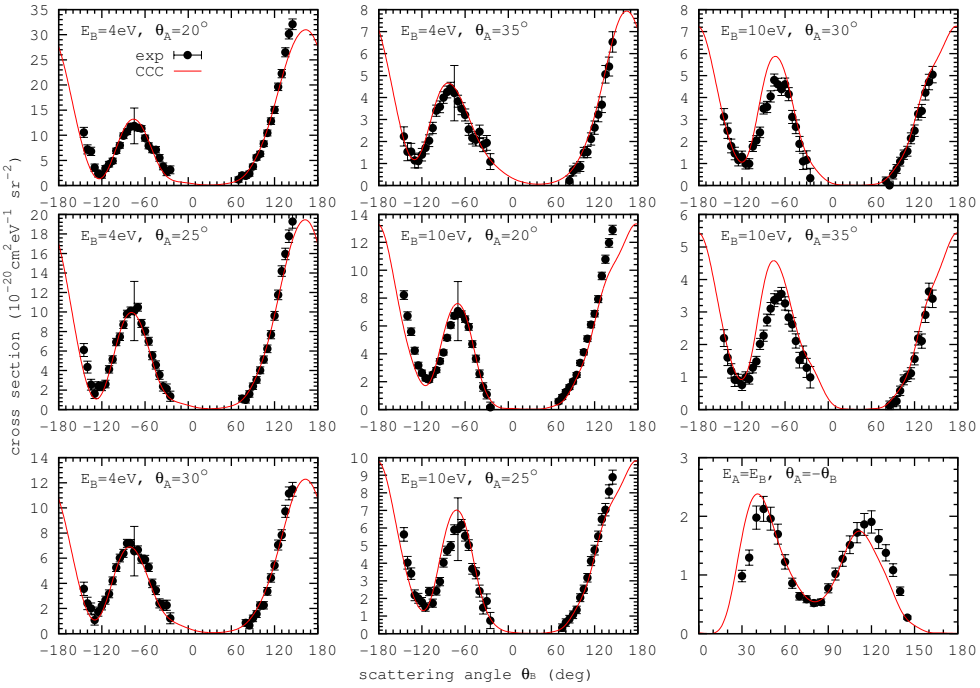

Figure 12: The 50 eV electron-impact on the ground state of helium coplanar fully differential cross sections at the specified secondary energies and geometries. The absolute experiment at $E_B = 4, 10$ eV is due to Röder et al. [111], while the relative equal-energy measurements of Rösel et al. [112] have been normalised to theory. The present CCC calculations are described in the text.

highlight two independent issues using just the CCC theory for clarity of presentation.

Begining with the perpendicular plane case ($\psi = 90°$), we see outstanding agreement between theory and experiment. The fact that the three geometries have the $\theta_A = 90°$ point in common (see Fig. 3) means that the full data set is internormalised, and so we are not free to normalise each case separately. If we are to believe that the CCC theory is correct for $\psi = 90°$ that would suggest that the absolute uncertainty is of the order of 0.01 of the specified units. However, the much larger coplanar case ($\psi = 0°$) the discrepancy arond $\theta_A = 40°$ is 200 times bigger! The situation would be resolved to a substantial extent if we were allowed to normalise the two cases separately, but the small error bars do not allow for the required movement.

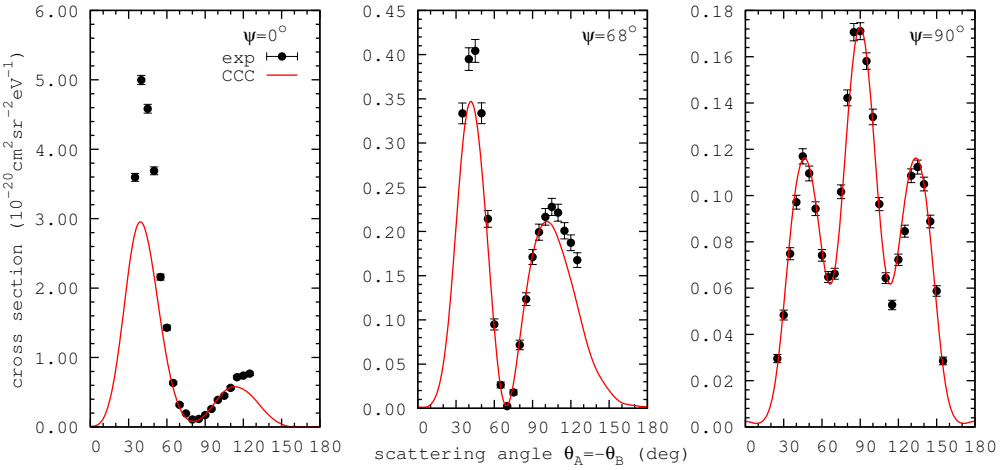

Figure 13: The 64.6 eV electron-impact on the ground state of helium fully differential cross sections with 20 eV outgoing electrons for the geometries as specified in Fig. 3. The relative experimental data [116] has been normalised to the CCC calculations [113] at the $\theta_A = 90°$ point, which is common for all ψ.

The second issue we'd like to bring to the attention of the reader is the $\psi = 68°$ case, where the cross section appears to go to zero at $\theta_A \approx 70°$. As has been extensively studied by Colgan et al. [115], this minimum comes about from a destructive interference of the contributing partial waves. We found that taking $\psi = 62.7°$ the minimum was five orders of magnitude less than the maximum of the cross section. By excluding contributions from the larger orbital angular momenta the minimum rises rapidly. Accordingly, there is no readily identifiable mechanism that is responsible for this, and it is conceivable that the minimum is an actual zero.

We next turn to one of the most spectacular experimental achievements in the field in recent times. This is the application of the cold-target recoilion momentum spectroscopy (COLTRIMS) technique, for a given incident energy, to measure absolute fully differential ionization cross sections simultaneously for many kinematical and geometrical combinations of the outgoing electrons. Given the CCC cross section behaviour identified in Fig. 1, this is ideal in testing the CCC theory as the secondary energy E_B varies in small steps from the minimum ($E_B = 3$ eV) to the maximum value ($E_B = E_A = 23$ eV) measurable. Comparison of experiment with the Laguerre based CCC results in the coplanar case is presented in Fig. 14. We

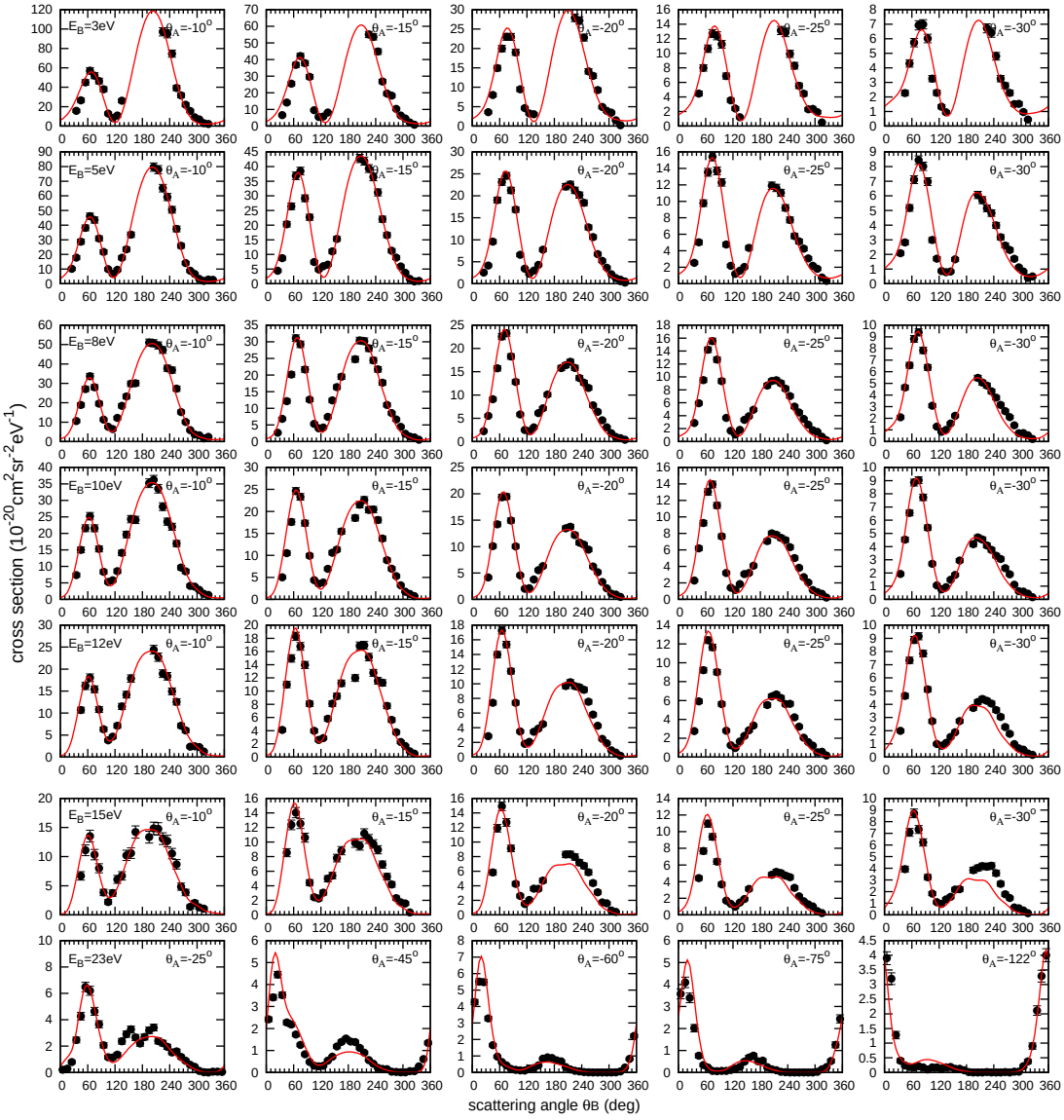

Figure 14: The 70.6 eV electron-impact on the ground state of helium fully differential cross sections for the coplanar geometry. The absolute experiment and CCC theory are due to Ren et al. [104].

see generally outstanding agreement across 35 separate cases, all of which arise from a single experiment and a single calculation. Incidentally, the TDCC results are also presented by Ren et al. [104], but they suffer from a systematic discrepancy with experiment for the asymmetric energy sharing cases.

In addition to the coplanar data Ren et al. [104] also extracted data where one of the electrons is ejected perpendicular to the plane formed by the incident and the so-called scattered electron. Given the discrepancy identified at 64.6 eV in Fig. 13 it is helful to see if the CCC theory is able to yield consistent agreement with absolute experiment for both coplanar and perpendicular-plane geometries. The perpendicular case is presented in Fig. 15. Once more we see generally excellent agreement of the CCC calculations with experiment, particularly given the experimental energy and angle resolution considerations. It is important to remember that being a unitary theory the T-matrix elements that arise from a single calculation are all coupled, and thereby contribute in some way to all of the presented cross sections. Though not conclusive, the weight of comparison between the CCC theory and experiment at 70.6 eV suggests similarly good agreement should be expected at 64.6 eV.

4.2.3. High energies

For completeness we say a few words about the higher energies. As for atomic hydrogen such data have been the most studied and is the fundamental starting point for the testing of any theory, including CCC [73]. Here perturbative methods are a very efficient way of yielding accurate cross sections. Hence, the intracacies of the definition of the ionization amplitude are not so relevant here.

Most of the experimental data is several decades old as are the calculations, but there have been a few more recent developments. Dürr et al. [117] have measured 102 eV electron-impact ionization of helium using the COLTRIMS techniques and found good agreement with various theories. This case was also studied with some success using the TDCC theory [66].

Catoire et al. [118] measured 730 eV electron-impact ionization of helium with a coplanar ejection of a 205 eV electron, and found some disagreement with various perturbative theories. This improved substantially upon application of the CCC theory [119], however being relative measurements the comparison is not able to be definitive.

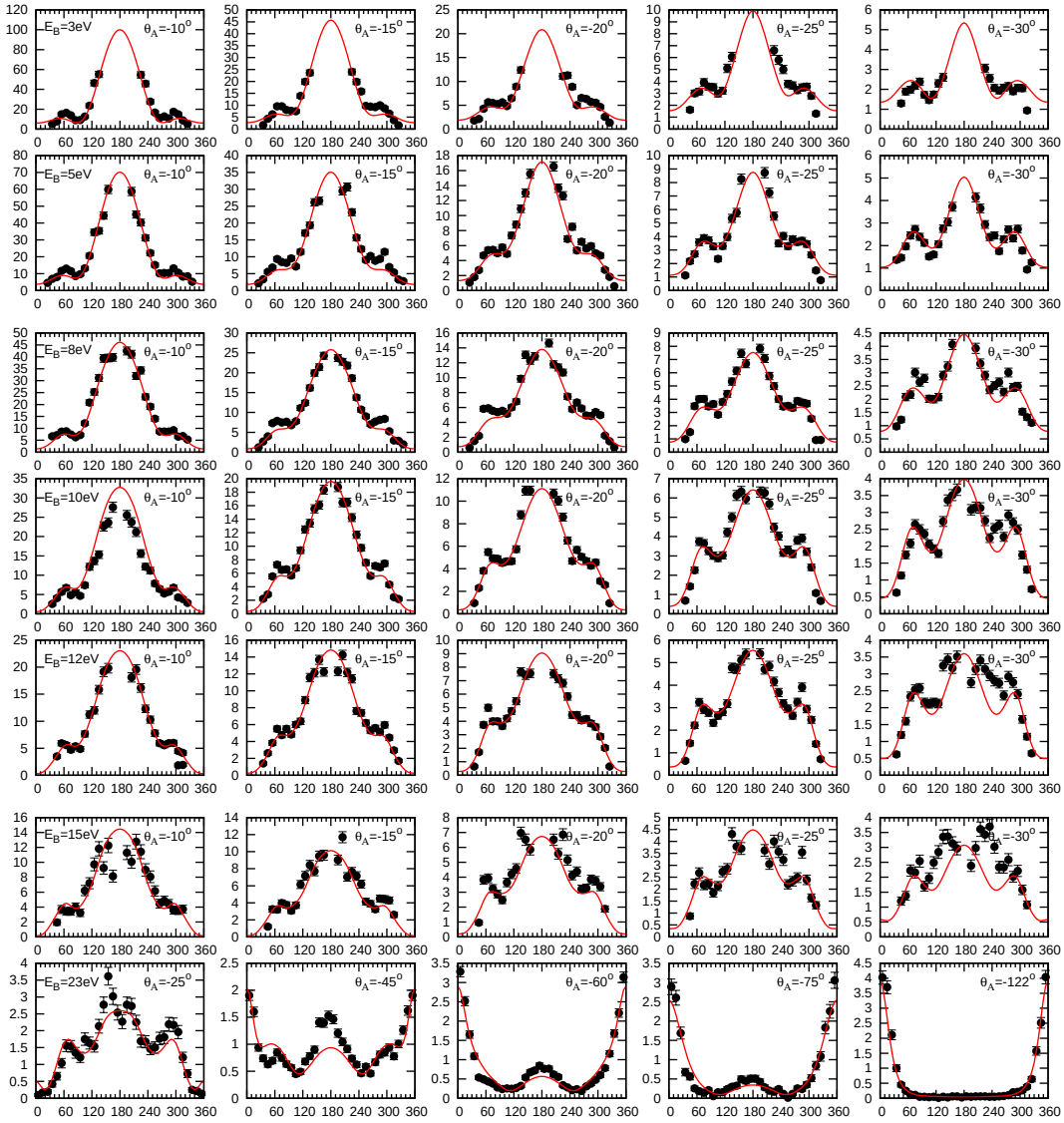

Figure 15: The 70.6 eV electron-impact on the ground state of helium fully differential cross sections for the perpendicular plane geometry. The absolute experiment and CCC theory are due to Ren et al. [104].

4.2.4. Ionization plus excitation

Thus far we have considered electron-impact ionization of helium in the case where the residual electron is left in the ground state of the He^+ ion. The formal theory for the definition of the ionization amplitude is unchanged for the case where the residual ion is left in an excited $n_f \geq 2$ state. However, perhaps surprisingly, the computation of such processes is not a trivial extension of what has been presented thus far. In a close-coupling based theory the same definition (106) for the ionization amplitude applies

$$f_i^{(N)}(\boldsymbol{q}_f, \boldsymbol{k}_f) = \sum_{n=1}^{N} \langle \boldsymbol{q}_f^{(-)} | \phi_n^{(N)} \rangle \langle \boldsymbol{k}_f \phi_n^{(N)} | (\overleftarrow{H} - E) | \Psi_i^{(N+)} \rangle, \qquad (124)$$

where now $\langle \boldsymbol{q}_f|$ is a continuum wave obtained as a close-coupling solution of e-He^+ scattering that includes at least the lowest three energy states, and the helium states $|\phi_n^{(N)}\rangle$ are constructed from configurations that contain at least the lowest three states of He^+ for one of the electrons. One consequence of this is that it is no longer possible to obtain $\langle \boldsymbol{q}_f^{(-)} | \phi_n^{(N)} \rangle = \delta_{fn} \langle \boldsymbol{q}_f^{(-)} | \phi_n^{(N)} \rangle$ for any $q_f^2/2$. Since $\langle \boldsymbol{k}_f \phi_n^{(N)} | (\overleftarrow{H} - E) | \Psi_i^{(N+)} \rangle$ exists only on the energy shell ($k_f^2/2 + \epsilon_n^{(N)} = E$), we have a fundamental computational problem.

There are several hybrid approaches to ionization plus excitation processes, see [120–124] for example. However, as stated at the outset, here we only concern ourselves with those approaches that aim to fully solve the problem, i.e. obtain an accurate ionization amplitude at any energy. As far as we are aware only Zatsarinny and Bartschat [10] have attempted to do this. Utilising their close-coupling formalism they effectively replaced $\boldsymbol{k}_f$ with $\boldsymbol{k}_n$ on the RHS of Eq. (124), and thereby avoided the above-mentioned problem. This means that the summation brings contributions from excitation amplitudes with rather different kinematics than in the experiment of interest, depending on the magnitudes of the $\langle \boldsymbol{q}_f^{(-)} | \phi_n^{(N)} \rangle$. Nevertheless, the results, reproduced here in Fig. 16, are quite spectacular. We see very good agreement of the B-spline R-matrix (BSR) calculations with the ratio measurements of Bellm et al. [124]. At times the "$n_f = 1$" cross section is two orders of magnitude bigger than the "$n_f = 2$" one. This indicates that the absolute "$n_f = 2$" cross sections are being calculated very accurately even though they are particularly small.

As this is only a very recent development more studies are required to determine the validity of the approach at other energies, and for the residual ion being in $He^+(n_f > 2)$ states.

5. Double photoionization

The process of *non-sequential* single-photon double photoionization (DPI), and a closely related process of photoionization-excitation, both involve absorption of a single photon which results in simultaneous change of quantum numbers of two or more atomic electrons. These are fundamentally important processes as they constitute a direct probe of electron correlation [125]. In the independent electron approximation, at most practical photon energies, the electromagnetic field can only couple to a single electron. Changing the quantum state of the second and further electrons can only take place via *many-electron correlation*, either in the initial bound state of the target or the final multiply ionized state. The bound state correlation is a static process which can be described relatively easily by various configuration-interaction schemes. Dynamical correlation in the photoelectron continuum is much more difficult to describe theoretically. Due to a long range of the Coulomb interaction, the continuum correlation cannot be treated perturbatively and a non-perturbative approach has to be taken.

A two-electron continuum state can be treated very efficiently by the convergent close-coupling (CCC) method in which one of the electrons is represented by a complete set of discrete (positive and negative energy) Laguerre basis pseudostates while the second electron is treated as a true continuum state. Details of the CCC method, as applied to electron-atom scattering, are outlined in the previous chapters.

5.1. Helium

Application of the CCC method do DPI of the helium atom is straightforward [126]. After the photon is absorbed and the first electron is ejected into the continuum, the atomic system evolves through elastic and inelastic scattering of the photoelectron on the He^+ ion. This process can be described by the multi-channel expansion for the final state wave function:

$$|\Psi_j^{(-)}(\boldsymbol{k})\rangle = |j\boldsymbol{k}_b^{(-)}\rangle + \sum_i \sum\!\!\!\!\!\!\int d^3p \frac{\langle \boldsymbol{p}^{(+)} i|T|j\boldsymbol{k}^{(-)}\rangle}{E - p^2/2 - \epsilon_i + i0} |i\boldsymbol{k}^{(+)}\rangle \ , \qquad (125)$$

with boundary conditions corresponding to an outgoing wave in a given channel $|j\boldsymbol{k}^{(-)}\rangle$ and incoming waves in all other channels $|i\boldsymbol{p}^{(+)}\rangle$. The total integrated cross section (TICS) of the helium photoionization, as a function of

the photon energy ω, corresponding to a particular bound electron state j (degenerate with magnetic sublevels m_j) is given by

$$\sigma_j(\omega) = \frac{4\pi^2}{\omega c} \sum_{m_j} \int \mathrm{d}^3k \, |\langle \Psi_j^{(-)}(\boldsymbol{k}) \, |\mathcal{D} \cdot \boldsymbol{e}| \, \Phi_0 \rangle|^2 \, \delta(\omega + E_0 - k^2/2 - \epsilon_j) \ . \quad (126)$$

Here $c \simeq 137$ is the speed of light in atomic units and $\boldsymbol{e}$ is the polarization vector of light. The energy of the system in the initial state $E_0 + \omega$ and the final state $k^2/2 + \epsilon_j$ is conserved. The dipole electromagnetic operator $\mathcal{D}$ can be written in one of the following three forms commonly known as length, velocity, and acceleration gauges [127]:

$$\mathcal{D}^r = \omega(\boldsymbol{r}_1 + \boldsymbol{r}_2), \quad \mathcal{D}^\nabla = \vec{\nabla}_1 + \vec{\nabla}_2, \quad \mathcal{D}^{\dot{\nabla}} = \frac{2}{\omega} \left(\frac{\boldsymbol{r}_1}{r_1^3} + \frac{\boldsymbol{r}_2}{r_2^3} \right). \quad (127)$$

The choice of the He atom ground state in Eq. (126) is discussed in detail in Ref. [128]. The most accurate representation is given by a Hylleraas expansion $\Phi_0 = Ne^{-zs} \sum_{ijk} a_{ijk} \, u^i s^j t^k$ over the powers of $u = |\boldsymbol{r}_1 - \boldsymbol{r}_2|$, $s = r_1 + r_2$, and $t = r_1 - r_2$. With the Hylleraas ground state, all the three gauges of the dipole operator produce identical cross-section results for the He atom and its isoelectronic sequence of ions [129]. As an alternative, the ground state can be represented by a multi-configuration Hartree–Fock (MCHF) expansion. which is less accurate than the Hylleraas one. However, it can be readily extended beyond helium and its isoelectronic sequence of ions towards more complex quasi two-electron targets with a frozen core.

We separate the contribution from the final channels $|j\boldsymbol{k}^{(-)}\rangle$ into single and double ionization according to the energy of the ϵ_j which is positive for the double ionized channels and negative for the singly ionized channels. We also ensure that the negative-energy state cross sections, which contribute to the ionization plus excitation cross sections, are multiplied by the projection of the state onto the true target discrete subspace [43]. This way we have a relatively clear separation between the discrete and continuous spectrum of the e-He^+ excitation.

The dipole matrix element in Eq. (126) can be used to calculate the fully resolved triply differential cross section (TDCS) of the DPI [67], which corresponds to two photoelectrons emerging with energies E_1, E_2 within solid angles Ω_1, Ω_2, respectively. This is achieved by projecting of one, usually slow, electron onto a positive energy pseudostate of the matching energy

$\epsilon_j = E_2$ and by using the partial wave expansion:

$$\langle \boldsymbol{k}_2|j\rangle\langle\Psi_j^{(-)}(\boldsymbol{k}_1)|\mathcal{D}_M|\Phi_0\rangle = \sum_{l_1m_1}\sum_{l_2m_2}(-i)^{l_1+l_2}e^{i[\delta_{l_1}(k_1)+\delta_{l_2}(k_2)]}$$

$$\times Y_{l_1m_1}(\boldsymbol{k}_1)Y_{l_2m_2}(\boldsymbol{k}_2)\begin{pmatrix} l_1 & 1 & l_2 \\ m_1 & M & m_2 \end{pmatrix} D_{l_1l_2}(k_1j)\langle k_2l_2 \parallel n_jl_j\rangle. \quad (128)$$

Here, we introduced the reduced (or stripped of angular dependence) dipole matrix element $D_{l_1l_2}(k_1j)$ and the overlap integral $\langle k_2l_2 \parallel n_jl_j\rangle$ between the positive–energy pseudostate and the Coulomb wave. The former is calculated by integrating the first-order dipole matrix with the dipole singlet T-matrix of the e–He^+ scattering system. The first-order dipole matrix is obtained as a transition amplitude of the dipole operator between the correlated ground state and the final state containing one continuum Coulomb wave and one discrete pseudostate.

Eq. (128) leads to the following form of TDCS:

$$\sigma_M = \frac{4\pi^2}{3\omega c}\left|\sum_{l_1l_2}(-\mathrm{i})^{l_1+l_2}\mathcal{Y}_{1M}^{l_1l_2}(\hat{\boldsymbol{k}}_1,\hat{\boldsymbol{k}}_2)\sum_{l_1l_2}\mathrm{e}^{\mathrm{i}(\delta_{l_1}+\delta_{l_2})}D_{l_1l_2}(E_1,E_2)\right|^2, \quad (129)$$

where $\mathcal{Y}_{1M}^{l_1l_2}(\hat{\boldsymbol{k}}_1,\hat{\boldsymbol{k}}_2)$ is a bipolar harmonics [130] and

$$D_{l_1l_2}(E_1,E_2) = D_{l_1l_2}(k_1j)\langle k_2l_2 \parallel n_jl_j\rangle\ .$$

The index M indicates polarization of light and is set to 0 for linearly polarized light along the z–direction and to ±1 for circularly polarized light depending on the helicity.

The TDCS for the linear polarization can be written in a compact form [131]

$$\sigma_0 = \frac{4\pi^2}{3\omega c}\Big|(\cos\theta_1+\cos\theta_2)\mathcal{M}_g(E_1,E_2)+(\cos\theta_1-\cos\theta_2)\mathcal{M}_u(E_1,E_2)\Big|^2, \quad (130)$$

where the symmetric and antisymmetric (gerade-g and ungerade-u) DPI amplitudes

$$\mathcal{M}_{\substack{g\\u}} = \frac{1}{4\pi}\sum_{l=0}^{\infty}\frac{(-1)^l}{\sqrt{l+1}}\left[P'_{l+1}(\cos\theta_{12}) \mp P'_l(\cos\theta_{12})\right]D^{\pm}_{ll+1}(E_1,E_2) \quad (131)$$

depend on the photoelectron energies and their mutual angle $\cos\theta_{12} = \boldsymbol{k}_1 \cdot \boldsymbol{k}_2/(k_1 k_2)$. Following the pioneering work by Schwarzkopf et al. [132], it is customary to describe the symmetric amplitude by a Gaussian ansatz

$$\left|\mathcal{M}^g(\theta_{12})\right| \approx A \exp\left[-2\ln 2\left(\frac{\pi-\theta_{12}}{\Delta\theta}\right)^2\right] . \tag{132}$$

The full width at half maximum parameter $\Delta\theta$ depends on the energy of the photon as prescribed by the Wannier theory [133].

5.1.1. Total integrated cross-sections

The double-to-single photoionization cross-section ratio σ^{2+}/σ^{+} in helium has been studied very thoroughly across a wide photon energy range [134–137]. Our CCC calculation with a 20-parameter Hylleraas ground state [129], which is illustrated on the right panel of Fig. 17, is essentially gauge independent and provides a good benchmark for various measurements. This calculation can be carried out from the threshold, where it reproduces the Wannier law $\sigma(E) = \sigma_0\ E^{1.056}$, all the way to the limit of infinite photon energy, indicated by the arrow on the right panel of Fig. 17. This limit is a static property of the atomic ground state [138]. While the CCC calculation in the length gauge looses its accuracy in the high photon energy regime, the two other gauges remain stable and reliable.

Along with the DPI calculation, the CCC model provides the full set of cross-sections for the ionization accompanied by excitation. These cross-sections for excitations up to $n = 6$ ionic states were evaluated for the He atom and its isoelectronic sequence of ions [129]. The cross section ratios σ_n/σ_1 for single photoionization of He with excitation to $n = 2$, 3 and 4 states are presented in Fig. 18. These data are compared with the experimental results of Wehlitz et al. [136]. The calculations generally agree very well with experiment and reach the non-relativistic limit of infinite photon energy.

In a more recent work, Czasch et al. [139] reported partial photoionization cross sections and angular distributions for double excitation of helium up to the $n = 13$ threshold. To reproduce this measurement, the original Laguerre based CCC method was modified to allow for the use of a box basis, which discretizes the target spectrum by forcing all target wave functions to vanish at the box boundary [140].

5.1.2. Fully differential cross-sections

The fully resolved TDCS of DPI of helium provide the most stringent test of theory. The CCC results have been tested in a number of experiments starting from the benchmark measurement by Bräuning et al. [141] who established the first good agreement with theory on the absolute scale. These tests continued in later years across a wide range of photon energies and polarization state of light which are summarized in Table 1. In all these cases, agreement between the CCC theory and experiment was very satisfactory.

Ref Linear	ω, eV	Ref Circular	ω, eV
[142]	119	[150]	88
[143]	139	[151]	127
[144]	159	[152]	179, 529
[145, 146]	119		
[147]	529		
[148, 149]	179, 529		

Table 1: Experimental tests of the fully-resolved TDCS of He calculated by the CCC method at specific photon energies ω and polarization state of light.

One of the most stringent tests of the CCC theory was performed in a measurement of the circular dichroism, i.e. the difference between the TDCS obtained with left- and right-hand circularly polarized light. Although the initial measurement by Mergel et al. [153] was found in disagreement with predictions of the CCC theory [154], subsequent refined measurement by the same group [155] agreed perfectly well with these predictions as is illustrated in Fig. 19

5.1.3. Symmetrized amplitudes

The quintessential dynamical information on the DPI process can be condensed into the symmetrized amplitudes (131). These amplitudes had been evaluated by the CCC method both for the case of equal [156] and arbitrary [157] energy sharing. Even though the Gaussian ansatz (132), as derived from the Wannier threshold theory, should be strictly valid at small excess energies, it can be used as a practical tool at a much wider range of photon energies. The Gaussian width parameters $\Delta\theta$ deduced from the CCC calculations at various equal energy sharings are presented in Fig. 20 in comparison with available experimental data.

Modern experimental techniques allow for direct DPI amplitude measurements without any specific reliance on the Gaussian ansatz [146, 149, 151]. These measurements supported predictions of the CCC theory both for the gerade and ungerade amplitudes and their relative phase. In a recent development [166], it was demonstrated that that an additional information on the *absolute* individual phases of the DPI amplitudes can be obtained by a time delay measurement in a short XUV pulse. Such a measurement, which is yet to be performed, opens up a possibility of a complete DPI experiment in which both the magnitudes and phases of the symmetrized DPI amplitudes can be determined.

5.2. Other targets

The CCC formalism, as outlined in the previous section for helium, can be readily applied to the isoelectronic sequence of He-like ions [129]. The only required change is modification of the expansion coefficients a_{ijk} in the Hylleraas ground state and the exponential fall-off parameter in the Laguerre basis. The same formalism, with the MCHF ground state, can be applied to the helium atom in its metastable state [167]. More essential modifications of the formalism is required for other targets.

5.2.1. Quasi two-electron targets

Alkaline-earth metal atoms can be treated by the CCC method in the so-called frozen-core approximation. In this approximation, all the atomic electrons, apart from the outermost valence shell, are considered as passive spectators and form a frozen core. Photoionization of the valence shell is described by the helium-like formalism with the only modification that both the target states and the continuum waves entering Eq. (125) are calculated in the frozen-core Hartree-Fock (FCHF) potential. The atomic ground state is described by a MCHF expansion which contains two-electron excitations from the valence shell.

This formalism was applied to Be [168, 169], Mg and Ca [169]. The double-to-single photoionization cross-sections ratios in Be and Mg are compared with experimental data on the left and right panels of Fig. 21, respectively. Generally, good agreement is achieved with experiment for both targets. Qualitatively, the double-to-single ratio in alkaline-earth metal atoms is similar to that of He shown in Fig. 17. These ratios can be scaled to that of He by measuring the excess energy above the DPI threshold in units of the

ionization potential of the corresponding singly charge ion [169]. An explanation of the this scaling property is that the DPI near threshold proceeds mainly via the electron impact ionization of the singly charged ion. The cross-section of the former process is a universal function of the reduced excess energy for all hydrogen-like targets. Qualitative difference of DPI of He and the alkaline-earth metal atoms can be observed in their angular correlation pattern in two-electron continuum which is described by the Gaussian function. As compared to He, there is a systematic reduction of the Gaussian width in the sequence of atoms from Be to Ca [169, 173]. This reduction is explained by an expansion of the target orbitals in the coordinate space and corresponding increase of the partial waves of the two-electron continuum emitted by these orbitals.

Similarly to the valence shell DPI, CCC technique can be applied to the K-shell DPI of alkaline-earth metal atoms from the threshold to the non-relativistic limit of infinite photon energy [174]. Theoretical double-to-single photoionization cross-sections ratios for Mg and Ca are compared favourably with experimental values derived from high-resolution X-ray spectra following the radiative decay of the K-shell double vacancy [175].

5.2.2. Three-electron targets

Recently, the CCC method was expanded to treat the DPI of three-electron targets like the lithium atom [176]. Application of the CCC method to DPI of Li is a natural extension of the previous work on DPI of He. This connection is illustrated in Fig. 22 where we draw schematically the amplitudes of single-photon two-electron ionization of He (left diagram) and Li (right diagram). Here we use the following graphical symbols. A thin solid line with an arrow to the right (the direction of time propagation) exhibits a one-electron state. The dashed line indicates a photon. A shaded oval stands for the multiple Coulomb interaction summed to infinite order (the T-matrix). Thick solid lines on the bottom diagram (Li) represent two-electron states.

Results of CCC calculations of DPI of Li are presented in Fig. 23. Good agreement with experiment is seen, especially in the near-threshold region where the calculation clearly adheres to the Wannier threshold law. Except for the total integrated cross-sections calculations [176], the CCC model was used to evaluate the differential cross-sections [179] including spin effects in the final state [180].

5.3. Other related processes

The process of electron impact double ionization can be similar to the DPI. If the incident electron is fast, its interaction with the target can be treated in the first Born approximation. In this case, the amplitude of the double ionization process can be presented as a matrix element of the Born operator between the two-electron ground and final states. Subsequent treatment is identical to that of the DPI with the only difference that instead of the dipole photoionization operator (127) one has to use the electron impact Born operator. Such a treatment was applied to He at a very high incident energy of 5.5 keV where the first Born approximation was well justified [181]. When the CCC calculation was compared with experimental data, the fully-resolved differential cross-sections were found in good agreement in shape but a considerable rescaling was required to get agreement in magnitude also. This disagreement in absolute values remains unresolved to date [182]. Contributions beyond the first Born approximation were identified comparing experimental data with first order CCC calculations for He at a smaller incident energy of 2 keV [183] including impulsive regime of large momentum transfer [184]. Extension of the CCC theory to include the second-Born corrections was attempted [185]. This technique was also applied to treat the process of non-sequential two-photon double ionization of He [186, 187] while the first-Born CCC treatment was given to the process of electron-impact ionization with simulateneous excitation [122].

6. Concluding remarks

We have presented a surface integral approach to break-up problems that is valid for both short- and long-ranged potentials. It yields clear definitions of the break-up amplitudes, which have been related to the various computational methods for calculating such processes. Given how both formal theory and computational techniques have come together, with such a broad agreement with experiment, it is tempting to conclude that electron-impact ionization and double photoionization of simple atomic targets are solved problems. Keeping in mind that single genuine discrepancy between theory and experiment can bring down the theory we have highlighted some such cases. We are hopeful that they are due to some as yet undetermined systematic experimental problem.

Not all questions raised have been answered. The ionization-plus-excitation problem is currently under intense investigation. Application to more com-

plex targets has the added complexity of generating the structure sufficiently accurately, but within constraints associated with subsequent application to ionizing collisions.

Nevertheless, we feel that immense progress has occurred in the field during the last decade, and arguably more than in any other before it. Much of this was due to the ever growing computational power. As so often happens in the field of physics, new technologies lead to new levels of understanding. It has to be acknowledged that the somewhat fortuitous computational progress was the catalyst for us to revisit the formal theory of breakup with long-range potentials in order to understand the computational success.

Acknowledgments

We thank Klaus Bartschat, James Colgan, XueGuang Ren, Jochen Röder, and Mark Baertschy for providing their data in quantitative form. We acknowledge the support of the Australian Research Council, the Australian National Computational Infrastructure Facility and its Western Australian node iVEC.

References

[1] T. N. Rescigno, M. Baertschy, W. A. Isaacs, C. W. McCurdy, Collisional breakup in a quantum system of three charged particles, Science 286 (1999) 2474–2479.

[2] M. Baertschy, T. N. Rescigno, C. W. McCurdy, Accurate amplitudes for electron-impact ionization, Phys. Rev. A 64 (2001) 022709.

[3] P. L. Bartlett, A. T. Stelbovics, I. Bray, Propagating exterior complex scaling method for electron-hydrogen collisions, J. Phys. B 37 (2004) L69.

[4] I. Bray, A. T. Stelbovics, Explicit demonstration of the convergence of the close-coupling method for a Coulomb three-body problem, Phys. Rev. Lett. 69 (1992) 53–56.

[5] I. Bray, Close-coupling approach to coulomb three-body problems, Phys. Rev. Lett. 89 (2002) 273201.

[6] I. Bray, D. V. Fursa, A. S. Kadyrov, A. T. Stelbovics, Single ionization of helium by electron impact, Phys. Rev. A 81 (2010) 062704.

[7] K. Bartschat, E. T. Hudson, M. P. Scott, P. G. Burke, V. M. Burke, Electron-atom scattering at low and intermediate energies using a pseudo-state/R-matrix basis, J. Phys. B 29 (1996) 115–123.

[8] K. Bartschat, The r-matrix with pseudo-states method: Theory and applications to electron scattering and photoionization, Comp. Phys. Comm. 114 (1998) 168–182.

[9] K. Bartschat, Bsr: B-spline atomic r-matrix codes, Comp. Phys. Comm. 174 (2006) 273–356.

[10] O. Zatsarinny, K. Bartschat, Nonperturbative treatment of ionization with excitation of helium by electron impact, Phys. Rev. Lett. 107 (2011) 023203.

[11] J. Colgan, M. S. Pindzola, Double- and triple-differential cross sections for the low-energy electron-impact ionization of hydrogen, Phys. Rev. A 74 (2006) 012713.

[12] A. S. Kadyrov, A. M. Mukhamedzhanov, A. T. Stelbovics, I. Bray, Integral representation for the ionization amplitude which is free of ambiguity and divergence problems, Phys. Rev. Lett. 91 (2003) 253202.

[13] A. S. Kadyrov, A. M. Mukhamedzhanov, A. T. Stelbovics, I. Bray, Theory of electron-impact ionization of atoms, Phys. Rev. A 70 (2004) 062703.

[14] A. S. Kadyrov, I. Bray, A. M. Mukhamedzhanov, A. T. Stelbovics, Coulomb breakup problem, Phys. Rev. Lett. 101 (2008) 230405.

[15] A. S. Kadyrov, I. Bray, A. M. Mukhamedzhanov, A. T. Stelbovics, Surface-integral formulation of scattering theory, Ann. Phys. 324 (2009) 1516–1546.

[16] H. van Haeringen, Charged-particle Interactions, Coulomb Press Leyden, Leiden, 1985.

[17] L. D. Faddeev, Scattering theory for a three-particle system, Sov. Phys. -JETP 12 (1961) 1014–1019.

[18] L. D. Faddeev, Mathematical Aspects of the Three-Body Problem in the Quantum Scattering, Israel Program for Scientific Translations, Jerusalem, 1965.

[19] E. O. Alt, W. Sandhas, H. Ziegelmann, Coulomb effects in three-body reactions with two charged particles, Phys. Rev. C 17 (1978) 1981–2005.

[20] R. K. Peterkop, , Opt. Spectrosc. 13 (1962) 87.

[21] R. G. Newton, Scattering theory of waves and particles, Springer-Verlag New York, 2nd edition, 1982.

[22] M. Brauner, J. S. Briggs, H. Klar, Triply differential cross sections for ionisation of hydrogen atoms by electrons and positrons, J. Phys. B 22 (1989) 2265–2287.

[23] S. Jones, D. H. Madison, A. Franz, P. L. Altick, Three-body distorted-wave Born approximation for electron-atom ionization, Phys. Rev. A 48 (1993) R22–R25.

[24] S. P. Lucey, J. Rasch, C. T. Whelan, On the use of analytic ansatz three-body wf ..., Proc. R. Soc. A 455 (1999) 349–383.

[25] S. Jones, D. H. Madison, M. Baertschy, Perturbative and nonperturbative calculations of electron-hydrogen ionization, Phys. Rev. A 67 (2003) 012703.

[26] R. K. Peterkop, , Opt. Spektrosk. 13 (1962) 153.

[27] R. K. Peterkop, Theory of Ionization of Atoms by Electron Impact, Colorado Associated University Press, Boulder, 1977.

[28] G. Arfken, Mathematical Methods for Physicists, Academic Press, New York, 2nd edition, 1971.

[29] R. K. Peterkop, , Izv. Akad. Nauk Latv. SSR Riga 9 (1960) 79.

[30] C. W. McCurdy, D. A. Horner, T. N. Rescigno, Practical calculation of amplitudes for electron-impact ionization, Phys. Rev. A 63 (2001) 022711.

[31] R. K. Peterkop, Teoriya Ionizatsii Atomov Elektronnym Udarom, Zinatne, Riga, 1971.

[32] R. G. Newton, The asymptotic form of three-particle wavefunctions and cross sections, Ann. Phys. 74 (1972) 324–351.

[33] J. Schwinger, Coulomb green's function, J. Math. Phys. 5 (1964) 1606–1608.

[34] P. A. M. Dirac, Does renormalization make sense?, in: D. W. Duke, J. F. Owens (Eds.), AIP Conf. Proc. 74, AIP, New York, 1981, pp. 129–130.

[35] W. Pauli, Nobel Lectures, Physics 1942-1962, Elsevier, Amsterdam, pp. 27–43.

[36] R. P. Feynman, QED, The Strange Theory of Light and Matter, Princeton University Press, Princeton, pp. 128–129.

[37] V. B. Berestetskii, E. M. Lifshitz, L. P. Pitaevskii, Quantum electrodynamics, Pergamon press, 2nd edition, pp. 3–4.

[38] L. H. Ryder, Quantum Field Theory, Cambridge University Press, Cambridge, 2nd edition, p. 390.

[39] A. Temkin, Nonadiabatic theory of electron-hydrogen scattering, Phys. Rev. 126 (1962) 130–142.

[40] R. Poet, The exact solution for a simplified model of electron scattering by hydrogen atoms, J. Phys. B 11 (1978) 3081–3094.

[41] R. Poet, Symmetrically coupled partial differential equations in scattering I. Model electron-hydrogen collisions, J. Phys. B 13 (1980) 2995–3008.

[42] I. Bray, A. T. Stelbovics, Convergent close-coupling calculations of electron-hydrogen scattering, Phys. Rev. A 46 (1992) 6995–7011.

[43] I. Bray, A. T. Stelbovics, Calculation of the total ionization cross section and spin asymmetry in electron-hydrogen scattering, Phys. Rev. Lett. 70 (1993) 746–749.

[44] T. N. Rescigno, M. Baertschy, D. Byrum, C. W. McCurdy, Making complex scaling work for long-range potentials, Phys. Rev. A 55 (1997) 4253–4262.

[45] C. W. McCurdy, T. N. Rescigno, D. Byrum, Approach to electron-impact ionization that avoids the three-body coulomb asymptotic form, Phys. Rev. A 56 (1997) 1958–1969.

[46] G. Gaseano, L. U. Ancarani, D. M. Mitnik, On the applicability of the exterior complex scaling method for scattering problems including coulombic potentials, Eur. Phys. J. D (2012) under review.

[47] I. Hornyak, A. T. Kruppa, Two-body coulomb scattering and complex scaling, Phys. Rev. A 85 (2012) in press.

[48] M. Baertschy, T. N. Rescigno, W. A. Isaacs, C. W. McCurdy, Benchmark single-differential ionization cross section results for the s-wave model of electron-hydrogen scattering, Phys. Rev. A 60 (1999) R13–R16.

[49] S. Jones, A. T. Stelbovics, Complete numerical solution of Electron-Hydrogen Model Collision Problem above the Ionization Threshold, Phys. Rev. Lett. 84 (2000) 1878–1881.

[50] S. Jones, A. T. Stelbovics, Efficient solution of theree-body quantum collision problems, Phys. Rev. A 66 (2002) 032717.

[51] P. L. Bartlett, I. Bray, S. Jones, A. T. Stelbovics, A. S. Kadyrov, K. Bartschat, G. ver Steeg, M. P. Scott, P. G. Burke, Unambiguous ionization amplitudes for electron-hydrogen ionization, Phys. Rev. A 68 (2003) 020702(R).

[52] J. M. Randazzo, F. Buezas, A. L. Frapiccini, F. D. Colavecchia, G. Gasaneo, Solving three-body-breakup problems with outgoing-flux asymptotic conditions, Phys. Rev. A 84 (2011) 052715.

[53] D. A. Konovalov, I. Bray, Calculation of electron-impact ionization using the j-matrix method, Phys. Rev. A 82 (2010) 022708.

[54] J. F. Williams, P. L. Bartlett, I. Bray, A. T. Stelbovics, A. G. Mikosza, Differential cross sections for excitation to the 3s, 3p and 3d states of

atomic hydrogen by electron impact at energies from 16.5 to 54 eV, J. Phys. B 39 (2006) 719–728.

[55] P. L. Bartlett, A. T. Stelbovics, Complete direct method for electron-hydrogen scattering: Application to the collinear and Temkin-Poet models, Phys. Rev. A 69 (2004) 022703.

[56] G. H. Wannier, Treshold ionization by electron impact ..., Phys. Rev. 90 (1953) 817–825.

[57] P. L. Bartlett, A. T. Stelbovics, Threshold behavior of e-H ionizing collisions, Phys. Rev. Lett. 93 (2004) 233201.

[58] D. A. Horner, C. W. McCurdy, T. N. Rescigno, Electron-helium scattering in the S-wave model using exterior complex scaling, Phys. Rev. A 71 (2005) 012701.

[59] D. A. Horner, C. W. McCurdy, T. N. Rescigno, Electron-impact excitation autoionization of helium in the S-wave limit, Phys. Rev. A 71 (2005) 010701(R).

[60] P. L. Bartlett, A. T. Stelbovics, Electron-helium S-wave model benchmark calculations. I. Single ionization and single excitation, Phys. Rev. A 81 (2010) 022715.

[61] P. L. Bartlett, A. T. Stelbovics, Electron-helium S-wave model benchmark calculations. II. Double ionization, single ionization with excitation, and double excitation, Phys. Rev. A 81 (2010) 022716.

[62] W. Ihra, M. Draeger, G. Handke, H. Friedrich, Time-dependent approach to electron scattering and ionization in the s-wave model, Phys. Rev. A 52 (1995) 3752–3762.

[63] M. S. Pindzola, D. R. Schultz, Time-dependent close-coupling method for electron-impact ionization of hydrogen, Phys. Rev. A 53 (1996) 1525–1536.

[64] J. Colgan, M. S. Pindzola, F. J. Robicheaux, D. C. Griffin, M. Baertschy, Time-dependent close-coupling calculations of the triple-differential cross section for electron-impact ionization of hydrogen, Phys. Rev. A 65 (2002) 042721.

[65] M. S. Pindzola, F. Robicheaux, J. Colgan, Energy and angle differential cross sections for the electron-impact double ionization of helium, J. Phys. B 41 (2008) 235202.

[66] J. Colgan, M. Foster, M. S. Pindzola, I. Bray, A. T. Stelbovics, D. V. Fursa, Triple differential cross sections for the electron-impact ionization of helium at 102 ev incident energy, J. Phys. B 42 (2009) 145002 (6pp).

[67] A. S. Kheifets, I. Bray, Convergent close coupling calculations of helium double photoionization triply differential cross sections, J. Phys. B 31 (1998) L447–L453.

[68] A. S. Kadyrov, I. Bray, Convergence of two-center expansions in positron-hydrogen collisions, J. Phys. B 33 (2000) L635–L640.

[69] A. S. Kadyrov, I. Bray, A. T. Stelbovics, Near-threshold positron-impact ionization of atomic hydrogen, Phys. Rev. Lett. 98 (2007) 263202.

[70] I. B. Abdurakhmanov, A. S. Kadyrov, I. Bray, A. T. Stelbovics, Coupled-channel integral-equation approach to antiproton-hydrogen collisions, J. Phys. B 44 (2011) 075204.

[71] J. T. Broad, Gauss quadrature generated by diagonalization of H in finite L^2 bases, Phys. Rev. A 18 (1978) 1012–1027.

[72] I. Bray, K. Bartschat, D. V. Fursa, A. T. Stelbovics, Box-based and Laguerre-based convergent close-coupling calculations of electron-helium ionisation, J. Phys. B 36 (2003) 3425–3432.

[73] I. Bray, D. V. Fursa, Calculation of ionization within the close-coupling formalism, Phys. Rev. A 54 (1996) 2991–3004.

[74] E. P. Curran, H. R. J. Walters, Triple differential cross sections for electron impact ionisation of atomic hydrogen - a coupled psedostate calculation, J. Phys. B 20 (1987) 337–365.

[75] I. Bray, D. A. Konovalov, I. E. McCarthy, A. T. Stelbovics, Calculation of triple-differential cross sections in electron scattering on hydrogen, Phys. Rev. A 50 (1994) R2818–R2821.

[76] P. G. Burke, A. Hibbert, W. D. Robb, Electron scattering by complex atoms, J. Phys. B 4 (1971) 153–161.

[77] P. G. Burke, W. D. Robb, The R-matrix theory of atomic processess, Adv. Atom. Mol. Phys. 11 (1975) 143–214.

[78] V. M. Burke, C. J. Noble, Farm - a flexible asymptotic r-matrix package, Comp. Phys. Comm. 85 (1995) 471–500.

[79] M. R. H. Rudge, Theory of the ionization of atoms by electron impact, Rev. Mod. Phys. 40 (1968) 564–590.

[80] I. Bray, D. V. Fursa, Calculation of singly-differential cross sections of electron-impact ionization of helium at 100 eV, J. Phys. B 28 (1995) L435–L441.

[81] I. Bray, Close-coupling theory of ionization: successes and failures, Phys. Rev. Lett. 78 (1997) 4721–4724.

[82] A. T. Stelbovics, Calculation of ionization within the close-coupling formalism, Phys. Rev. Lett. 83 (1999) 1570–1573.

[83] K. Bartschat, I. Bray, The s-wave model for electron–hydrogen scattering, Phys. Rev. A 54 (1996) R1002–R1005.

[84] I. Bray, Low energy electron-impact ionization of atomic hydrogen with equal energy outgoing electrons, J. Phys. B 33 (2000) 581–595.

[85] M. B. Shah, D. S. Elliot, H. B. Gilbody, Pulsed crossed-beam study of the ionisation of atomic hydrogen , J. Phys. B 20 (1987) 3501–3514.

[86] J. Röder, H. Ehrhardt, C. Pan, A. F. Starace, I. Bray, D. V. Fursa, Absolute Triply Differential (e,2e) Cross Section Measurements for H with Comparison to Theory, Phys. Rev. Lett. 79 (1997) 1666–1669.

[87] P. Schlemmer, T. Rösel, K. Jung, H. Ehrhardt, (e,2e) investigation of atomic hydrogen and helium close to threshold, Phys. Rev. Lett. 63 (1989) 252–254.

[88] J. Röder, M. Baertschy, I. Bray, Ionization of atomic hydrogen by 17.6 ev electrons: experiment and theory, Phys. Rev. A 67 (2003) 010702(R).

[89] J. Röder, J. Rasch, K. Jung, C. T. Whelan, H. Ehrhardt, R. J. Allan, H. R. J. Walters, Coulomb three-body effects in low-energy impact ionization of h(1s), Phys. Rev. A 53 (1996) 225–233.

[90] C. T. Whelan, R. J. Allan, J. Rasch, H. R. J. Walters, X. Zhang, J. Röder, K. Jung, H. Ehrhardt, Coulomb three-body effects in (e,2e) collisions: The ionization of h in coplanar symmetric geometry, Phys. Rev. A 50 (1994) 4394–4396.

[91] J. Berakdar, J. S. Briggs, I. Bray, D. V. Fursa, Electron angular distributions in low-energy (e,2e) reactions, J. Phys. B 32 (1999) 895–913.

[92] M. Brauner, J. S. Briggs, H. Klar, J. T. Broad, T. Rösel, K. Jung, H. Ehrhardt, Triply differential cross sections for ionisation of hydrogen atoms by electrons: the intermediate and threshold energy regions, J. Phys. B 24 (1991) 657–673.

[93] H. Ehrhardt, K. Jung, G. Knoth, P. Schlemmer, Differential cross sections of direct single electron impact ionization, Z. Phys. D 1 (1986) 3–32.

[94] J. G. Childers, K. E. James, M. Hughes, I. Bray, M. Baertschy, M. A. Khakoo, Absolute measurements of electron-hydrogen ionization, Phys. Rev. A 68 (2003) 030702(R).

[95] S. Jones, D. H. Madison, M. K. Srivastava, Near-threshold ionization of hydrogen and helium by electron impact, J. Phys. B 25 (1992) 1899–1914.

[96] I. Bray, Electron-impact ionization of atomic hydrogen at 2 ev above threshold, J. Phys. B 32 (1999) L119–L126.

[97] I. Bray, On convergence of the close-coupling method for calculating electron-hydrogen ionisation, J. Phys. B 36 (2002) 2203–2209.

[98] Jochen Röder, Untersuchung der Elektronenstoßionisation, Ph.D. thesis, University of Kaiserslautern, Germany, 1996.

[99] D. V. Fursa, I. Bray, Calculation of electron-helium scattering, Phys. Rev. A 52 (1995) 1279–1298.

[100] D. V. Fursa, I. Bray, Topical review: Convergent close-coupling calculations of electron-helium scattering, J. Phys. B 30 (1997) 757–785.

[101] A. T. Stelbovics, I. Bray, D. V. Fursa, K. Bartschat, Electron-impact ionization of helium for equal-energy sharing kinematics, Phys. Rev. A 71 (2005) 052716(13).

[102] I. Bray, D. V. Fursa, Benchmark cross sections for electron-impact total single ionization of helium, J. Phys. B 44 (2011) 061001.

[103] M. S. Pindzola, F. Robicheaux, S. D. Loch, J. C. Berengut, T. Topcu, J. Colgan, M. Foster, D. C. Griffin, C. P. Ballance, D. R. Schultz, T. Minami, N. R. Badnell, M. C. Witthoeft, D. R. Plante, D. M. Mitnik, J. A. Ludlow, U. Kleiman, The time-dependent close-coupling method for atomic and molecular collision processes, J. Phys. B 40 (2007) R39–R60.

[104] X. Ren, I. Bray, D. Fursa, J. Colgan, M. Pindzola, T. Pflüger, A. Senftleben, S. Xu, A. Dorn, J. Ullrich, Electron-impact ionization of helium: A comprehensive experiment benchmarks theory, Phys. Rev. A 83 (2011) 052711.

[105] R. Rejoub, B. G. Lindsay, R. F. Stebbings, Determination of the absolute partial and total cross sections for electron-impact ionization of the rare gases, Phys. Rev. A 65 (2002) 042713.

[106] A. A. Sorokin, I. L. Beigman, S. V. Bobashev, M. Richter, L. A. Vainshtein, Total electron-impact ionization cross sections of helium, J. Phys. B 37 (2004) 3215.

[107] T. Rösel, J. Röder, L. Frost, K. Jung, H. Ehrhardt, Measurement of absolute, near-threshold triple differential cross sections for electron impact ionization, J. Phys. B 25 (1992) 3859–3872.

[108] J. Röder, H. Ehrhardt, I. Bray, D. V. Fursa, I. E. McCarthy, Absolute triple differential cross section for electron-impact ionization of helium at 40 eV, J. Phys. B 29 (1996) 2103–2114.

[109] S. Rioual, J. Röder, B. Rouvellou, H. Ehrhardt, A. Pochat, I. Bray, D. V. Fursa, Absolute (e,2e) cross sections for the electron-impact

ionization of helium in energy sharing kinematics at 44.6 eV, J. Phys. B 31 (1998) 3117–3127.

[110] J. Röder, H. Ehrhardt, I. Bray, D. V. Fursa, Absolute double differential cross sections for electron impact ionization of helium, J. Phys. B 30 (1997) 1309–1322.

[111] J. Röder, H. Ehrhardt, I. Bray, D. V. Fursa, I. E. McCarthy, Absolute triple differential cross section for electron-impact ionization of helium at 50 eV, J. Phys. B 29 (1996) L67–L73.

[112] T. Rösel, C. Dupre, J. Röder, A. Duguet, K. Jung, A. Lahmam-Bennani, H. Ehrhardt, symmetric coplanar e,2e for e-He, J. Phys. B 24 (1991) 3059–3067.

[113] I. Bray, T. Lepage, D. V. Fursa, A. T. Stelbovics, Ionization of helium by 64.6 ev electrons, J. Phys. B 43 (2010) 074028.

[114] I. Bray, D. V. Fursa, A. S. Kadyrov, A. T. Stelbovics, J. Colgan, M. S. Pindzola, Close-coupling calculations of 64.6 ev e-he ionization, Journal of Physics: Conference Series 288 (2011) 012002.

[115] J. Colgan, O. Al-Hagan, D. H. Madison, A. J. Murray, M. S. Pindzola, Deep interference minima in non-coplanar triple differential cross sections for the electron-impact ionization of small atoms and molecules, J. Phys. B 42 (2009) 171001 (6pp).

[116] A. J. Murray, F. H. Read, exploring the helium (e, 2e) differential cross section at 64.6 ev with symmetric scattering angles but non-symmetric energies, J. Phys. B 26 (1993) L359–L365.

[117] M. Dürr, C. Dimopoulou, A. Dorn, B. Najjari, I. Bray, D. V. Fursa, Z. Chen, D. H. Madison, K. Bartschat, J. Ullrich, Single ionization of helium by 102 ev electron impact: three-dimensional images for electron emission, J. Phys. B 39 (2006) 4097–4111.

[118] F. Catoire, E. M. Staicu-Casagrande, M. Nekkab, C. D. Cappello, K. Bartschat, A. Lahmam-Bennani, Investigation of the (e, 2e) single ionization of he and ar at large energy loss close to minimum momentum transfer, J. Phys. B 39 (2006) 2827–2838.

[119] I. Bray, D. V. Fursa, A. T. Stelbovics, Electron-impact ionization of helium with large energy transfer, Phys. Rev. A 74 (2006) 034702.

[120] L. Avaldi, R. Camilloni, R. Multari, G. Stefani, J. Langlois, O. Robaux, R. J. Tweed, G. N. Vien, Absolute measurement of ionization-excitation of helium at intermediate energies and their interpretation, J. Phys. B 31 (1998) 2981–2997.

[121] P. J. Marchalant, J. Rasch, C. T. Whelan, D. H. Madison, H. R. J. Walters, First and second born calculations of (e, 2e) excitation-ionization of helium, J. Phys. B 32 (1999) L705–L710.

[122] A. S. Kheifets, I. Bray, K. Bartschat, Convergent calculations for simultaneous electron-impact ionization–excitation of helium, J. Phys. B 32 (1999) L433–L438.

[123] Y. Fang, K. Bartschat, Convergent second-order calculations for simultaneous electron-impact ionization-excitation of helium, J. Phys. B 34 (2001) L19–L25.

[124] S. Bellm, J. Lower, K. Bartschat, X. Guan, D. Weflen, M. Foster, A. L. Harris, D. H. Madison, Ionization and ionization-excitation of helium to the $n = 1 - 4$ states of he^+ by electron impact, Phys. Rev. A 75 (2007) 042704.

[125] J. Briggs, V. Schmidt, Differential cross sections for photo-double-ionization of the helium atom, J. Phys. B 33 (2000) R1–R48.

[126] A. S. Kheifets, I. Bray, Calculation of double photoionization of helium using the convergent close-coupling method, Phys. Rev. A 54 (1996) R995–R998.

[127] M. Y. Amusia, Atomic photoeffect, Plenum Press, New York, 1990.

[128] A. S. Kheifets, I. Bray, Effect of the ground state correlations on the helium double photoionization and ionization with excitation, Phys. Rev. A 57 (1998) 2590–2595.

[129] A. S. Kheifets, I. Bray, Photoionization with excitation and double photoionization of the helium isoelectronic sequence, Phys. Rev. A 58 (1998) 4501–4511.

[130] D. A. Varshalovich, A. N. Moskalev, V. K. Khersonskii, Quantum theory of angular momentum, World Scientific, Singapore, 1988.

[131] A. S. Kheifets, I. Bray, Energy-sharing double photoionization of helium from near-threshold to high energies, Phys. Rev. A 62 (2000) 65402.

[132] O. Schwarzkopf, B. Krässig, J. Elmiger, V. Schmidt, Energy- and angle-resolved double photoionization in helium, Phys. Rev. Lett. 70 (1993) 3008–3011.

[133] A. Huetz, P. Selles, D. Waymel, J. Mazeau, Wannier theory for double photoionization of noble gases, J. Phys. B 24 (1991) 1917.

[134] R. Dörner, T. Vogt, V. Mergel, H. Khemliche, S. Kravis, C. L. Cocke, Ratio of cross sections for double to single ionization of He by 85–400 eV photons, Phys. Rev. Lett. 76 (1996) 2654–2657.

[135] J. C. Levin, G. B. Armen, I. A. Sellin, Photoionization and compton double ionization of helium from threshold to 20 kev, Phys. Rev. Lett. 76 (1996) 1220–1223.

[136] R. Wehlitz, I. A. Sellin, O. Hemmers, S. B. Whitfield, P. Glans, H. Wang, D. W. Lindle, B. Langer, N. Berrah, J. Viefhaus, U. Becker, Photon energy dependence of ionization-excitation in helium at medium energies, J. Phys. B 30 (1997) L51.

[137] J. A. R. Samson, W. C. Stolte, Z. X. He, J. N. Cutler, R. J. Bartlett, Double photoionization of helium, Phys. Rev. A 57 (1998) 1906–1911.

[138] T. Aberg, Asymptotic double-photoexcitation cross sections of the helium atom, Phys. Rev. A 2 (1970) 1726–1729.

[139] A. Czasch, M. Schöffler, M. Hattass, , S. Schössler, T. Jahnke, T. Weber, A. Staudte, J. Titze, C. Wimmer, S. Kammer, M. Weckenbrock, S. Voss, R. E. Grisenti, O. Jagutzki, L. P. Schmidt, H. Schmidt-Böcking, R. Dörner, J. M. Rost, T. Schneider, C.-N. Liu, I. Bray, A. Kheifets, K. Bartschat, Partial photoionization cross sections and angular distributions for double excitation of helium up to the N=13 threshold, Phys. Rev. Lett. 95 (2005) 243003.

[140] I. Bray, K. Bartschat, A. T. Stelbovics, Box-based convergent close-coupling for solving Coulomb few-body problems, Phys. Rev. A 67 (2003) 060704(R).

[141] H. Bräuning, R. Dörner, C. L. Cocke, M. H. Prior, B. Krässig, A. Kheifets, I. Bray, A. Bräuning-Demian, K. Carnes, S. Dreuil, V. Mergel, P. Richard, J. Ullrich, H. Schmidt-Böcking, Absolute triple differential cross sections for photo double ionization of helium — experiment and theory, J. Phys. B 31 (1998) 5149–5160.

[142] S. Cvejanović, J. P. Wightman, T. Reddish, F. Maulbetsch, M. A. MacDonald, A. S. Kheifets, I. Bray, Photodouble ionisation of helium at an excess energy of 40 eV, J. Phys. B 33 (2000) 265–283.

[143] C. Dawson, S. Cvejanovič, D. P. Seccombe, T. J. Reddish, F. Maulbetsch, A. Huetz, J. Mazeau, A. S. Kheifets, Helium (γ,2e) triple differential cross sections at an excess energy of 60 eV, J. Phys. B 34 (2001) L525–L533.

[144] G. Turri, L. Avaldi, P. Bolognesi, R. Camilloni, M. Coreno, J. Berakdar, A. S. Kheifets, G. Stefani, Double photoionization of he at 80 ev excess energy in the equal-energy-sharing condition, Phys. Rev. A 65 (2002) 034702.

[145] P. Bolognesi, R. Camilloni, M. Coreno, G. Turri, J. Berakdar, A. Kheifets, L. Avaldi, Complementary TDCS for the photo-double ionisation of He at 40 eV above threshold in unequal energy sharing conditions, J. Phys. B 34 (2001) 3193–3203.

[146] P. Bolognesi, A. S. Kheifets, I. Bray, L. Malegat, P. Selles, A. K. Kazansky, L. Avaldi, A procedure to extract the complex amplitudes of He photodouble ionisation from experimental data, J. Phys. B 36 (2003) L241–L247.

[147] A. Knapp, A. Kheifets, I. Bray, T. Weber, A. L. Landers, S. Schössler, T. Jahnke, J. Nickles, S. Kammer, O. Jagutzki, L. P. Schmidt, T. Osipov, J. Rösch, M. H. Prior, H. Schmidt-Böcking, C. L. Cocke, R. Dörner, Mechanisms of photo double ionization of helium by 530 eV photons, Phys. Rev. Lett. 89 (2002) 033004.

[148] A. Knapp, A. Kheifets, I. Bray, T. Weber, A. L. Landers, S. Schössler, T. Jahnke, J. Nickles, S. Kammer, O. Jagutzki, L. P. Schmidt, T. Osipov, M. H. Prior, H. Schmidt-Böcking, C. L. Cocke, R. Dörner, Photo double ionization of helium 100 eV and 450 eV above threshold: I. linearly polarized light, J. Phys. B 38 (2005) 615.

[149] A. Knapp, A. Kheifets, I. Bray, T. Weber, A. L. Landers, S. Schössler, T. Jahnke, J. Nickles, S. Kammer, O. Jagutzki, L. P. Schmidt, T. Osipov, M. H. Prior, H. Schmidt-Böcking, C. L. Cocke, R. Dörner, Photo double ionization of helium 100 eV and 450 eV above threshold: III. Gerade and ungerade amplitudes and their relative phase, J. Phys. B 38 (2005) 645.

[150] A. S. Kheifets, I. Bray, K. Soejima, A. Danjo, K. Okuno, A. Yagishita, Experimental and theoretical study of linear and circular dichroism in helium double photoionization, J. Phys. B 32 (1999) L501–L509.

[151] P. Bolognesi, V. Feyer, A. Kheifets, S. Turchini, T. Prosperi, N. Zema, L. Avaldi, Photodouble ionization of he with circularly polarized synchrotron radiation: complete experiment and dynamic nodes, J. Phys. B 41 (2008) 051003.

[152] A. Knapp, A. Kheifets, I. Bray, T. Weber, A. L. Landers, S. Schössler, T. Jahnke, J. Nickles, S. Kammer, O. Jagutzki, L. P. Schmidt, T. Osipov, M. H. Prior, H. Schmidt-Böcking, C. L. Cocke, R. Dörner, Photo double ionization of helium 100 eV and 450 eV above threshold: II. circularly polarized light, J. Phys. B 38 (2005) 635.

[153] V. Mergel, M. Achler, R. Dörner, K. Khayyat, T. Kambara, Y. Awaya, V. Zoran, B. Nyström, L. Spielberger, J. H. McGuire, J. Feagin, J. Berakdar, Y. Azuma, H. Schmidt-Böcking, Helicity dependence of the photon-induced three-body coulomb fragmentation of helium investigated by cold target recoil ion momentum spectroscopy, Phys. Rev. Lett. 80 (1998) 5301–5304.

[154] A. S. Kheifets, I. Bray, Calculation of circular dichroism in helium double photoionization, Phys. Rev. Lett. 81 (1998) 4588–4591.

[155] M. Achler, V. Mergel, L. Spielberger, R. Dorner, Y. Azuma, H. Schmidt-Böcking, Photo double ionization of he by circular and

linear polarized single-photon absorption, J. Phys. B 34 (2001) 965–981.

[156] A. S. Kheifets, I. Bray, Equal energy-sharing double photoionization of helium from near-threshold to high energies, Phys. Rev. A 62 (2000) 065402.

[157] A. S. Kheifets, I. Bray, Symmetrized amplitudes of the helium atom double photoionization, Phys. Rev. A 65 (2002) 022708.

[158] O. Schwarzkopf, B. Krassig, J. Elmiger, V. Schmidt, Energy resolved and angle resolved double photoionization in helium, Phys. Rev. Lett. 70 (1993) 3008–3011.

[159] O. Schwarzkopf, V. Schmidt, Experimental determination of the absolute value of the triple differential cross section for double photoionization in helium, J. Phys. B 28 (1995) 2847–2862.

[160] G. Dawber, L. Avaldi, A. G. Mcconkey, H. Rojas, M. A. Macdonald, G. C. King, Near threshold tdcs for photo-double ionization of helium, J. Phys. B 28 (1995) L271–L277.

[161] R. Dörner, H. Bräuning, J. M. Feagin, V. Mergel, O. Jagutzki, L. Spielberger, T. Vogt, H. Khemliche, M. H. Prior, J. Ullrich, C. L. Cocke, H. Schmidt-Böcking, Photo-double-ionization of He: fully differential and absolute electronic and ionic momentum distributions, Phys. Rev. A 57 (1998) 1074–1090.

[162] L. Malegat, P. Selles, A. Huetz, Double photoionization-1: A new parametrization of the triple differential cross section from first principles, J. Phys. B 30 (1997) 251–261.

[163] J. P. Wightman, S. Cvejanović, T. J. Reddish, (γ, 2e) cross section measurements of D_2 and He, J. Phys. B 31 (1998) 1753.

[164] K. Soejima, A. Danjo, K. Okuno, A. Yagishita, Linear and circular dichroism in the double photoionization of helium, Phys. Rev. Lett. 83 (1999) 1546 – 1549.

[165] L. Malegat, A. Kazansky, P. Selles, Extended Wannier ridge model versus $\mathcal{R}$-matrix treatment for double photoionization of helium, J. Phys. B 32 (1999) 4667–4675.

[166] A. S. Kheifets, I. A. Ivanov, I. Bray, Timing analysis of two-electron photoemission, J. Phys. B 44 (2011) 101003.

[167] A. S. Kheifets, A. Ipatov, M. Arifin, I. Bray, Double photoionization calculations of the helium metastable $2^{1,3}s$ states, Phys. Rev. A 62 (2000) 052724(10).

[168] A. S. Kheifets, I. Bray, Frozen-core model of the double photoionization of beryllium, Phys. Rev. A 65 (2001) 012710.

[169] A. S. Kheifets, I. Bray, Valence-shell double photoionization of alkaline-earth-metal atoms, Phys. Rev. A 75 (2007) 042703.

[170] R. Wehlitz, D. Lukic, J. B. Bluett, Single and double photoionization of beryllium below 40 ev, Phys. Rev. A 71 (2005) 012707.

[171] R. Wehlitz, S. B. Whitfield, Valence double photoionization of beryllium, J. Phys. B 34 (2001) L719–L725.

[172] R. Wehlitz, P. N. Juranić, D. V. Lukić, Double photoionization of magnesium from threshold to 54 eV photon energy, Phys. Rev. A 78 (2008) 033428.

[173] A. S. Kheifets, I. Bray, Angular correlation in the two-electron continuum, Phys. Rev. A 73 (2006) 020708(R).

[174] A. S. Kheifets, I. Bray, J. Hoszowska, K-shell double photoionization of be, mg, and ca, Phys. Rev. A 79 (2009) 042504.

[175] J. Hoszowska, A. K. Kheifets, J.-C. Dousse, M. Berset, I. Bray, W. Cao, K. Fennane, Y. Kayser, M. KavCiC, J. Szlachetko, M. Szlachetko, Physical mechanisms and scaling laws of k-shell double photoionization, Phys. Rev. Lett. 102 (2009) 073006.

[176] A. S. Kheifets, D. V. Fursa, I. Bray, Two-electron photoionization of ground-state lithium, Phys. Rev. A 80 (2009) 063413.

[177] M.-T. Huang, R. Wehlitz, Y. Azuma, L. Pibida, I. A. Sellin, J. W. Cooper, M. Koide, H. Ishijima, T. Nagata, Single and double photoionization of lithium, Phys. Rev. A 59 (1999) 3397–3401.

[178] R. Wehlitz, J. B. Bluett, S. B. Whitfield, Comparison of the double- to single-photoionization ratio of li with he, Phys. Rev. A 66 (2002) 012701.

[179] A. S. Kheifets, D. V. Fursa, I. Bray, J. Colgan, M. S. Pindzola, Differential cross sections of double photoionization of lithium, Phys. Rev. A 82 (2010) 023403.

[180] A. S. Kheifets, D. V. Fursa, C. W. Hines, I. Bray, J. Colgan, M. S. Pindzola, Spin effects in double photoionization of lithium, Phys. Rev. A 81 (2010) 023418.

[181] A. S. Kheifets, I. Bray, A. Lahmam-Bennani, A. Duguet, I. Taouil, A comparative experimental and theoretical investigation of the electron impact double ionization of he in kev regime, J. Phys. B 32 (1999) 5047–5065.

[182] A. S. Kheifets, I. Bray, Convergent calculations of double ionization of helium:
from (γ,2e) to (e,3e) processes, Phys. Rev. A 69 (2004) 050701(R).

[183] A. Dorn, A. Kheifets, C. D. Schröter, B. Najjari, C. Höhr, R. Moshammer, J. Ullrich, Double ionization of helium by electron-impact: Complete pictures of the four-body break up dynamics, Phys. Rev. Lett. 86 (2001) 3755–3758.

[184] A. Dorn, A. Kheifets, C. D. Schröter, B. Najjari, C. Höhr, R. Moshammer, J. Ullrich, Double ionization of helium by electron-impact in the impulsive regime, Phys. Rev. A 65 (2002) 032709.

[185] A. S. Kheifets, Second-order born model for two-electron atomic ionization by fast charged-particle impact, Phys. Rev. A 69 (2004) 032712.

[186] A. S. Kheifets, I. A. Ivanov, Convergent close-coupling calculations of two-photon double ionization of helium, J. Phys. B 39 (2006) 1731.

[187] A. S. Kheifets, I. A. Ivanov, I. Bray, Angular anisotropy parameters and recoil-ion momentum distribution in two-photon double ionization of helium, Phys. Rev. A 76 (2007) 025402.

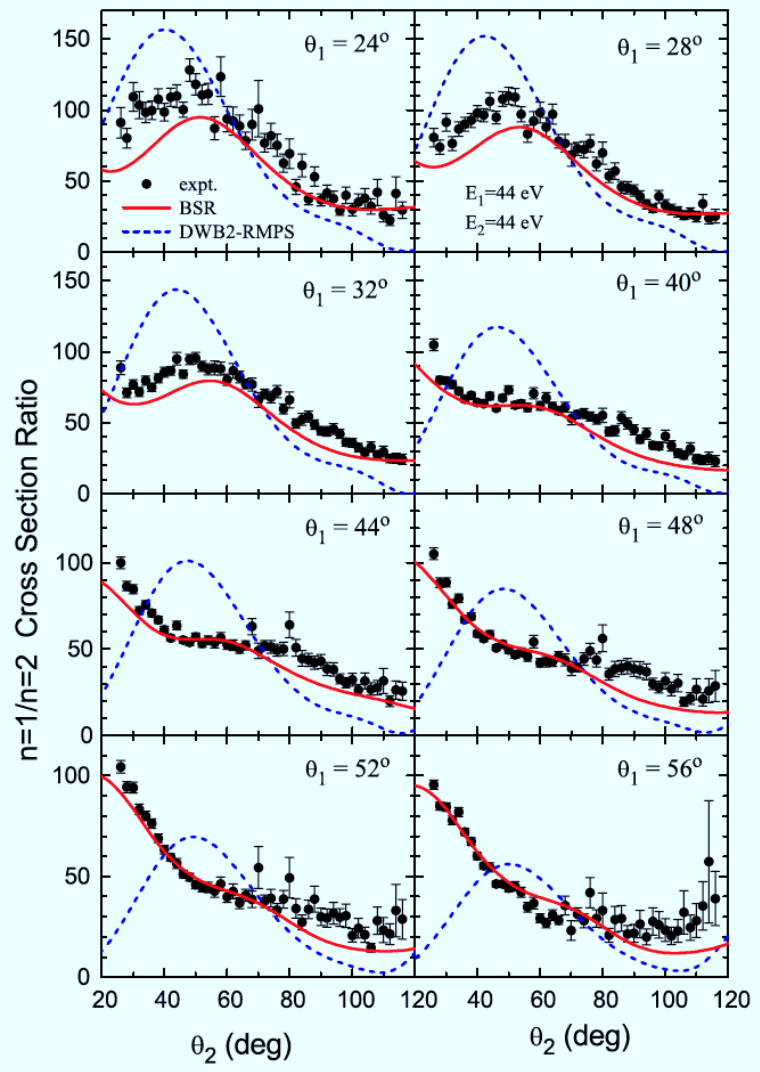

Figure 16: Coplanar fully differential cross sections $n = 1/n = 2$ ratios for electron-impact single ionization of the ground state of helium leaving the residual He^+ ion in the $n = 1$, or $n = 2$ states. The two outgoing electrons have $E_1 = E_2 = 44$ eV. The experimental data is due to Bellm et al. [124]. The figure is reproduced with permission of Zatsarinny and Bartschat [10], who performed the calculations.

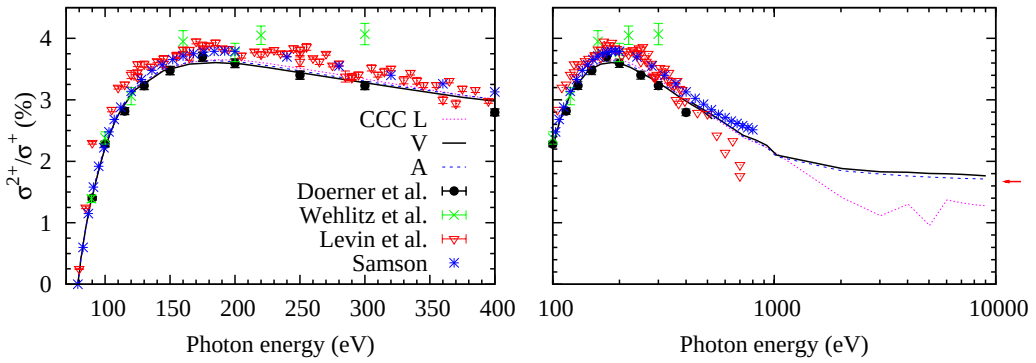

Figure 17: The ratio of double to single photoionization cross sections in He. The CCC calculations are presented in the three gauges of the electro-magnetic interaction with a 20-parameter Hylleraas ground state. Experimental data are from Dörner *et al.* [134], Levin *et al.* [135], Wehlitz *et al.* [136] and Samson *et al.* [137]. The arrow on the right panel visualizes the limit of infinite photon energy.

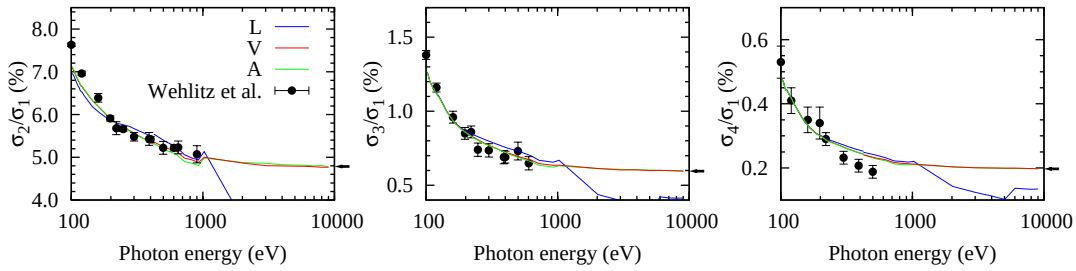

Figure 18: The cross sections ratio σ_n/σ_1 for the photoionization of He with simultaneous excitation to the $n = 2$, 3 and 4 final ionic state. Experimental data are from Wehlitz et al. [136]. The asymptotic ratio in the limit of infinite photon energy is indicated by an arrow.

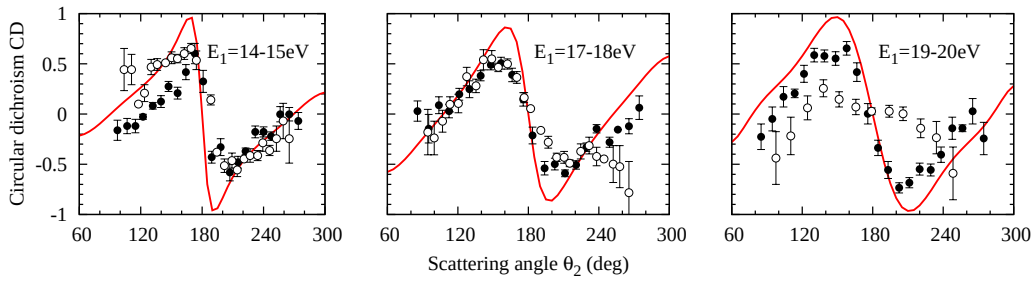

Figure 19: Circular dichroism CD=$(\sigma_+ - \sigma_-)/(\sigma_+ + \sigma_-)$ at excess energy $E_1 + E_2 = 20\,\mathrm{eV}$, with electron of energy E_1 detected at $\theta_1 = 0°$. Experimental data are from Mergel et al. [153] (open circles) and Achler et al. [155] (filled circles)

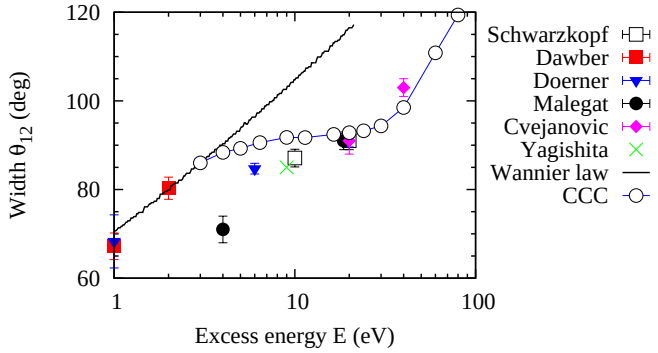

Figure 20: The width parameter $\Delta\theta$ of the Gaussian function (132). Experimental data are due to Schwarzkopf et al. [158], Schwarzkopf and Schmidt [159] (open squares), Dawber *et al.* [160] (filled squares), Dörner *et al.* [161] (filled triangles), Malegat *et al.* [162] (filled circles), Cvejanović *et al.* [142, 163] (filled diamonds), Soejima *et al.* [164] (asterisk). The CCC results are shown as open circles joint by a solid line. The straight line is the Wannier exponent by Malegat et al. [165].

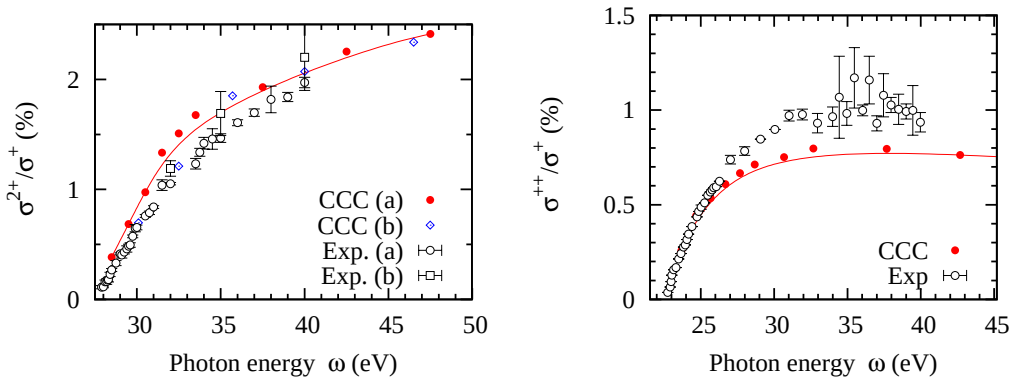

Figure 21: Left: Double-to-single photoionization cross-sections ratio in Be (left) and Mg (right) shown as a function of the photon energy. On the left plot, the CCC results (a) [168] and (b) [169] are shown by the red filled circles and blue open diamonds. Experimental data (a) [170] and (b) [171] are displayed by open circles and squares, respectively. On the right plot, the CCC results [169] are compared with experiment [172].

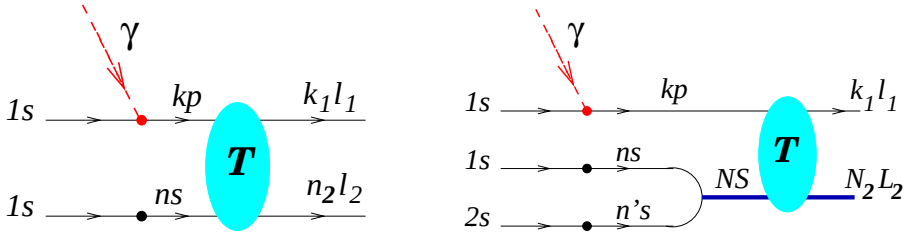

Figure 22: (Color online) Graphical representation of the amplitudes of single-photon two-electron ionization of He (left diagram) and Li (right diagram)

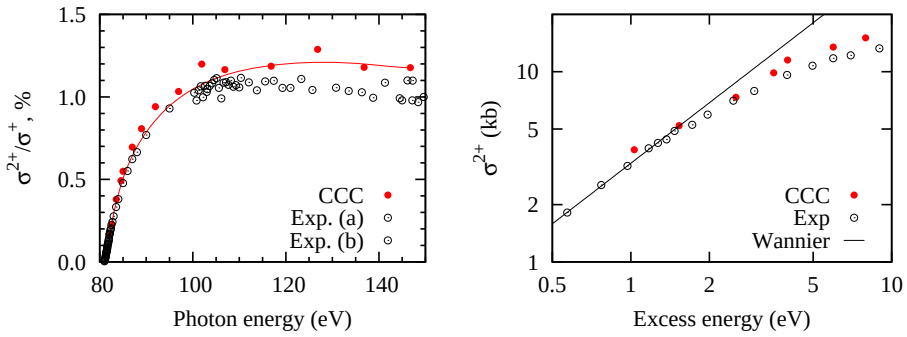

Figure 23: (Color online) Left: Double-to-single photoionization cross-sections ratio in Li is plotted as a function of the photon energy. The CCC calculation [176] is compared with experiment (a) [177] and (b) [178]. Right: DPI cross-section near threshold is plotted in log scale as a function of the excess energy. The CCC calculation [176] is compared with experiment [178] and the Wannier threshold law drawn with a straight line line.